Hepatic AMPK signaling and pharmacological activation during liver injury.

Julia Rolim Cavalcanti Nunes

Thesis submitted to the University of Ottawa

in partial fulfillment of the requirements for the

Doctorate in Philosophy degree in Biochemistry

Supervisor: Dr. Morgan Fullerton

The Department of Biochemistry, Microbiology, and Immunology

Faculty of Medicine

University of Ottawa

© Julia Rolim Cavalcanti Nunes, Ottawa, Canada, 2024

Abstract

Liver injury instigates a proinflammatory response in tissue-resident macrophages, called Kupffer cells (KCs), resulting in the recruitment of monocytes and neutrophils. The high energy demand required for a rapid proinflammatory response in macrophages like KCs is achieved through metabolic reprogramming. This is supported by increased glycolysis. On the other hand, injury resolution requires hepatic macrophages to undergo an anti-inflammatory polarization, which relies on oxidative phosphorylation (OXPHOS). In addition to shifts in mechanisms of adenosine triphosphate (ATP) production, lipid metabolic reprogramming supplies metabolic intermediates and lipids for membrane remodeling and the production of inflammatory mediators. AMP-activated protein kinase (AMPK) is a master metabolic regulator that influences the metabolic reprogramming of macrophages. While AMPK activation promotes an anti-inflammatory polarization, disruption of activity exacerbates proinflammatory signaling. For this thesis work, we addressed whether macrophage AMPK is protective against liver injury by altering immunometabolism**.** Specifically, we investigated this question in the context of chronic (non-alcoholic steatohepatitis (NASH)) and acute (acetaminophen (APAP) overdose) liver injury.

While APAP overdose is a robust and directly translational model of acute injury, models of NASH-induced hepatic fibrosis rely on nutrient-deficient diets like the choline-deficient high-fat diet (CDAHFD) or genetic manipulation. Despite the utility of these models, they seldom mirror the pathogenesis of human NASH, with diets like CDAHFD being completely dissociated from metabolic syndrome. Moreover, models are required to address the divergence between male and female mice. Recently, there has been a shift towards addressing other variables that drive inflammation and metabolism. At room temperature (RT) (22 °C), mice experience cold stress that alters various biological functions. Cold stress drives brown adipose tissue (BAT) activation

and upregulates corticosterone production and immunosuppression, all processes that blunt NASH progression. Giles *et al.* (2016) demonstrated that housing mice at thermoneutrality (T_N) (30 °C) exacerbated metabolic-dysfunction associated fatty liver disease (MAFLD) progression toward NASH in both male and female mice. Since then, we and others have implemented T_N housing with different dietary interventions and mice strains. We determined that 16-week Western diet (WD) feeding of male and female mice at 29 °C was insufficient to drive hepatic fibrosis, however alterations in glucose tolerance and elevated liver injury enzymes as well as profibrotic gene expression in male mice may indicate that a longer timeline is necessary (24 weeks).

Given that our T_N NASH model did not produce hepatic fibrosis, we implemented the CDAHFD to investigate macrophage AMPK in chronic liver injury. Male and female AMPK Flox (*Prkaa1* fl/fl/*Prkaa2* fl/fl) and MacKO (Flox-LysM-Cre+) mice were fed CDAHFD for 8 weeks. In this time frame, CDAHFD produces a lean euglycemic phenotype with hepatic steatosis, inflammation, and fibrosis, to which AMPK MacKO had no influence. Moreover, intervention with a low dose of metformin had no effect, contrary to the reduction in hepatic steatosis observed in HFD-fed mice. Although macrophage AMPK is dispensable in the CDAHFD model of chronic liver injury, acute liver injury needed to be addressed. We found that priming with systemic activation of a direct AMPK activator MK-8722 did not influence hepatic injury and necrosis in our model of APAP-induced liver injury (AILI). Moreover, deletion of hepatocellular AMPK (Flox-Alb-Cre+) or AMPK MacKO did not influence injury at 24 hours post overdose. Despite the lack of effect of systemic AMPK activation, we were interested in a nanoparticle-based targeting of direct AMPK activator MK-8722 (NP-MK8722) delivery. We determined that PLGA-PEG nanoparticles (NPs) accumulated in hepatic macrophages as early as 2 hours post-injection, but NP-MK8722 did not alter hepatic necrosis, injury, or immune infiltration.

Overall, my thesis work has advanced our knowledge of the effects of housing temperatures on NASH pathogenesis. Moreover, we are the first to address the effects of macrophage AMPK signaling in NASH and AILI. This is especially true for assessing how AMPK deficiency and targeted activation influences KC immunometabolism during injury.

Viver e não ter a vergonha de ser feliz

Cantar, e cantar e cantar

A beleza de ser um eterno aprendiz

Eu sei que a vida devia ser bem melhor e será

Mas isso não impede que eu repita

É bonita, é bonita e é bonita!

Gonzaguinha (O Que e o Que E? 1999)

Acknowledgements

The past six years have been a period of tremendous growth for me. Many people have inspired me to persevere through challenging times but also celebrate every success. First and foremost, I owe the success and completion of my Ph.D. thesis to my supervisor, Dr. Morgan Fullerton. I was extremely fortunate to be mentored by such a fantastic and experienced researcher. His guidance and patience have been vital to the development of my critical thinking and communication skills. His mentorship style has shaped me into an intellectually curious and independent thinker. In light of all the mistakes I have made, Dr. Fullerton has always been open to my ideas, both conceptual and experimental. Most of all, Dr. Fullerton has always been a champion of work-life balance and the biggest advocate for my career advances.

I would also like to thank my thesis advisory committee members, Dr. Thomas Lagace, Dr. Julie St-Pierre, and Dr. Erin Mulvihill. Their expertise and fresh perspective have helped me drive my research. Amongst all our collaborators, I especially thank Dr. Suresh Gadde for providing the nanoparticles crucial to one of my studies. A special thanks to Dr. Vera Tang for all the interesting conversations at the cytometer and for answering my endless flow cytometry questions. Finally,

the staff of the histology core has processed and imaged so many liver sections for my research; it's incredible.

I am also so lucky to have such a supportive lab. These people have seen me during highs and lows and are always willing to lend an ear or a helping hand. My lab has greatly shaped my graduate experience, from large animal studies to experimental advice. However, this support was also found outside the lab. I have made so many fantastic friends throughout the years. We have bonded over shared experiences, and I will always treasure our conversations. Friends outside of research, thank you for your encouragement and understanding of the different phases of my graduate studies. Although we have not seen each other as frequently as I would have liked, I still care for you dearly.

To my family, minha mãe, meu pai e Camilla, thank you for being my biggest fan. I love you all more than words can say. I would not be where or who I am today without you. This gratitude also extends to my family abroad; I know how proudly you speak of me. Also, thank you to Genia and Andrzej Olender for opening your home to Tom and I over the past 3 years; we are eternally grateful.

Finally, to my other half, my fiancé, Thomas, you have picked me up many times and helped me believe in myself. We are coming out of this phase of our lives as better and more mature people. I am so happy to have shared all the moments with you, no matter how small. I look forward to our next chapter. Just keep swimming.

Abbreviations

KCs: Kupffer cells
OXPHOS: oxidative phosphorylation
ATP: adenosine triphosphate
AMPK: AMP-activated protein kinase
NASH: non-alcoholic steatohepatitis
APAP: acetaminophen
CDAHFD: choline-deficient high-fat diet
RT: room temperature
BAT: brown adipose tissue
T_N: thermoneutral or thermoneutrality
MAFLD: metabolic dysfunction associated liver disease.
WD: Western diet
Flox: Prkaa1 $^{fl/fl}$ /Prkaa2$^{fl/fl}$
MacKO: Flox-*LysM*-Cre^{+}
AILI: APAP-induced liver injury
NP: nanoparticles
FAO: fatty acid oxidation
NPCs: non-parenchymal cells
HSCs: hepatic stellate cells
LSECs: liver sinusoidal endothelial cells
ALT: alanine transaminase
ALF: acute liver failure
HCC: hepatocellular carcinoma
DAMPs: danger-associated molecular patterns
NLRP3: NOD-like receptor pyrin domain containing 3
TLR: toll-like receptors
IL-1β: interleukin-1
TNF: tumour necrosis factor
VCAM1: vascular adhesion molecule 1
CCL2: chemokine ligand 2
ROS: reactive oxygen species
NO: nitric oxide
TGFβ: transforming growth factor beta
NAPQI: N-acetyl-p-benzoquinone
CYP450: cytochrome P450
GSH: glutathione
NAC: N-acetylcysteine
JNK: c-jun N-terminal kinase
HMGB1: high mobility box protein 1
NAFLD: non-alcoholic fatty liver disease
IR: insulin resistance
VLDL: very low-density lipoprotein
DNL: de novo lipogenesis
FFA: free fatty acid
TG: triglycerides
CE: cholesterol esters
LXR: liver X receptor
SREBP: sterol regulatory element binding protein
FC: free cholesterol
HMGCR: 3-hydroxy-3-methylglutaryl coenzyme A reductase
LDL: low-density lipoprotein
ER: endoplasmic reticulum
SERCA: sarco/endoplasmic reticulum Ca^{2+}-ATPase
LPS: lipopolysaccharide
MoKCs: monocyte-derived KCs
TIMD4: T-cell immunoglobulin and mucin domain containing 4
RTMs: recruited temporary macrophages.
LAMs: lipid-associated macrophages
SAMs: scar-associated macrophages
HCLSs: hepatic crown-like structures
CCL_4: carbon tetrachloride
MCD: methionine-choline deficient
DIAMOND: diet-induced animal model of NAFLD
ACC: Acetyl-CoA Carboxylase
α-KD: amino-terminal kinase domain
α-AID: autoinhibitory domain
α-CTD: C-terminal domain
β-CTR: C-terminal region
β-CBM: carbohydrate-binding module
ADaM: allosteric drug and metabolite
CBS: cystathionine-β-synthase
T172: threonine-172
LKB1: liver kinase B1
mTORC1: mammalian target of rapamycin complex 1
CAMKK: Ca^{2+}/Calmodulin -dependent serine-threonine protein kinase
S108: serine-108

ULK1: unc-51-like autophagy-activating like kinase 1
FBP: fructose-1,6-bisphosphate
TCA: tricarboxylic acid
DN-AMPKα1: dominant negative AMPKα1
CA-AMPKα1: constitutively active AMPKα1
NF-κB: nuclear factor kappa-light-chain-enhancer of activated B cells
GSK3-β: glycogen synthase kinase β
KO: knockout
WT: wildtype
RIPK1: receptor-interacting serine/threonine-protein kinase 1
S79A: serine-to-alanine mutation at S79
DKI: double knockin
AMPK hepDKO: hepatocyte-specific KO of AMPKα1 and α2
D316A: aspartic acid residue 316 to alanine
BMDMs: bone marrow-derived macrophages
GTT: glucose tolerance test
ITT: insulin tolerance test
CD: control diet
AST: aspartate transaminase
ALP: alkaline phosphatase
TBIL: total bilirubin
LFD: low-fat diet

List of Figures and Tables

Figure 1.1. The anatomy and zonation of the hepatic lobule.
Figure 1.2. The mechanisms of hepatic repair following acute or repeated injury.
Figure 1.3. APAP hepatic metabolism.
Figure 1.4. Histological differences between human and mouse MAFLD/NASH.
Figure 1.5. Structure of AMPK
Figure 1.6. Hierarchical activation of AMPK during increasing nutrient starvation and compartmentalized signaling.
Figure 2.1.T_N housing and WD feeding have select effects in male and female mice.
Figure 2.2. T_N housing and WD feeding do not alter liver enzyme or lipid levels.
Figure 2.3. T_N housing does not exacerbate progression toward NASH beyond that observed with WD feeding.
Figure 2.4. WD feeding changes select hepatic fibrosis transcripts and increases liver macrophage markers of WD-T_N mice.
Supplemental Figure 2.1. T_N housing and WD feeding effects on gut permeability and hepatic fibrosis.
Supplemental Figure 2.2. T_N housing and WD feeding have little effect on liver inflammatory and gluconeogenic transcript expression.
Supplemental Table 2.1. Primer sequences
Figure 3.1. Myeloid AMPK signaling and metformin intervention does not influence hepatic steatosis or circulating lipids.
Figure 3.2. Myeloid AMPK signaling and metformin intervention does not influence hepatic fibrosis or circulating liver enzymes.
Figure 3.3. Myeloid AMPK signaling and metformin intervention do not affect markers of hepatic inflammation.
Supplemental Figure 3.1. CDAHFD does not induce weight loss in male or female mice.
Supplemental Figure 3.2. Myeloid AMPK signaling and metformin intervention does not influence hepatic fibrosis.
Supplemental Figure 3.3. Resident macrophage populations disappear after a CDAHFD.
Supplemental Table 3.1. Primer sequences
Figure 4.1. Hepatocellular and macrophage AMPK do affect AILI.
Figure 4.2. Systemic MK-8722 is not protective against APAP-induced hepatic necrosis.
Figure 4.3. NPs accumulate in hepatic macrophages.
Figure 4.4. NP-MK8722 targeting of KC AMPK does not influence AILI.
Supplemental Figure 4.1. Macrophage AMPK does not influence APAP-induced hepatic necrosis or recovery.
Supplemental Figure 4.2. Empty NPs exhibit no effect in AILI.
Supplemental Figure 4.3. LysM-Cre has no off-target effects on AILI.
Supplemental Figure 4.4. NP-A76 exhibit a more potent and sustained activation of AMPK than free drug.
Supplemental Table 4.1. Flow stain
Supplemental Figure 4.5. Flow cytometry gating strategy for hepatic NPCs, blood leukocytes and hepatocytes.

Table of Contents

Abstract ii
Acknowledgements v
Abbreviations vii
List of Figures and Tables ix
Chapter 1: General Introduction 1
1.1 Liver physiology 1
1.1.1 Function of the liver as a metabolic hub 1
1.1.2 Hierarchical structure of the liver 1
1.1.3 Non-parenchymal populations 2
1.2 Liver injury and inflammation 3
1.2.1 Acute vs. chronic liver injury 3
1.2.2 Acetaminophen overdose 6
1.2.3 Metabolic-dysfunction associated liver disease. 10
1.2.4 Models of Liver Injury 16
1.3 AMP-activated protein kinase 23
1.3.1 AMPK structure and function 23
1.3.2 AMPK signaling and macrophage immunometabolism 30
1.4 AMPK signaling in the liver 34
1.4.1 Disruption of hepatocellular AMPK signaling 34
1.4.2 Activation of hepatocellular AMPK signaling 35
1.4.3 Hepatocellular AMPK signaling during NASH and hepatic fibrosis 37
1.5 Rationale, hypothesis, and objectives 38
Chapter 2: Thermoneutral housing does not accelerate metabolic dysfunction-associated fatty liver disease in male or female C57Bl/6J mice fed a Western diet 42
2.1 Preface 42
2.2 Abstract 43
2.3 Introduction 44
2.4 Materials and Methods 46
2.5 Results 50
2.6 Discussion 53
2.7 Figures 59

2.8 Acknowledgments 65
2.9 Funding 66
Chapter 3: Myeloid AMPK is dispensable for and low-dose metformin does not improve diet-induced NASH in male and female mice 67
3.1 Preface 67
3.2 Abstract 68
3.3 Introduction 68
3.4 Material and Methods 71
3.5 Results 74
3.6 Discussion 76
3.7 Figures 82
3.8 Acknowledgments 87
3.9 Funding 87
Chapter 4: Macrophage and hepatocyte AMPK signaling do not influence acetaminophen-induced liver injury 88
4.1 Preface 88
4.2 Abstract 89
4.3 Introduction 89
4.4 Material and Methods 92
4.5 Results 96
4.6 Discussion 99
4.7 Figures 104
4.8 Acknowledgments 111
4.9 Funding 111
Chapter 5: General Discussion and Future Directions 112
References 120
Appendix 141
Rights and Permissions 141
Metformin again? Atheroprotection mediated by macrophage AMPK and ATF1 145
Curriculum vitae 147

Chapter 1: General Introduction

1.1 Liver physiology

1.1.1 Function of the liver as a metabolic hub

The liver regulates a wide range of physiological processes, from metabolism, immunity, detoxification, and blood volume regulation. The liver maintains systemic glucose homeostasis by storing glycogen during feeding and upregulating gluconeogenesis during fasting. Bile production and lipoprotein synthesis by the liver also allow for excess lipid secretion into the duodenum and storage in adipose tissue, respectively[1,2]. Finally, the liver is the major site for amino acid processing and management of nitrogenous waste through urea metabolism[2].

1.1.2 Hierarchical structure of the liver

The hepatic lobule is defined as the functional unit of the liver (**Figure 1.1**)[3]. Each corner of this hexagonal structure is demarcated by a portal triad composed of the portal vein, hepatic artery, and bile duct[4]. Around the central vein is an array of hepatocytes segmented into three zones[5]. Zonation is defined by the primary hepatocellular function of that zone that is influenced by the proximity to oxygenated blood and nutrients derived from the periportal region[6–9]. Zone I is composed of highly regenerative hepatocytes that perform oxidative processes like fatty acid oxidation (FAO) and gluconeogenesis[5,9,10]. Zone III hepatocytes are pericentral and involved in glycolysis, glycogen production and lipogenesis, while zone II is an intermediate region[11].

1.1.3 Non-parenchymal populations

Hepatocytes and cholangiocytes make up the hepatic parenchyma. However, a significant proportion of the liver is composed of non-parenchymal cells (NPCs)[12]. Like hepatocytes, hepatic stellate cells (HSCs), liver sinusoidal endothelial cells (LSECs) and KCs have an embryological origin and are capable of self-renewal[13]. HSCs are a dynamic population of pericytes that reside in the space of Disse (**Figure 1.1**)[3]. HSCs are responsible for retinol storage in their quiescent state and extracellular matrix remodeling when activated during liver injury[14]. LSECs lack a basement membrane and contain fenestrations that form the permeable lining of hepatic sinusoids[15–17]. KCs are hepatic resident macrophages that occupy the sinusoidal lumen[18](**Figure 1.1**)[3]. KCs recognize and phagocytose inflammatory antigens released into portal circulation but also maintain the tolerogenic nature of the liver in the presence of harmless gut-derived molecules[19–23].

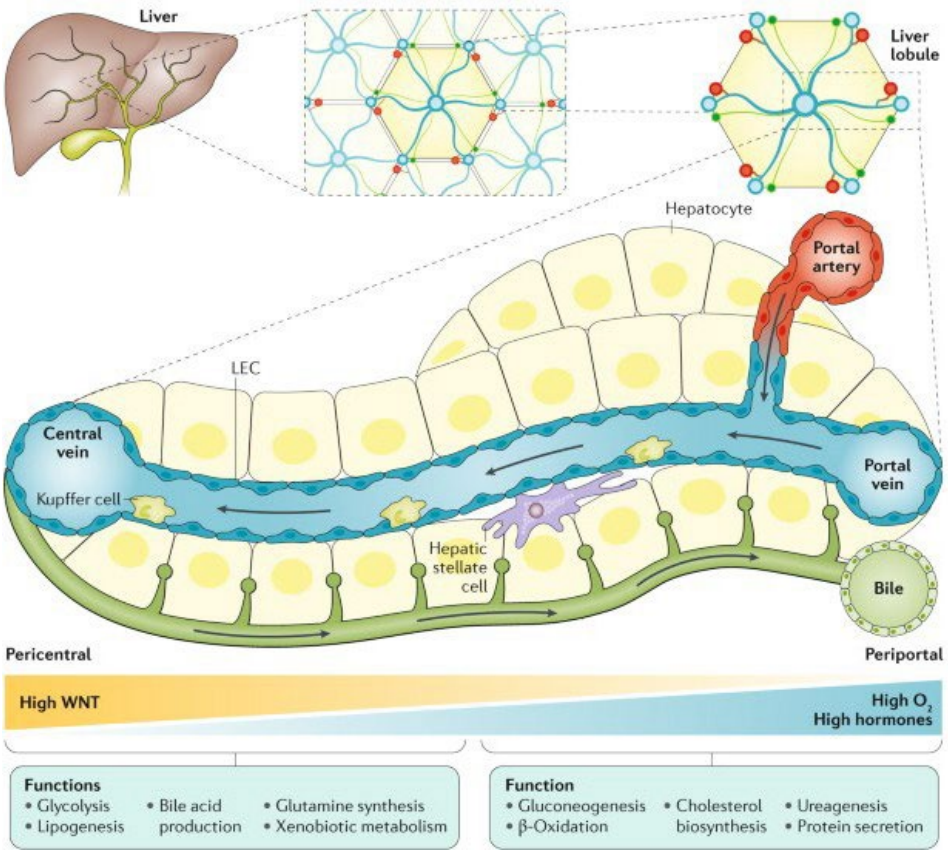

Figure 1.1. The anatomy and zonation of the hepatic lobule. The portal triad consists of the portal artery, portal vein, and bile duct. Bile secreted from hepatocytes flows from the central vein through the bile canaliculi and into the bile duct. Blood rich in nutrients and oxygen runs through the sinusoids and drains into the central vein, creating a spatially defined gradient. This gradient of nutrients and oxygen, in turn, determines the primary function of different hepatocellular zones. NPCs that support liver function are KCs present in the sinusoids, LSECs that make up the sinusoids and HSCs that reside in the space of Disse. *Reproduced image used with permission from Springer Nature from "Spatial heterogeneity in mammalian liver", Ben-Moshe & Itzkovitz (2019)[3]; permission conveyed through Copyright Clearance Center, Inc. under license: 5632791270020.*

1.2 Liver injury and inflammation

1.2.1 Acute vs. chronic liver injury

Acute liver injury is clinically diagnosed by a 2-3 fold increase in circulating liver enzymes such as alanine transaminase (ALT), jaundice and coagulopathy[24]. The most common insults include

drug overdose (APAP), supplements and acute viral hepatitis. Immense hepatocellular death occurs, followed by an intense immune response. In severe cases, injury can cause life-threatening acute liver failure (ALF), requiring an organ transplant[25,26]. Chronic liver injury such as fatty liver disease (alcoholic or metabolic) or viral hepatitis, is characterized by continuous low-grade inflammation and ongoing hepatocellular death[27]. While collagen is an important component of the extracellular matrix, chronic liver injury induces the deposition of excess collagen, known as fibrosis, as a wound-healing response[28,29]. Persistent inflammation can exacerbate fibrosis to the point of cirrhosis or hepatocellular carcinoma (HCC), leading to death by hepatic decompensation or non-hepatic malignancies, respectively[30].

The onset of sterile inflammation (non-viral) induced by acute and chronic liver injury share common mechanisms. Danger-associated molecular patterns (DAMPs) released from dying hepatocytes trigger the activation of KCs via toll-like receptors (TLR). Binding to these pattern recognition receptors results in the assembly and activation of the NOD-like receptor pyrin domain containing 3 (NLRP3) inflammasome for the secretion of interleukin-1 (IL-1β) and IL-18 and induces cell death (pyroptosis)[31]. The release of proinflammatory cytokines initiates the innate immune response to the site of injury by amplifying KC activation. Activated KCs can secrete additional proinflammatory cytokines such as tumour necrosis factor (TNF), which induces hepatocellular apoptosis and production of adhesion molecules (vascular cell adhesion molecule 1; VCAM1) by LSECs. KCs (as well as hepatocytes and HSCs) also recruit circulating monocytes through various chemokines, including chemokine ligand 2 (CCL2), that eventually adhere to the sinusoidal wall through VCAM1. Neutrophils infiltrate the hepatic environment by sensing DAMPs and KC-mediated recruitment (CXCL1, CXCL2 and CXCL8) for the production of

reactive oxygen species (ROS) and reactive nitrogen species as well as proinflammatory cytokines that, in turn, activate KCs[29,32–34].

In contrast, the chronicity of the injury influences the hepatic immune system and crosstalk with the rest of the tissue. Infiltrating proinflammatory monocytes that aggravate the necroinflammatory phase of acute liver injury differentiate in pro-restorative macrophages and aid KCs in the clearance of cell debris and hepatocyte regeneration[35](**Figure 1.2**)[36]. Persistent inflammation observed during chronic liver injury leads to the transdifferentiation of HSCs to fibrogenic myofibroblasts. This activation is mediated directly by hepatic DAMPS and macrophage-dependent signaling, especially profibrogenic mediator transforming growth factor beta (TGFβ)[37–39]. Myofibroblasts upregulate the production of extracellular collagen, smooth muscle actin-α and connective tissue growth factors, including inhibitors of matrix degradation[38]. If the balance between fibrinolysis and fibrogenesis is tipped towards the latter, functional parenchyma is replaced by an extracellular matrix. This marks a turning point in wound healing, where fibrosis is no longer maintaining organ integrity, but the transition to cirrhosis is defined by impaired liver function and a point of no return[36] (**Figure 1.2**)[36].

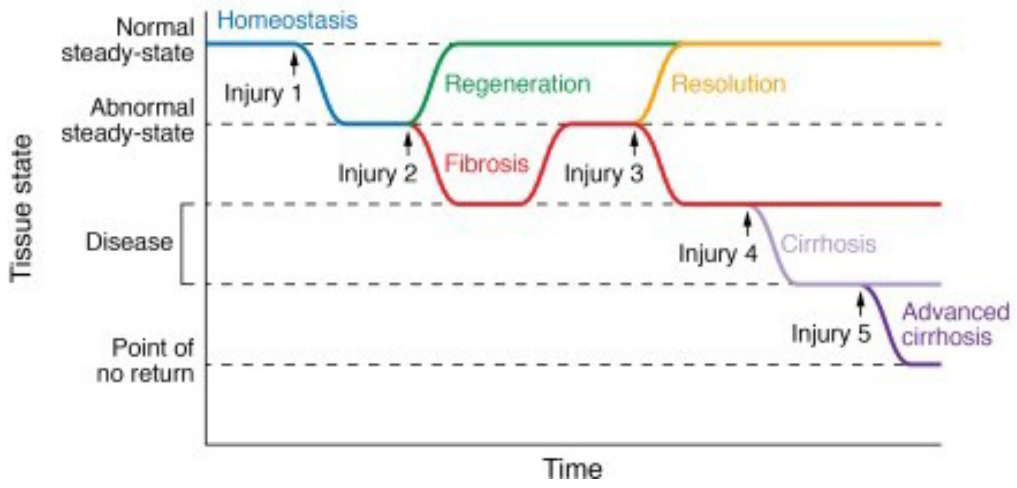

Figure 1.2. The mechanisms of hepatic repair following acute or repeated injury. In response to acute injury, the liver is capable of regenerating, thereby returning to normal steady state. During repeated or chronic injury, fibrosis occurs as a wound-healing mechanism. If the source of damage is removed, then fibrinolysis and injury resolution takes place. Persistent damage, however, may exacerbate fibrosis to the point of cirrhosis, making a recovery highly unlikely. *Adapted image used with permission of American Society for Clinical Investigation from "The balancing act of the liver: tissue regeneration versus fibrosis", Cordero-Espinoza and Huch, 128(1), 2018*[36]*; permission conveyed through Copyright Clearance Center, Inc. under license: 1398453-1.*

1.2.2 Acetaminophen overdose

APAP or N-acetyl-para-aminophenol is a commonly used safe analgesic. However, overdose accounts for almost 50% of ALF cases[40,41]. Especially at risk are individuals with chronic liver disease (acute-on-chronic liver injury), making them susceptible to AILI even at the recommended dosages[42,43].

A large proportion of APAP is metabolized in the liver and converted to non-toxic glucuronosylated or sulfated metabolites as well as excreted in the urine[41,44] (**Figure 1.3**)[41]. Toxicity lies in the conversion of APAP to N-acetyl-p-benzoquinone (NAPQI) by cytochrome P450 (CYP450)[45]. At therapeutic doses, hepatic glutathione (GSH) scavenges NAPQI; however,

excess APAP results in GSH depletion and NAPQI accumulation. The current clinical intervention for AILI is N-acetylcysteine (NAC), a precursor of GSH, aimed to buffer NAPQI-induced toxicity in the face of GSH depletion. While effective early on, NAC requires high doses due to its low bioavailability. This can introduce a series of side effects, including allergic reactions and, in rare cases, death. Moreover, once the therapeutic window of NAC is missed, a liver transplant remains as the only viable treatment plan[46].

NAPQI highly reacts with protein sulfhydryl groups to form APAP adducts. In comparison with its isomer N-acetyl-meta-aminophenol, which does not cause liver injury, it was determined that mitochondrial APAP adducts explain the initial events that ultimately induce hepatic necrosis[47]. NAPQI directly binds and interferes with the function of several mitochondrial proteins. Disruption of the electron transport chain via binding to complex I and II results in the formation of superoxide radicals and blocked ATP synthesis. Superoxides interact with NO to yield peroxynitrite, which accumulates as a result of APAP-induced GSH depletion. Nitration of mitochondrial proteins by peroxynitrite interferes with the antioxidant capacity through proteins like mitochondrial superoxide dismutase 2. Nitrosative stress also leads to c-jun N-terminal kinase (JNK) phosphorylation, which further amplifies oxidative stress. JNK-mediated BCL2 associated-X protein and glycogen synthase kinase-3β translocation results in mitochondrial permeability transition pore opening. Nuclear localization of endonuclease G and apoptosis-inducing factor induces DNA fragmentation and programmed necrosis through receptor-interacting serine-threonine kinase (RIPK) 1 and 3 activation. All these events culminate in the release of hepatic DAMPs[46,48].

As described in section 1.2.1., KCs are activated by various hepatic DAMPS, including high mobility box protein 1 (HMGB1), nuclear DNA fragments, mitochondrial DNA, and ATP. Specifically, during ALF, 51.5% of KCs are activated, representing the main phagocytes during injury onset[49]. Many reports have investigated the protective effects of stimulating KC proliferation and survival in the early stages of AILI[50–52]. On the other hand, liposome or clodronate-mediated depletion of KCs aggravates injury because of the reduction in cytokines like IL-10 that induces hepatocyte regeneration near the site of injury[52,53]. Despite all this promising evidence, other studies have demonstrated the complete opposite effect[54,55].

Neutrophils also become activated in response to hepatic DAMPs and are the first innate immune population to infiltrate the liver and migrate toward the site of injury[56]. In murine models of AILI, neutrophils are most prominent 6- and 24 hours post overdose, followed by a steady decline thereafter[57]. Like the AILI research on KCs, the role of neutrophils in APAP-induced necrosis remains unclear[58,59]. One study reported that antibody-mediated neutrophil depletion or blocking of neutrophil extracellular traps by enzymatic hydrolysis drastically reduced HMGB1 levels and hepatocellular necrosis[60]. Others have also observed a protective effect of neutrophil depletion against AILI. Despite these striking results, several studies have reported that manipulation of neutrophil recruitment and function did not alter APAP-induced injury, and AILI is mainly driven by intracellular signaling in hepatocytes[61]. It is important to note, however, that neutrophils promote ROS-mediated conversion of proinflammatory ($Ly6C^{hi}CX3CR1^{lo}$) monocytes/macrophages to pro-resolving macrophages ($Ly6C^{lo}CX_3CR1^{hi}$) during the recovery phase of AILI (beyond 24 hours), highlighting the dichotomy of ROS during injury and recovery[62].

Circulating $CCR2^{+}Ly6C^{hi}$ monocytes ($CD14^{++}CD16^{-}$ for humans) are also recruited 12-24 hours post overdose and promote injury through the secretion of proinflammatory cytokines and ROS[50,54,63,64]. After 48-72 hours of AILI, these proinflammatory monocytes differentiate into pro-resolving $Ly6C^{lo}$ macrophages, a process facilitated by neutrophils[62,64]. While $Ly6C^{hi}$ monocytes promote neutrophil survival, their pro-resolving descendants are responsible for neutrophil clearance. Importantly, macrophages have a pro-phagocytic phenotype that drives liver repair and hepatocyte regeneration[65,66]. The effects of phagocytosis in the recovery phase of AILI were clearly shown in the persistent injury of mice deficient in a phagocytic receptor Mer tyrosine kinase[67,68].

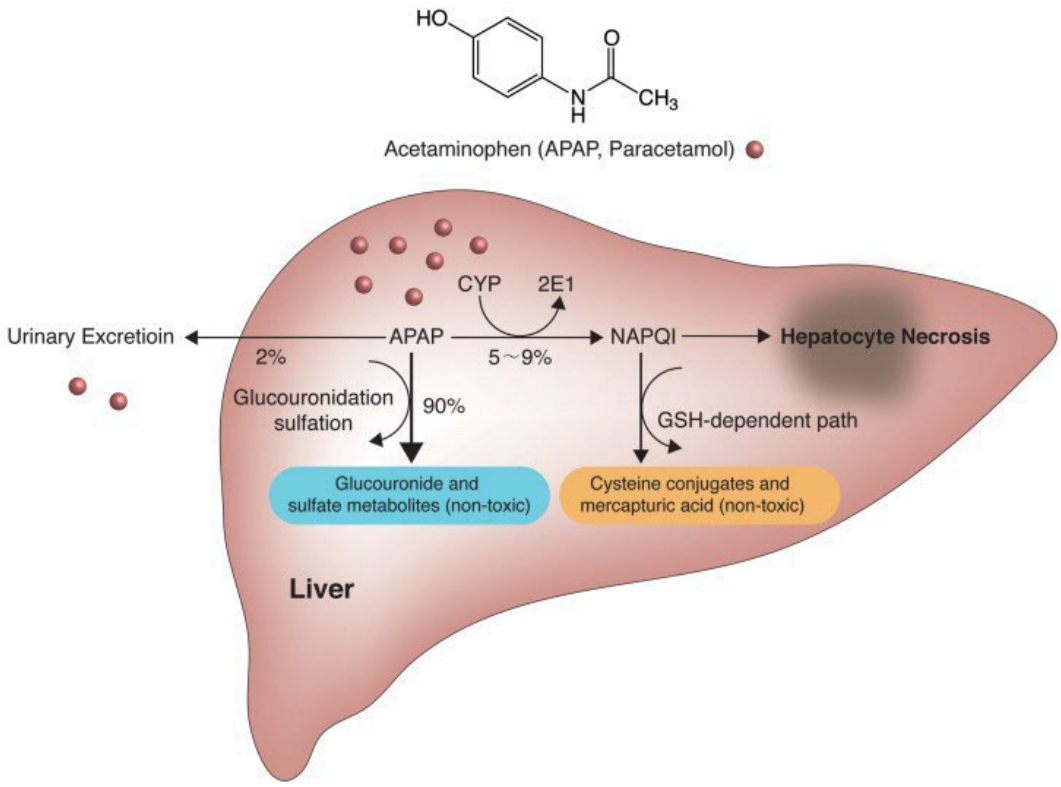

Figure 1.3. APAP hepatic metabolism. Approximately 90% of APAP is metabolized by hepatic glucuronidation and sulfation, with just 2% excretion in the urine. The remaining APAP is metabolized by CYP450 into the toxic metabolite NAPQI. When APAP is taken at therapeutic doses, hepatic GSH can scavenge NAPQI and convert it to non-toxic derivatives (cysteine conjugates and mercapturic acid). During overdose, this process is saturated, resulting in the depletion of GSH and accumulation of NAPQI that drives necrosis. *Reproduced image used is Copyright © 2016 The Second Affiliated Hospital of Chongqing Medical University from "Acetaminophen-Induced Hepatotoxicity: a Comprehensive Update" Yoon et al. (2016)*[41]*; permission conveyed through Creative Commons Attribution-Noncommercial 4.0 Unported License. (Creative Commons — Attribution-NonCommercial 4.0 International — CC BY-NC 4.0)*

1.2.3 Metabolic-dysfunction associated liver disease.

The term non-alcoholic fatty liver disease (NAFLD) was first coined by Ludwig in the 1980s as a fatty liver disease in the absence of alcohol abuse[69]. However, a new nomenclature is being adopted to highlight the positive determinants of the pathology[70,71]. MAFLD is the accumulation of lipids (>5%) in the liver, denoted as simple hepatic steatosis. It is characterized as the hepatic

manifestation of metabolic syndrome, driven by obesity and insulin resistance (IR) and is an independent risk factor for the development of cardiovascular disease[71]. By 2030, it is projected that approximately 30% of the population will be afflicted by this chronic liver disease[72]. While hepatic steatosis is considered benign and reversible, the transition to NASH is pathological[73–75]. The primary histological marker of MAFLD is macrovesicular steatosis, while NASH is also characterized by hepatocellular ballooning and injury, as well as inflammation and the presence of Mallory Denk bodies and apoptotic bodies[76]. NASH can also display varying degrees of fibrosis. The scaling for hepatic fibrosis ranges from F0, histologically defined as no fibrosis, to F4, classified as cirrhosis[77]. While the main causes of death in patients are cardiovascular disease and non-hepatic malignancies stemming from HCC, hepatic decompensation supersedes all causes of NASH-related mortality once cirrhosis is established[30].

Healthy liver lipid metabolism consists of a balance between lipid uptake and synthesis as well as oxidation and secretion and minimal local lipid stores. In the fed state, gut-derived chylomicron remnants are taken up by the liver, and lipids undergo FAO or very low-density lipoprotein (VLDL)-mediated delivery to peripheral tissues. Carbohydrates also promote *de novo* lipogenesis (DNL) through insulin- and glucose-mediated transcriptional upregulation. In the fasted state, adipose tissue immobilizes free fatty acids (FFAs) to the liver through lipolysis. Lipid storage consists of triglycerides (TG) and cholesterol esters (CE) packaged into lipid droplets[78]. As previously mentioned, simple hepatic steatosis occurs when these stores exceed 5% of the tissue. Expansion of adipose tissue during obesity and insulin-resistant adipocytes increase lipolysis and flux of FFAs and glycerol to the liver[75,79,80]. IR also drives hyperinsulinemia and hyperglycemia, which activates liver X receptor (LXR)-mediated upregulation of sterol regulatory element binding

protein (SREBP)1c as well as activation of carbohydrate response element-binding protein, both master transcription factors that promote DNL[81–85]. As a consequence of DNL, FA intermediate malonyl-CoA inhibits carnitine palmitoyltransferase-1, reducing the rate of FAO, which is compounded by FA-induced mitochondrial oxidative stress. Chronic activation of SREBP1c suppresses the expression of the main hepatic insulin signaling molecule, insulin receptor substrate 2, driving hepatic IR and exacerbating steatosis[86–88]. Hepatic IR is worsened by the accumulation of lipotoxic intermediates of TG synthesis, such as diacylglycerol, resulting in the inhibition of insulin-signaling mediators phosphatidylinositol 3 and Akt[37,89]. In addition to the interplay between obesity, IR and hepatic steatosis, high dietary intake of certain FAs (saturated) and carbohydrates themselves contributes to lipid droplets and DNL, respectively[90–92].

The progression of MAFLD to NASH was first described as a two-hit hypothesis where the "first hit" encompasses IR-driven steatosis (MAFLD), and "the second hit" describes the mechanisms that drive hepatocellular death and inflammation (NASH)[93]. Over the past decade, "multi-hit" and "multi-parallel hit" hypotheses have been proposed to capture the complexity and dynamics of the "perfect storm" of NASH, starting with lipotoxicity[94,95]. Lipotoxicity occurs when the influx of FFAs exceeds the liver's ability to convert to neutral lipids[96]. On the same note, individuals that can buffer the accumulation of the lipotoxic species have been speculated to be "good fat storers" able to stave off the development of NASH[97]. Lipotoxic species include FFAs (saturated ex. palmitate), diacylglycerol and ceramides[98]. Free cholesterol (FC) is also a major contributor to NASH development. Accumulation of FC stems from high dietary intake and dysregulated endogenous metabolism. Handling of hepatic cholesterol occurs in various ways: excretion via VLDL or efflux into nascent high-density lipoproteins, excretion through bile and

incorporation into bile acid synthesis, or storage as CE[99]. In human NAFLD livers, decreased expression of ATP-binding cassette sub-family G member 8 (transporter responsible for cholesterol efflux to bile) and increased expression of neutral CE hydrolase (enzyme responsible for CE hydrolysis) have been reported[100]. Several studies have also observed elevated activity of SREBP2, along with increased expression of its cholesterol synthetic gene targets and activity of the rate-limiting enzyme of cholesterol synthesis, 3-hydroxy-3-methylglutaryl coenzyme A reductase (HMGCR)[101]. Despite the elevated activity of SREBP2, expression of the SREBP2 target low-density lipoprotein (LDL) receptor is decreased in human NAFLD, which would indicate decreased LDL uptake[100]. However, an alternative scavenger receptor, CD36, is increased, thereby exacerbating cholesterol uptake via oxidized LDL[102].

The main targets of hepatocellular lipotoxicity are the endoplasmic reticulum (ER) and mitochondria. Cholesterol synthesis occurs at the ER, enzymatically and transcriptionally controlled by proteins such as HMGCR and SREBP2, respectively[103]. Sarco/endoplasmic reticulum Ca^{2+}-ATPase (SERCA) is responsible for the maintenance of ER Ca^{2+} concentrations necessary for proper protein folding. FC accumulation at the ER alters the ratio between FC: phospholipids thereby increasing ER membrane rigidity and impairing SERCA function[104]. As a consequence of Ca^{2+} depletion, unfolded protein response is activated. While unfolded protein response acts as a protective mechanism against ER stress, chronic activation induces the NLRP3 inflammasome and cell death. FFAs, particularly saturated FAs like palmitate and stearate, can also induce ER stress. However, it remains unclear how this occurs[105–107]. In comparison to the ER, mitochondria contain very low levels of cholesterol[108]. Increased flux of cholesterol to mitochondria has been attributed to increased mRNA levels of steroidogenic acute regulatory

protein during NASH[101]. Like at the ER, increased mitochondrial FC increases membrane rigidity, affecting the function of ATP synthase[109–111]. Mitochondrial-reduced GSH is also depleted due to the sensitivity of the 2-oxoglutarate carrier to increased membrane cholesterol. As previously mentioned, depletion of this antioxidant enables the production of mitochondrial ROS[112]. GSH protects against the peroxidation of cardiolipin, a unique mitochondrial phospholipid whose structure controls mitochondrial membrane permeability[108]. FFA overload at the mitochondria also induces oxidative stress due to increased flux through FAO. Electron leakage occurs, and superoxide and hydrogen peroxide formation initiate lipid peroxidation, including the formation of highly reactive aldehydes like 4-hydroxy-2-nonenal[102]. All these events culminate in hepatocellular apoptosis and necrosis via JNK1 activation, resulting in the release of hepatic DAMPs.

As described in section 1.2.1. and 1.2.2., KCs are activated by hepatic DAMPs, including HMGB1. However, extrahepatic signalling is also a potent driver of NASH inflammation. Diets high in fructose alter the gut microbiome, causing dysbiosis and increasing intestinal permeability[90]. This leads to a high influx of gut-derived pathogen-associated molecular patterns like lipopolysaccharide (LPS) that infiltrate the liver and exacerbate inflammation[113]. Moreover, the crosstalk between the liver and adipose tissues amplifies lipolysis, and adipose tissue-derived leptin sensitizes KCs to endotoxins and activates the profibrogenic responses of HSCs[114,115].

As with AILI, neutrophils are some of the first responders to liver injury; however, in chronic low-grade inflammation, neutrophil production of ROS, cytokines and proteases exacerbates the

disease. While neutrophil depletion or disintegration of neutrophil extracellular traps limits inflammation, these effects are lost as NASH progresses[116].

The hepatic macrophage pool is drastically increased during NASH, with studies constantly uncovering the diversity and plasticity of this population under different pathological conditions. Two subsets of KCs have been described in HFD-fed mice – a major fraction of KC1 ($CD206^{lo}$ $ESAM^{-}$) and a minor fraction of KC2 ($CD206^{hi}$ $ESAM^{+}$) that have a higher CD36 expression and is metabolically primed (even at steady state) to manage lipid processing and induce oxidative stress[117]. It has been shown in more aggressive models of NASH that the capacity of self-renewal of KCs in chronic liver injury is impaired, resulting in an immunological void that must be replaced[118]. In models of NASH and experimental depletion of KCs, monocytes differentiate into monocyte-derived KCs (MoKCs) in response to HSC- and LSEC-derived signaling[118–121]. This subset of macrophages localizes to sinusoids to occupy the KC niche and share the same lipotoxicity gene signature as KCs. However, MoKCs do not express embryonic markers like T-cell immunoglobulin and mucin domain containing 4 (TIMD4) surface expression, have higher TG stores and have a more proinflammatory phenotype[118]. Moreover, transcriptional analysis indicates that MoKCs are unable to execute certain KC accessory functions, such as erythrophagocytosis. Recruited temporary macrophages (RTMs) are another subset present during NASH and distinct from KCs. The terms lipid-associated macrophages (LAMs) or scar-associated macrophages (SAMs) were coined to describe this population[122–126]. Characteristic markers include high expression levels of surface receptors such as CD9, Trem2 and Gpnmb, but no expression of embryonic marker TIMD4 or KC-specific markers like CLEC4F or VSIG4. Functionally, these macrophages form hepatic crown-like structures (HCLSs) around fibrotic

regions, a histological feature that distinguishes MAFLD from NASH. Interestingly, NASH-induced transcriptional changes are observed even in the bone marrow[127].

1.2.4 Models of Liver Injury

Preclinical models such as rodents allow for the phenocopying of human health and disease. To counteract disease pathology, mouse models are used to determine the mode of action, safety, and efficacy of therapeutic agents. While there has been a concerted effort for the development of culturing systems such as organoids, mouse models are still superior. Spheroids and liver-on-a-chip are unable to capture the heterogeneity and spatial organization of the liver under different pathological conditions, nor the crosstalk with other organ systems. Moreover, the pharmacodynamics and pharmacokinetics of human therapies can only be approximated when studying a whole multicellular organism[128]. As quoted from George E.P. Box, 'All models are wrong, but some are useful'[129].

Mouse models of acute liver injury are either surgical, pharmacological, or immunogenic. Surgical models are based on reducing or cutting off blood supply (ischemia) or hepatic resection[130,131]. Pharmacological agents typically induce hepatocellular death by depletion, binding, or modification of different molecules. Given the translational application of APAP overdose, it is one of the most common experimental models of acute liver injury. One of the limitations of this model is the susceptibility and, therefore, utility of male over female mice. This is partly explained by the faster recovery of GSH levels and the protective role of estrogen in females[132]. Carbon tetrachloride (CCl_4) is another agent that is commonly used to induce hepatic fibrosis when

administered repeatedly[129]. A single higher dose of CCl_4, on the other hand, induces acute liver injury. Conversion of CCl_4 to a trichloromethyl radical by CYP450, which binds non-specifically to several macromolecules (proteins, lipids, and nucleic acids). The trichloromethyl radical can also be oxidized to create trichloromethylperoxy radical, a molecule responsible for lipid peroxidation[130]. D-galactosamine, an important component of glycoproteins, induces cell death by depleting uridine, a component necessary for RNA and glycogen synthesis. In combination with LPS, D-galactosamine induces a robust immune-mediated liver injury. Finally, immunogenic models include forms of autoimmunity or viral hepatitis, induction of apoptosis (antibody-mediated) or direct immune-mediated injury (LPS)[130].

NASH models are determined by their ability to phenocopy human disease outcomes, unlike AILI, which is defined exclusively by the initial insult. Given the diversity of NASH models, we will exclusively focus on this type of chronic liver injury. Mouse models of NASH are dietary, genetic, or toxin-based, requiring different experimental timelines[129]. While useful and reproducible, these models display a combination of macro- and microsteatosis, unlike human NASH (macrosteatosis only) (**Figure 1.4**)[129]. The WD is a classic diet that closely represents, as appropriately named, the unhealthy dietary regime of Western countries[133]. Despite the various formulations, WD constitutes a high-fat (saturated and unsaturated) and high-carbohydrate diet (fructose, sucrose) with some percentage of cholesterol. This diet induces metabolic syndrome, hepatic steatosis, inflammation, and some degree of fibrosis within a 24+ week timeline[129]. To avoid ketogenesis, fat concentrations are maintained within 40-45%[134]. Fructose, in comparison to glucose, has a greater inflammatory capacity and deleterious effects on the gut microbiome. Moreover, fructose can also be administered in drinking water, given that liquid fructose has been demonstrated to

exacerbate hepatic steatosis and fibrosis[90]. Despite the different formulations of fats and carbohydrates, the amount of cholesterol remains one of the most important considerations. Cholesterol concentrations typically range from 0.1-2%. To overcome the lower absorption and metabolism of cholesterol in mice compared to humans, researchers typically opt for 1-2% cholesterol, a dose that produces hepatic fibrosis within 24+ weeks. For humans, this dietary intake of cholesterol is unrealistic and not reflective of NASH pathogenesis[135]. In contrast, lower doses (0.1%) seldom produce hepatic fibrosis despite this being a supra-physiological concentration for mice[136–138]. To address this issue, toxins (like CCl_4) are used alongside WD-feeding[129].

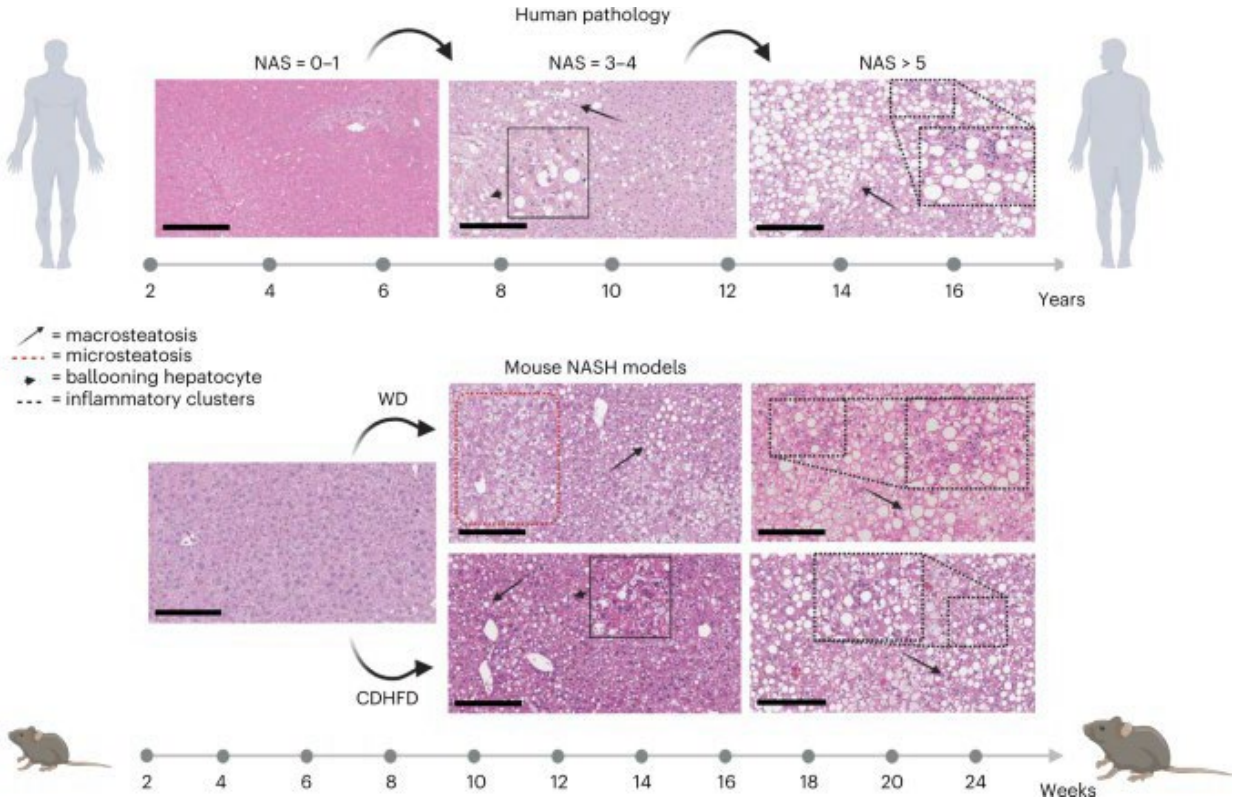

Figure 1.4. Histological differences between human and mouse MAFLD/NASH. While the development of human NASH takes years of unhealthy habits, dietary mouse models like the WD and CDAHFD phenocopy human NASH in a matter of weeks. Human NASH presents histologically with macrosteatosis (black arrow), hepatocellular ballooning (short black arrow) and clusters of inflammatory cells (black dashed areas). Mouse models display all these features, but unlike humans, mice have both microseatosis (red dashed area) and macrosteatosis (black dashed area): H&E-stained liver sections, scale 200 µm. *Reproduced image used with permission from Springer Nature from "A researcher's guide to preclinical mouse NASH models", Gallage et al. (2022)*[129]*; permission conveyed through Copyright Clearance Center, Inc. under license:5632800235222.*

A sharp contrast to the overnutrition of the WD is the choline-deficient dietary models. The methionine-choline deficient (MCD) diet is a reproducible model of NASH that displays hepatic fibrosis within 4-6 weeks[139]. The principal of choline deficiency is the lack of the phosphatidylcholine necessary for VLDL production. While choline deficiency impairs lipid export, methionine deficiency induces adipose lipolysis for hepatic uptake. Finally, choline and methionine are necessary for FAO. While the MCD diet is a robust inducer of hepatic steatosis

and NASH, the dramatic mobilization of FAs from adipose tissue results in dramatic weight loss. In combination with improved insulin sensitivity, MCD represents an intrahepatic model of NASH completely disassociated from metabolic syndrome[140,141]. A less aggressive dietary alternative is the CDAHFD, which has a higher fat content (45%) and sufficient methionine. Supplementation of high-fat results in mild weight gain and IR, and in combination with choline deficiency, NASH is observed after 4 weeks and fibrosis (F2) after 8 weeks[140]. Moreover, Wei *et al*. (2020) found that there was a fat dose dependence in the degree of fibrosis, where 60% fat CDAHFD-feeding of C57BL/6J mice was the most fibrogenic. Interestingly, high-fat supplementation in the MCD diet did not alter the progressive weight loss nor exacerbate fibrosis in fibrosis-prone BALB/cAnNCrl strain[142].

Genetic predisposition is an important factor in the pathogenesis of NASH, such as rs738409 polymorphism in the *patatin-like phospholipase domain-containing protein 3* gene[143]. In the same fashion, modifications in mouse genetics have been utilized to drive NASH pathogenesis. In recent years, a mouse strain derived from an isogenic cross between C57BL/6J and 129S1/Svlm mimics human NASH and metabolic syndrome when fed a 0.1% cholesterol WD with pericellular fibrosis in 16 weeks. This serendipitous discovery termed the diet-induced animal model of NAFLD (DIAMOND); however, it did not exhibit glucose intolerance and spontaneously developed HCC within 12 months of WD-feeding[138]. Moreover, investigation with other transgenic mice presents a serious challenge, given that most genetic modifications are on a pure C57BL/6J background. Another great example of strain influence on NASH is a comparison of substrains of C57BL/6 mice. Whereas the BL/6J stain develops a more pronounced degree of CCl_4-induced oxidative stress and fibrosis, its BL/6N counterpart is more susceptible to high fat-induced liver injury[144].

These phenotypic differences were attributed to the genetic drift that occurred during the generation of either strain. Finally, a genetic model that closely mimics human NASH is the *Foz*/*Foz* mouse. A mutation in the *Alstrom syndrome 1* gene drives a hyperphagic phenotype in this transgenic model that fully displays all features of metabolic syndrome and NASH, including fibrosis after 24 weeks of HFD-feeding with 0.2% cholesterol.

In addition to repeated CCl_4 injections, the STAM model of diabetes-induced NASH is generated by early injections of streptozotocin and pancreatic beta cell toxicity[145]. The STAM model is uncoupled from obesity or type II diabetes. Hepatoxin diethylnitrosamine, in combination with WD, induces NASH and HCC, while incorporation of an HFD fast tracks simple steatosis to liver cancer.

Another variable that is currently being explored is the effects of housing temperature. Barrier facilities, for economic reasons and the comfort of the staff, are typically set to 22-23°C, also referred to as RT. For rodents, RT induces chronic cold stress, which has a myriad of physiological implications. The large surface area: volume ratio of mice makes them vulnerable to minor differences in temperature, resulting in drastic means of thermoregulation. Humans are approximately 3000 times the size of mice, and therefore, thermoregulation is focused on heat dissipation[146]. Mice require mechanisms of heat generation and preservation to counteract increased heat loss. Methods of heat conservation include vasoconstriction, piloerection (muscle contraction causing the fur to erect) and huddling. In addition to heat conservation, the thermic effect of food also contributes to the maintenance of core temperature. When these methods are insufficient, mice expend energy through cold-induced thermogenesis. Cold-induced

thermogenesis accounts for approximately a third of energy expenditure and is classified as either shivering or non-shivering thermogenesis through BAT activation[147]. Because of increased energy demand, chronic cold stress also results in immunosuppression, at least in part due to elevated immunosuppressive corticosterone production. Increased β-adrenergic receptor activity during cold stress suppresses the production of proinflammatory cytokines in myeloid cells, which can have profound effects on NASH-induced chronic low-grade inflammation[148].

Given the implications of cold stress on energy expenditure and immunosuppression, researchers have explored the effect T_N housing has on NASH progression. When ambient temperature falls within the T_N zone, the basal metabolic rate of an organism is sufficient to maintain core temperature[146]. For mice, while this ambient temperature is currently under debate, it falls within a range of 28-30 °C. As previously mentioned, dietary models of hepatic fibrosis require high cholesterol, nutrient deficiency, genetic manipulation, or additional toxins. Overnutrition or "metabolically faithful" dietary models, like 0.1% cholesterol WD or HFD-feeding, seldom produce fibrosis. To address this limitation, Giles *et al.* (2016) housed male and female mice at 30 °C during HFD-feeding[148]. First, in response to LPS challenge, T_N-housed mice had elevated levels of serum TNF (and IL-6), a response that was blunted by exogenous corticosterone. Importantly, when fed an HFD, T_N-housed male C57BL/6J mice had a higher degree of hepatic steatosis and NAFLD severity score, as well as increased gene expression of chemokines (macrophage infiltration) and elevated levels of serum ALT. Although there were no histological indications of hepatic fibrosis, gene expression indicated induction of profibrotic programs. These changes also held for AKR mouse strain that only displayed hepatic fibrosis at 30 °C. Antibiotics and adrenalectomy demonstrated that gut dysbiosis and corticosterone played key roles in the T_N-

driven exacerbation of NAFLD progression. Most importantly, it was determined that T_N housing removed the sex-dependent protection of female mice, an effect that is widely observed across NASH mouse models but not as drastically observed in humans. Since then, we and others have explored the implementation of TN housing across different diets, including the WD and mouse strains[149–152]. Overall, given the relevance of T_N in the daily lives of humans, T_N housing in combination with a 'metabolically faithful' dietary model (0.1-0.2% cholesterol WD-feeding) may serve as a translationally relevant mouse model of NASH-induced hepatic fibrosis.

1.3 AMP-activated protein kinase

1.3.1 AMPK structure and function

In the 1970s, protein phosphorylation was emerging as an important posttranslational modification of enzymatic activity. In line with these observations was the work of KH Kim and David Gibson, who reported the phosphorylation-dependent inhibition of acetyl-CoA carboxylase (ACC) and HMGCR, regulatory enzymes of fatty acid and cholesterol synthesis, respectively[153,154]. Specifically, early studies observed that the HMGCR and ACC kinases were regulated by the "adenylate energy charge", a concept proposed by Daniel Atkinson years prior[155,156]. This concept states that these kinases are allosterically controlled by ratios of [ATP]: [AMP]/[ADP], resulting in the coupling of energy and metabolic homeostasis[157,158]. Throughout a couple of years, AMPK was discovered as the common regulator of both HMGCR and ACC and, in short, is responsible for promoting catabolic pathways while suppressing anabolic ones (details below about murine AMPK signaling, unless stated otherwise)[159,160].

Since the initial purification in 1994, the structure of AMPK has been characterized[161–163]. AMPK is a heterotrimeric complex consisting of an α-catalytic subunit and βγ-regulatory subunits[164–167]. Various isoforms of mammalian AMPK exist, arising from multiple genes (α1/2 and β1/2 isoforms) and gene duplications (γ1/2/3 isoforms). AMPK isoforms have the potential to form 12 unique heterotrimeric complexes, some with empirical evidence of cell-type specificity[168]. The AMPK α1 and α2 subunits (550 residues) share a conserved NH_2-terminal catalytic domain but diverge at the -COOH terminus[169]. This catalytic module consists of an amino-terminal kinase domain (α-KD) followed by the autoinhibitory domain (α-AID) that interacts with α-KD, positioning it in a less active conformation (**Figure 1.5**)[162,170,171]. Immediately following the α-AID is an α-linker connecting the catalytic and regulatory module of the α subunit, the C-terminal domain (α-CTD)[172,173]. At the core of the regulatory module is the β C-terminal region (β-CTR) that cross-links the α-CTD to the γ subunit. The β subunit also exerts regulatory function on the kinase activity via its carbohydrate-binding module (β-CBM), which contains the site for glycogen binding and the allosteric drug and metabolite (ADaM) site, a cleft between β-CBM and N-lobe of the α-KD[174]. AMPK β1 and β2 (270 residues) are highly conserved apart from the first 65 residues of the N-terminus that allow for regulation of kinase activity through myristoylation[169]. Finally, the γ subunits vary greatly in length, only sharing the last 300 residues of the C-terminus that contain 4 cystathione-β-synthase (CBS) repeats. These CBS repeats are arranged in pairs (CBS1:CBS2 and CBS3:CBS4) for binding of adenosine nucleotides. Specifically, while CBS1 is thought to bind to ATP or ADP permanently, the binding AMP to CBS4 enhances the affinity of CBS3 to AMP despite significantly higher levels of ATP and ADP[175–178].

Canonical activation of murine AMPK is centred on the phosphorylation and inhibition of dephosphorylation of threonine-172 (T172) present in the α-KD (T183 in human α1) and AMP-dependent allosteric activation. Liver kinase B1 (LKB1) is an upstream kinase of AMPK, responsible for phosphorylation of T172[179–181]. The key event of regulation occurs when AMP-binding to CBS3 pulls the catalytic and regulatory modules together through interaction with the α-linker, thereby shielding T172 from dephosphorylation by phosphatases like protein phosphatase 2[182]. On the other hand, displacement of AMP by ATP induces a massive rotation of the catalytic module away from the regulatory module[170,183,184]. In addition to dephosphorylation, Akt kinase and protein kinase A phosphorylate serine-186 in rats (serine-496 in humans) of the ST loops (serine/threonine rich sequences) of α-CTD. This phosphorylation event, specific to AMPKα1, inhibits T172 phosphorylation and AMPK activation[183,185,186]. Finally, mammalian target of rapamycin complex 1 (mTORC1) was recently discovered to directly inhibit AMPK via phosphorylation of serine-347 on α1 and serine-345 on α2, resulting in decreased T172 phosphorylation specifically on AMPKα2[187,188].

In 1995, the first AMP/ADP-independent mechanism of AMPK activation was revealed. Ca^{2+}/Calmodulin -dependent serine–threonine protein kinase (CAMKK), specifically CAMKK2, was shown to activate AMPK in a Ca^{2+}-dependent manner[189–192]. In turn, AMPK limits intracellular Ca^{2+} and depletion of ER stores by directly inhibiting stromal interaction molecule 1, an ER Ca^{2+} sensor[193]. Another upstream kinase of AMPK is TGFβ-activated kinase 1, highlighted as an important activator of AMPK during lysosomal damage and TNF-related apoptosis-inducing signaling[194–196]. Finally, the ADaM site is stabilized by autophosphorylation or unc-51-like autophagy-activating like kinase 1 (ULK1)-mediated phosphorylation of serine-108 (S108) on the

β-CBM of the β1 isoform[197,198]. It is the phosphorylation of S108 that sensitizes AMPKβ1 to ADaM site pharmacological activators independent of T172. Moreover, while several compounds have been developed for ADaM allosteric activation[199–201], only recently were CoA esters of long-chain FAs determined to be the natural ligands of this site in β1-containing AMPK heterotrimers[202].

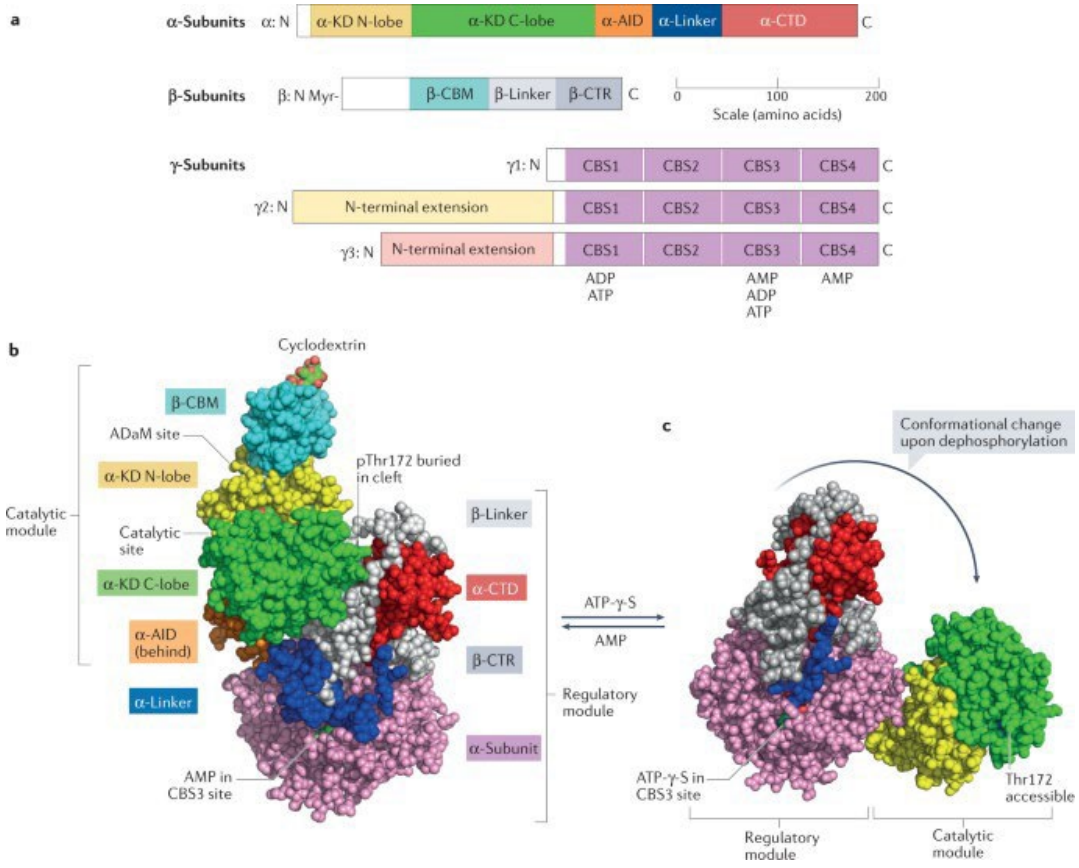

Figure 1.5. Structure of AMPK. A) Domain structures of AMPK α, β and γ subunits. B) Heterotrimeric structure of human α1β2γ1in the active conformation; AMP bound to CBS3 and phosphorylated T172 protected by the interaction between the catalytic and regulatory module. C) Inactive confirmation of AMPK heterotrimer; ATP analogue (ATP-γ-S) bound to CBS3 and T172 accessible for dephosphorylation. 3D structure drawn using Pymol 2.5.2 and PDB file 4RER. *Reproduced image used with permission from Springer Nature from "New insights into activation and function of the AMPK", Steinberg & Hardie (2023)[171]; permission conveyed through Copyright Clearance Center, Inc. under license:5632800512605.*

AMPK activity is also spatially regulated in a manner that is both dependent and independent of cellular AMP/ATP[203]. Zong *et al.* (2019) expanded on previous work that reported on compartmentalization of different pools of AMPK[204]. The yeast orthologue of AMPKα, sucrose non-fermenting 1 protein, had long been recognized as a glucose starvation-activated kinase, and mammalian AMPK was found to be no exception[205,206]. Although AMPK is not capable of directly sensing glucose, it is low levels of the glycolysis intermediate fructose-1,6-bisphosphate (FBP) that ultimately activates AMPK[207]. FBP is a substrate for aldolase, and its absence enables the interaction of aldolase to the v-ATPase-Ragulator complex that then binds to AXIN1-LKB1 at the lysosome. In combination with lysosomal localization of myristoylated AMPK, this complex brings LKB1 and AMPK together, leading to AMPK activation[204]. Conversely, high glucose disrupts the LKB1 complex. While glucose starvation alone can exclusively activate lysosomal AMPK, the degree of energy stress also influences AMPK and LKB1 dependency on AXIN1. During exposure to moderate levels of AMP, cytosolic and lysosomal AMPK still require AXIN1 for association of AMPK and LKB1. However, during severe nutrient starvation, high levels of AMP induce the conformational change in AMPK that allows for phosphorylation of T172 independent of AXIN1. Zong *et al*. (2019) noted that glucose starvation mediated lysosomal AMPK phosphorylation of autophagy-related targets. While moderate AMP levels induce phosphorylation of cytosolic and lysosomal targets (anabolic processes), mitochondrial targets of AMPK were exclusively phosphorylated under high AMP levels (catabolic processes) (**Figure 1.6**)[204]. Interestingly, pharmacological activation of AMPK by biguanide metformin also displays spatial regulation in a dose-dependent manner. For a long time, it has been recognized that metformin activates AMPK by increasing cellular AMP through complex I inhibition. At lower

doses, however, metformin mediates lysosomal activation of AMPK through direct binding to PEN2[208].

Since the identification of AMPK as the common inhibitor of ACC and HMGCR, over 130 phosphorylation sites have been identified across more than 100 downstream targets[171]. The recognition motif derived from variant peptides and proteins known to be phosphorylated by AMPK and used for prediction of novel sites is as follows: at position 0 is the serine or threonine to be phosphorylated; at position -4, -3 and ideally -6 are basic residues and positions -5 and +4 are hydrophobic residues[209–211].

Amongst its most well-known targets are regulators of FA and cholesterol metabolism. As previously stated, AMPK inhibits ACC, to which there are two isoforms, ACC1 (S79) and ACC2 (S212)[212]. As it relates to localization, ACC2 is found at the mitochondria, where the production of malonyl-CoA inhibits FAO through carnitine palmitoyl transferase I. Interestingly, when cellular AMP levels are induced by severe nutrient starvation, AMPK inhibits ACC2, thereby inducing FAO for energy supply. Meanwhile, ACC1 is cytosolic and AMPK-mediated inhibition of ACC1 during glucose starvation impedes further depletion of glucose through incorporation into FA synthesis[204]. Moreover, although AMPK exerts transcriptional control of FA synthesis through direct inhibition of SREBP1c (S372 in humans) and SREBP1c retention through insulin-induced gene 1 (human at T222)[213,214], SREBP1c overexpression demonstrated that ACC1 phosphorylation is the primary mechanism of AMPK-mediated FA synthesis inhibition[215]. Finally, as previously mentioned, AMPK directly phosphorylates HMGCR (S871), the rate-limiting enzyme of cholesterol synthesis, with some indications of SREBP2 targeting as well[213,216].

The dynamics between AMPK and mTORC1 have been described as the yin-yang of metabolism. As previously described, mTORC1 inhibits AMPKα. However, this regulation is bidirectional. AMPK inhibits mTORC1 complex activity by phosphorylation of the Regulator associated protein of mTOR subunit as well as activation upstream regulator tuberous sclerosis complex 2, thereby blocking mTORC1 phosphorylation of ribosomal proteins (S6K1 and 4EBP1)[217,218]. Recently, another AMPK mediator of mTORC1 inhibition was discovered. Inhibition of GAP activity towards Rags 2 by AMPK during glucose starvation and its role in amino acid sensing provides a mechanistic link for mTORC1's ability to sense both nutrients[219]. In addition to AMPK-mTORC1 inhibitory effects on protein synthesis, lysosomal AMPK promotes autophagy through mTORC1 inhibition[220,221]. AMPK also regulates autophagy by inhibiting and stabilizing ULK1 against caspase-mediated degradation. This ensures control over abrupt autophagy during energy stress while maintaining the autophagy components required for cellular homeostasis[222]. Lysosomal biogenesis may also be affected by mTORC1 or AMPK direct phosphorylation and activation of transcription factor E3, a master transcription factor for autophagy and lysosomal activity[223,224]. Mitophagy (autophagy specific for degradation of mitochondria) is also facilitated by AMPK phosphorylation of mitochondrial fission factor[225,226]. In turn, AMPK transcriptionally stimulates mitochondrial biogenesis through peroxisome proliferator-activated receptor gamma coactivator 1-α for the maintenance of mitochondrial function and long-term energy homeostasis[227].

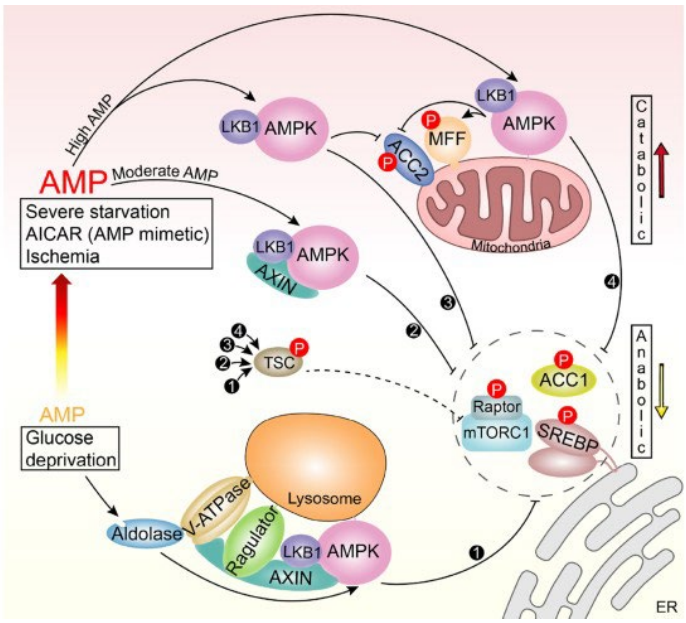

Figure 1.6. Hierarchical activation of AMPK during increasing nutrient starvation and compartmentalized signaling. Glucose deprivation in the presence of sufficient ATP triggers activation of AMPK at the lysosomal through the interaction of LKB1 and AXIN1 (complexed with FBP-sensitive aldolase and other lysosomal proteins). Activation of lysosomal AMPK (1) leads to targeting of lysosomal and cytosolic targets. During moderate AMP levels, cytosolic AMPK (2) is still dependent on AXIN1 for LKB1 activation and downstream phosphorylation of cytosolic targets. Severe starvation results in high AMP levels that allow for LKB1 activation of cytosolic (3) and mitochondrial AMPK (4) independent of AXIN1 and phosphorylation of targets in those compartments. All pools of AMPK (1-4) target TSC2. *Reproduced image used with permission from Springer Nature from "Hierarchical activation of compartmentalized pools of AMPK depends on severity of nutrient or energy stress", Zong et al. (2019)*[204]*; permission conveyed through Copyright Clearance Center, Inc. under license: 5632800837723.*

1.3.2 AMPK signaling and macrophage immunometabolism.

One of the first observations of the connection between inflammation and metabolism was observed by Hotamisligil *et al.* (1993), who reported the production of TNFα in the adipose tissue of obese and diabetic mice[228]. These observations and many since have demonstrated the relationship between metabolic syndrome and inflammation. However, despite the lack of appreciation of its influence on inflammation, the metabolism of macrophages themselves has been

studied as early as the 1960s[229]. Macrophages display unique metabolic signatures that support different polarization and activation states. At the same time, the microenvironment of the tissue where they reside greatly shapes intracellular metabolism. One classic example of metabolic plasticity is the Warburg effect. First described as a driver of oncogenic signaling, the Warburg effect refers to the significant upregulation of aerobic glycolysis[230]. Specifically, aerobic glycolysis supports the energy demand required for macrophage proinflammatory polarization (previously referred to as M1). Although glycolysis lacks the efficiency of the tricarboxylic acid (TCA) cycle, it is a rapid means of ATP production. Conversely, anti-inflammatory or pro-resolving macrophages (previously referred to as M2) display higher rates of OXPHOS[231]. In addition to meeting energy demands, several metabolic intermediates are integrated into inflammatory signaling. After stimulation with proinflammatory mediators, the TCA cycle is disrupted. Two breaks are induced to supply excess citrate and succinate, which support anabolism and inflammation, respectively[232]. At the same time, cis-aconitate is diverted from the TCA cycle for the production of antimicrobial metabolite, itaconate[233–236]. Itaconate, in turn, blocks the activity of succinate dehydrogenase, resulting in the accumulation of succinate and mitochondrial ROS. Overall, these disruptions to the TCA cycle reinforce the reliance on proinflammatory macrophages in glycolysis, while anti-inflammatory macrophages depend on OXPHOS.

Glycolysis also feeds acetyl-CoA into the TCA cycle for downstream FA synthesis. LPS stimulation leads to drastic lipid remodeling alongside an increased synthesis of eicosanoids, sphingolipids, and sterols[237]. On the contrary, anti-inflammatory macrophages use FAO as an energy source; however, whether FAO is vital for polarization is still under debate. Although cholesterol can not be catabolized for the production of ATP, upregulated synthesis of many

intermediate metabolites and cholesterol itself support inflammatory signaling[238]. Interestingly, increased flux through the mevalonate pathway furthers the anti-viral response through ER cholesterol sensing and activation of stimulator of interferon genes and type I interferon response[239]. Cholesterol is an important component of lipid rafts and alters membrane fluidity, thereby modulating the receptor function and downstream signaling[240]. Intermediates like farnesyl pyrophosphate and geranylgeranyl pyrophosphate support protein prenylation and GTPase signaling[241]. Moreover, mevalonate has been implicated in epigenetic reprogramming for trained immunity[242]. Temporally, TLR4-mTOR activates SREBP2, while the cholesterol derivative 25-hydroxycholesterol inhibits SREBP2 nuclear localization and activates LXR-mediated anti-inflammatory response[243]. Recently, it was identified that SCAP-SREBP2 associates with the NLRP3 inflammasome and mediates its activation during SREBP2 translocation from the ER to the Golgi[244]. Finally, SREBP2 perpetuates inflammation during prolonged TNF exposure, thereby inducing not only cholesterol synthesis but also expression of proinflammatory genes[245].

Seminal work of the early 2000s provided strong evidence for the role of AMPK in macrophage immunometabolism. *In vitro* studies showed that deletion of AMPKα1 (macrophages do not express AMPKα2) or expression of dominant negative AMPKα1 (DN-AMPKα1) exacerbates LPS-induced production of proinflammatory cytokines (IL-6, TNF) while suppressing anti-inflammatory signaling (IL-10)[246]. Conversely, stimulation of primary macrophages with IL-10 or TGFβ induces AMPK phosphorylation[246], while LPS and FFA (palmitate, stearate, oleate) suppress AMPK activity[247]. AMPK activation with AICAR or expression of constitutively active AMPKα1 (CA-AMPKα1) suppresses nuclear factor kappa-light-chain-enhancer of activated B cells (NF-κB) activity through the increased deacetylase activity of sirtuin 1. Moreover, the

expression of DN-AMPKα1 increases the degradation of IκB, resulting in the nuclear localization of NF-κB, while AICAR treatment has the opposite effect[248]. AMPK activity has also been implicated in the inhibition of the proinflammatory activity of glycogen synthase kinase β (GSK3-β) through enhancement of Akt phosphorylation, which also relieves GSK3-β-mediated inhibition of cyclic AMP responsive element binding protein for the expression of IL-10[246,249]. The AMPK-mTOR-pS6K pathway reduces protein synthesis of inducible NO synthase and production of NO for proinflammatory response to endotoxic shock as well as chronic inflammation[250]. In addition to AICAR, metformin blunts monocyte-to-macrophage differentiation and proinflammatory cytokine production through signal transducer and activator of transcription 3 inhibition[251]. The effects of metformin were also systematically investigated, and a distinction was made between its effect on acute and chronic LPS exposure. While chronic metformin treatment blocks ROS production, during acute inflammation, metformin dampens not only *Il1b* expression but a select set of LPS-response genes through AMPK signaling[252]. Finally, macrophage AMPK deficiency results in increased expression of enzymes related to itaconate synthesis, amongst several other metabolites[253].

Macrophage AMPK signaling has a wide range of physiological implications, including reducing inflammation during rheumatoid arthritis and sodium-sulphate-induced colitis[254,255]. AMPK signaling mediates glucocorticoid induction of pro-resolving macrophage polarization, where myeloid AMPKα1 deletion impaired skeletal muscle repair and resolution of acute lung inflammation[256]. On the same note, phagocytosis-driven skewing of macrophages from proinflammatory to pro-resolving during muscle regeneration requires myeloid AMPK signaling[257]. In another model of AMPK deletion, bone marrow transplantation of AMPK β1

knockout (KO) cells into wildtype (WT) mice (hematopoietic deletion of AMPK) promotes adipose tissue and liver inflammation during HFD-feeding, as well as increased hepatic macrophage infiltration and IR[258]. During acute liver injury, myeloid AMPK was found to phosphorylate and inhibit RIPK1 activity, thereby reducing inflammation and hepatocellular apoptosis[259]. Finally, primarily attributed to the diversity of mouse models, we and others observed diverging evidence of the importance of myeloid AMPK signaling in atherosclerosis[260–268].

1.4 AMPK signaling in the liver.

1.4.1 Disruption of hepatocellular AMPK signaling

Several studies have modulated hepatocyte AMPK primarily for the investigation of its role in MAFLD. Whole-body KO of AMPKβ1 shows a 90% reduction of hepatic AMPKα1 and α2 activity due to the exclusive expression of β1 in the mouse liver with no compensatory expression of AMPKβ2[269]. This effective KO of hepatocellular AMPK displayed elevated expression of gluconeogenic enzymes as well as increased rates of FA synthesis and reduced FAO in isolated hepatocytes. *In vivo*, HFD-feeding had the opposite effect that was attributed to reduced food intake and circulating levels of IL-6, which drove the improved IR and reduced hepatic steatosis in β1 KO mice[269]. Although this whole body β1 KO mice displayed reduced hepatic steatosis, ACC1 (serine-to-alanine mutation at S79, S79A) and ACC2 (S212A) double knockin (DKI) mice confirmed that disruption of the AMPK-ACC pathway was responsible for the elevated DNL and impaired FAO during NAFLD and exacerbated IR[212]. Regarding the input of AMPK in hepatic cholesterol metabolism, HMGCR KI mice (S871A) fed a high carbohydrate diet displayed dysfunctional hepatic lipid and glucose homeostasis[216]. Specifically, we noted that not only did

HMGCR KI mice have increased flux through the mevalonate pathway, as well as increased hepatic and serum cholesterol, but also elevated TG accumulation. This link between cholesterol and TG metabolism was mechanistically explained by the activation of liver LXRα mediated by oxysterols, which in turn activates SREBP1c[270]. While gain-of-function KI models clearly show the physiological implications of specific AMPK signaling pathways on MAFLD progression, these KI mutations were present in all tissues. Meanwhile, HFD-fed mice harbouring a hepatocyte-specific deletion of AMPKα1 and α2 (AMPK hepDKO) had similar hepatic TG and cholesterol levels and rates of DNL when compared to the Flox control mice[215]. This phenotype is likely due to the downregulation of hepatic AMPK activity as a consequence of lipid accumulation and decreased sirtuin-LKB1 activity[271]. Moreover, compared to ACC DKI, which exhibited hyperglycemia, AMPK hepDKO mice are normoglycemic, even in the inducible KO models (adenovirus-associated delivery of liver-specific Cre recombinase)[201,215].

1.4.2 Activation of hepatocellular AMPK signaling

While models of AMPK signaling (KO and KI models) saw differing responses to overnutrition, the effects of hepatic AMPK activation are relatively consistent. Small molecule agents that allosterically activate AMPK through the ADaM site have shown to be effective, including promise in phase II clinical trials[272]. These compounds robustly reduce serum and hepatic lipid content and synthesis in various MAFLD animal models and primary hepatocytes[200,216,273,274], with some compounds reported to reduce gluconeogenesis and improve glucose tolerance[200,274,275]. Moreover, it was found that despite overexpression of nuclear SREBP1c, small molecule A-769662 reduces DNL and promotes FAO through ACC inhibition, with synergistic effects with

indirect activators AICAR and metformin[215]. On the other hand, metformin alone has been shown to activate AMPK[208,276] and reduce hepatic DNL, gluconeogenesis and IR, while some reports state that the latter effect is independent of LKB1-AMPK[275]. In addition to systemic pharmacological activation, three different liver-specific gain-of-function models of AMPK were developed. First, Woods *et al.* (2017) determined that mutation of aspartic acid residue 316 to alanine (D316A) of γ1 subunit causes complete dissociation of AMP from CBS4[277]. This modification, in turn, shields AMPK from T172 dephosphorylation, resulting in a 7-fold increase in basal activity. Interestingly, the D316A mutation highly protected mice from hepatic steatosis, who, when fed a high-fructose diet, showed similar hepatic TG levels to chow-fed WT mice. In primary hepatocyte culture, this mutation translated to a robust reduction in DNL as well as basal and glucagon-induced glucose output (which was reflected in the expression of gluconeogenic genes). In contrast to pharmacological activators, D316A gain-of-function did not upregulate FAO. First reported in 1998 was a truncated AMPKα1 construct (amino acids 1-312) consisting solely of α-KD, resulting in a significant increase in basal activity[173]. The other two studies generated models for the inducible expression (doxycycline or liver-restricted adenovirus expression) of hepatocyte CA-AMPK (mentioned in section 1.3.2.)[278,279]. Consistent with some of the effects of D316A mutation, liver-specific CA-AMPK activity reduced hepatic steatosis (TG and cholesterol) through increased FAO and reduced DNL in chow and HFD-fed mice. Moreover, doxycycline-induced expression of liver-specific CA-AMPK not only improved glucose homeostasis and reduced hepatic steatosis and adiposity after 8 weeks of HFD but also proved to be beneficial as early as 4 weeks and following 4 weeks of HFD-feeding. Finally, transcriptome analysis revealed that AMPK inhibits HFD-induced liver inflammation and fibrosis.

1.4.3 Hepatocellular AMPK signaling during NASH and hepatic fibrosis.

In comparison to the literature on MAFLD progression, only a handful of studies have assessed the role of AMPK in the context of NASH; regarding the development of hepatic fibrosis, small molecule activators again proved to be protective. Whole liver transcriptome analysis had reduced expression of extracellular matrix genes with PF-06409577 treatment, including those for expression of different types of collagen[273]. In an STAM NASH model, MK-8722 and ACC inhibitor MK-4074 showed reductions in hepatic TG content as well as histological evidence of reduced hepatic fibrosis[280]. Moreover, it was through ACC inhibition that the authors reported a reduction in the profibrogenic cytokine TGFβ. Finally, chronic PXL770 treatment showed dose-dependent protection against different markers of NASH, including hepatocellular ballooning, immune infiltration, and steatosis. Lower expression of profibrogenic genes for expression of proteins such as TGFβ and TIMP1 were also observed, in addition to a dramatic reduction in the levels of hepatic smooth muscle actin-α, a marker of HSC activation[274].

In a recent report utilizing a CDAHFD model of NASH, it was found once again that AMPKα1 and α2 deletion did not influence hepatic steatosis. However, when assessing liver injury and hepatic fibrosis, AMPK hepDKO mice have elevated serum levels of ALT/AST, increased fibrosis, and hepatocellular death. It was found that behind the exacerbated NASH phenotype was the increased cleavage of proapoptotic Caspase-6. Moreover, activation of hepatocellular AMPK with A-769662 was protective against the effects of Caspase-6 cleavage and activation. AMPK motif analysis and *in vitro* kinase assay revealed that AMPKα1 and AMPKα2 directly phosphorylate Caspase-6 at serine 257, thereby inhibiting its pro-apoptotic function[281]. This

hepatocyte-specific phenotype on fibrosis was not observed in a whole-body KO of AMPKα1 and CCl_4-induced hepatic fibrosis. However, activation of AMPK in primary HSC inhibits fibrogenesis *in vitro*[282].

1.5 Rationale, hypothesis, and objectives

Macrophage polarization is characterized by a spectrum ranging from pro-inflammatory to anti-inflammatory phenotypes. Pro-inflammatory macrophages are considered the classical activation state, whereas anti-inflammatory macrophages are regarded as alternative activation, critical for inflammation resolution and wound healing. The high energy demand required for a rapid proinflammatory response is achieved through metabolic reprogramming. Specifically, pro-inflammatory macrophages meet this demand through increased glycolysis, while anti-inflammatory macrophage polarization enhances FAO and OXPHOS. In addition to shifts in mechanisms of ATP production, the pro-inflammatory phenotype requires lipid metabolic reprogramming. FA and cholesterol synthesis are upregulated to supply metabolic intermediates and lipids for membrane remodeling and the production of inflammatory mediators. An important regulator of macrophage metabolic reprogramming is AMPK. AMPK, through its ability to sense high [AMP][ADP]/[ATP] as well as different nutrient levels like glucose, couples energy homeostasis to metabolism. Amongst some of AMPK's best-characterized functions are the suppression of FA and cholesterol synthesis by inhibition of ACC and HMGCR, respectively. AMPK is also a strong promoter of FAO. To date, macrophage AMPK has been implicated in several inflammatory contexts, including atherosclerosis, skeletal muscle regeneration, obesity, and hepatic inflammation driven by HFD-feeding.

Tissue-resident macrophages, called KCs, amongst other hepatic immune cells, are responsible for maintaining immunosuppressive tolerance of harmless antigens derived from the portal vein. In contrast to homeostasis, liver injury instigates acute KC activation in response to DAMPs released from necrotic hepatocytes. While monocytes and neutrophils are more predominant during AILI, different macrophage subsets arise during chronic injury. MAFLD (and progression to NASH) represents a prevalent class of chronic liver injury, expected to affect 30% of adults by 2030. With the advent of new specific markers for different macrophage subsets, there is evidence that KCs may die off, and activated macrophages are derived from recruited monocytes. In the NASH environment, two populations of bone marrow-derived macrophages (BMDMs) arise, RTMs and MoKCs. In a recent report of a mouse model of NASH, RTMs were further characterized as LAMs, which occupy fibrotic regions of the hepatic lobule and form HCLSs. While recent studies have revealed the heterogeneity of hepatic macrophage populations, there are many unanswered questions regarding the metabolic reprogramming that drives inflammation and whether these processes are influenced by AMPK signaling.

Regarding hepatocyte metabolism, AMPK has been demonstrated to have a protective effect against MAFLD in various genetic models. Recently, this protective effect has been extended to NASH-induced hepatocellular death through direct inhibition of Caspase 6. Given the therapeutic potential of AMPK in various tissues, there has been a concerted effort for the development and repurposing of a wide range of pharmacological activators. Metformin, best known for its antidiabetic effects, is effective at reducing hepatic steatosis in HFD-fed mice via activation of AMPK. A synthetic direct activator of AMPK, A-769662, reduced hepatic necrosis in AILI and hepatic steatosis in MAFLD. Although these studies represent a small percentage of those

demonstrating the effects of AMPK activation, there is still much to be explored. Interesting avenues include the effects of pharmacological activation during more advanced stages of chronic liver injury, such as NASH-induced hepatic fibrosis. Moreover, considering the complexity of the hepatic environment under different types of injury, targeting specific hepatic populations such as macrophages warrants investigation.

While AILI is a robust, reproducible, and directly translational model of acute injury, models of NASH-induced hepatic fibrosis rely on nutrient-deficient diets like the CDAHFD and genetic manipulation that drives the obesity phenotype observed in *ob/ob* mice. Despite the utility of these models, they seldom mirror the pathogenesis of human NASH, with diets like CDAHFD being completely dissociated from metabolic syndrome. Moreover, these models are required to address the divergence between male and female mice. In recent years, there has been a shift towards addressing other variables that drive inflammation and metabolism. At RT (22 °C) of barrier facilities, mice experience cold stress that alters various biological functions. Cold stress drives BAT activation and upregulates corticosterone production and immunosuppression, all processes that blunt NASH progression. Giles *et al.* (2016) demonstrated that housing mice at T_N (30 °C) exacerbated MAFLD progression toward NASH in both male and female mice.

Given the implication of cold stress-induced corticosterone signaling of energy expenditure and inflammation, we **hypothesized** that TN housing could accelerate NASH progression toward hepatic fibrosis.

We addressed this hypothesis with the following aim.

Chapter 2. Determine the effects of T_N-housing on NASH progression of male and female mice at 0.2% WD for 16 weeks.

Publication title: Thermoneutral housing does not accelerate metabolic dysfunction-associated fatty liver disease in male or female C57Bl/6J mice fed a Western diet.

Given the importance of AMPK in macrophage immunometabolism and the effects of hepatic activation on liver injury, we **hypothesized** that macrophage AMPK signaling would be protective against chronic and acute liver injury. We addressed this hypothesis with the following aims.

Chapter 3. Determine the importance of macrophage AMPK in CDAHFD-fed male and female mice.

Running title: Myeloid AMPK signaling is dispensable for, and low-dose metformin does not improve diet-induced NASH in male and female mice.

Chapter 4. Determine the importance of hepatic AMPK in APAP-induced necrosis and inflammation.

Running title: Macrophage and hepatocyte AMPK signaling do not influence acetaminophen-induced liver injury.

Chapter 2: Thermoneutral housing does not accelerate metabolic dysfunction-associated fatty liver disease in male or female C57Bl/6J mice fed a Western diet

2.1 Preface: This chapter has been published as a research article[149].

Julia R.C. Nunes[1,2], Tyler K.T. Smith[1,2], Peyman Ghorbani[1,2], Conor O'Dwyer[1,2], Natasha A. Trzaskalski[1,4], Habiba Dergham[1], Ciara Pember[1,2], Marisa K. Kilgour[1,2], Erin E. Mulvihill[1,2,4], Morgan D. Fullerton* [1,2,3] (2023). Thermoneutral housing does not accelerate metabolic dysfunction-associated fatty liver disease in male or female C57Bl/6J mice fed a Western diet. Am J Physiol Endocrinol Metab 325: E10–E20, 2023. doi:10.1152/ajpendo.00124.2023.

Copyright©2023 the American Physiological Society.

[1] Department of Biochemistry, Microbiology and Immunology, Faculty of Medicine, University of Ottawa, Ottawa, ON, K1H 8M5, Canada

[2] University of Ottawa Centre for Infection, Immunity and Inflammation, Ottawa ON K1N 6N5, Canada

[3] University of Ottawa Centre for Catalysis Research and Innovation, Ottawa ON K1N 6N5, Canada

[4] University of Ottawa Heart Institute, Ottawa, ON K1Y 4W7, Canada

Contributions

Author Contributions: J.R.C.N., T.K.T.S., P.G., C.O., N.A.T., H.D., C.P. and M.K.K. performed the experiments and testing. E.E.M. and M.D.F. provided funding. J.R.C.N. and M.D.F. wrote the

manuscript. All authors edited the manuscript and provided comments. M.D.F. is the guarantor of this work and, as such, has full access to all the data in the study and takes responsibility for the integrity of the data and the accuracy of the analysis.

2.2 Abstract

MAFLD represents a growing cause of mortality and morbidity and encompasses a spectrum of liver pathologies. While dozens of preclinical models have been developed to recapitulate stages of MAFLD, few achieve fibrosis using an experimental design that mimics human pathogenesis. We sought to clarify whether the combination of T_N housing and consumption of a classical WD would accelerate the onset and progression of MAFLD. Male and female C57Bl/6J mice were fed a nutrient-matched low-fat control or WD for 16 weeks. Mice were housed with littermates at either standard temperature (T_S; 22 °C) or T_N-like conditions (T_N; ~29 °C). Male but not female mice housed at T_N and fed a WD were significantly heavier than T_S-housed control animals. WD-fed mice housed under T_N conditions had lower levels of circulating glucose compared to T_S mice; however, there were select but minimal differences in other circulating markers. While WD-fed T_N males had higher liver enzymes and higher liver TG levels, no differences in markers of liver injury or hepatic lipid accumulation were observed in females. Housing temperature had little effect on histopathological scoring of MAFLD progression in males; however, while female mice retained a level of protection, WD-T_N conditions trended toward a worsened hepatic phenotype, which was associated with higher macrophage transcript expression and content. Our results indicate that interventions coupling T_N housing and WD-induced MAFLD should be longer than 16 weeks to accelerate hepatic steatosis and increase inflammation in both sexes of mice.

News and Noteworthy

Mouse models leading to accelerated fatty liver onset will be a useful translational tool. Here, we show that coupling T_N-like housing and WD feeding in mice for 16 weeks does not lead to significant disease progression in either sex. However, the molecular phenotype indicates priming of immune-related and fibrotic pathways.

2.3 Introduction

MAFLD[71] is the hepatic manifestation of obesity and metabolic syndrome. MAFLD is one of the largest global causes of chronic liver disease (with an unsettlingly high prevalence in children[286–288]) and is expected to affect over a third of adults by 2030[72]. MAFLD encompasses a continuum of liver pathologies that begins with benign steatosis in hepatocytes. In certain at-risk individuals, lipotoxic species can accumulate, leading to the onset of inflammation (NASH) and fibrosis. Severe cases of NASH lead to hepatic cirrhosis or HCC[289–291]. Despite the identification of metabolic, fibrotic and inflammatory pathways for therapeutic targeting, there are currently no approved drugs to treat or halt the progression of NASH, although clinical trials are ongoing[292]. Currently, only the early stages of benign steatosis are considered reversible with lifestyle changes and weight loss.

Critical to the effort to combat this chronic liver condition are the preclinical models used to interrogate potential targets. Rodent models of MAFLD typically involve dietary intervention and/or genetic manipulation[129,284,285]. Dietary models include deficiency of choline and methionine, first introduced in the 1930s, and excess dietary fat being one of the most consistently altered components[293]. Genetic alterations consist of various naturally occurring human disease

variants or mutations that alter metabolism, such as leptin receptor mutations in obesogenic *ob/ob* mice. While these models achieve the phenotype of various MAFLD stages, the mechanisms by which the NASH-induced fibrosis is achieved are not always translationally relevant[294].

While diet and genetics have been at the forefront of controllable variables in mouse models, housing temperature has presented a new consideration. Conventional housing at 21-22°C induces cold stress in mice, unlike the human population who, when clothed, are comfortable within this range[295]. This results in immunosuppression and BAT-mediated thermogenesis in mice, two mechanisms that highly blunt NASH progression[296]. In recent years, numerous groups have highlighted the impact of housing temperature on different disease contexts. The progression toward fatty liver disease was exacerbated in HFD-fed male and female mice housed at 30°C[148] and C57Bl/6 mice fed a typical WD developed hypercholesterolemia and early atherosclerosis, although markers of fatty liver were not described[297]. Mice housed at ~30°C or T_N-like conditions, accumulated more fat mass due to lower BAT-mediated energy expenditure. Further, lower levels of corticosterone, an immunosuppressive stress hormone, exacerbated hepatic inflammation. Lastly, since female mice are more resistant to NASH development, the exacerbated phenotype observed at T_N-like conditions highlights the importance of housing temperature[148]. This potential paradigm shift presents an opportunity to investigate key drivers of fatty liver progression that could better mimic human pathophysiology but also calls into question whether past mechanistic insights hold true.

Mice fed a WD high in fat, sucrose and supplemented with a high dose of cholesterol, progress toward NASH after long periods (greater than 24 weeks)[298–300]. Accelerating this progression

usually requires the addition of supraphysiological concentrations of cholesterol (>0.2%), fructose and/or extreme dietary, chemical, or genetic manipulations (i.e., choline/methionine-deficient diets, CCl_4 injections or various genetic models) to achieve hepatic fibrosis[294,301]. Here, we sought to address whether feeding a WD high in fat, sucrose, and 0.2% cholesterol in conjunction with T_N housing could accelerate the progression toward NASH-induced fibrosis in C57Bl/6J male and female mice. While both sexes gained significantly more weight when fed a WD, only male mice housed under T_N conditions gained significantly more weight compared to those at ambient RT (T_S). There were select differences in the hepatic lipid levels and markers of hepatic injury in male mice, and we observed an increase in the expression of certain macrophage and extracellular related transcripts in both sexes. However, no histological differences in hepatic steatosis, collagen deposition or overall pathological scoring were seen between WD-fed T_N and T_S mice. Finally, sex-specific and sex-independent effects were observed on markers of glucose homeostasis and insulin tolerance.

2.4 Materials and Methods

Mice: C57Bl/6J mice were obtained from Jackson Laboratory (000664) and bred at the University of Ottawa for 6 generations prior to the initiation of this study, while housed at 22 °C. Male and female mice (12-15 weeks old) were acclimated for 2 weeks at either 22°C or 29°C in static cages. Mice were co-housed with littermates in groups of 2-5 mice. Once acclimated, mice were fed a 0.2% cholesterol high fat (41% Kcal) WD (Research diets – D12079B) or a macronutrient-matched low-fat (10% Kcal) control diet (Research diets – D14020502) for 16 weeks. Mice were fasted for 4 hours prior to the tissue harvest, where the food was removed at the beginning of the

light cycle. All animal protocols were approved by the uOttawa Animal Care Committee (BMIe3744).

Non-terminal parameters: During week 15 of dietary intervention, mice underwent the following noninvasive procedures. Body composition was determined by ECHO MRI prior to the intraperitoneal glucose tolerance test (GTT). For the GTT, food was removed at 7 am and 4 h-fasted mice were injected with D-glucose (1.5 mg/kg *i.p.,* made up in saline). For the insulin tolerance tests (ITT), food was removed at 7 am and 4 h-fasted mice were injected with insulin (0.8 U/kg *i.p*., made up in saline; NovoRapid ®). Glucometer measurements for both tests were taken at baseline, 20-, 40-, 60-, 90- and 120 minutes post-injection. The above-mentioned tests were performed at 22°C to avoid the acute effects of temperature on glucose clearance[302]. GTT and ITT were performed two days apart. For determination of intestinal permeability, mice were fasted for 6 hours, starting at 7 am, followed by oral gavage of 150 µL of 80 mg/mL FITC-dextran (Sigma, 4 kDa). Blood was collected via tail vein at baseline and 1-hour post-gavage. Serum was collected via centrifugation, and fluorescence was measured by spectrophotometry (excitation 485 nM, emission 530 nM). Baseline serum readings were subtracted from 1-hour serum readings of each biological replicate. All samples were carefully protected from light.

Serum and liver biochemical analysis: Terminal blood was collected via cardiac puncture of the left ventricle and placed on ice. Once clotted, serum was collected by centrifugation. Circulating insulin was determined by ELISA (Mouse High-sensitive Plus Mouse Insulin ELISA Kit (#32393)– Toronto BioScience Inc). Serum ALT, AST, ALP, TG, cholesterol, LDL and HDL were measured using the Beckman Coulter AU480 clinical chemistry analyzer in combination with

appropriate reagents, calibrators and quality control materials. These readouts were performed by the Pathology core at the Toronto Centre for Phenogenomics. Liver was snap frozen in liquid nitrogen and chipped on dry ice for Bligh and Dyer lipid extraction[303] and BCA protein quantification. Total liver cholesterol and TG were determined with colorimetric assay kits (L-Type TG M – Fujifilm Wako, Infinity Cholesterol Liquid Stable Reagent – Thermo Fisher) and normalized to total protein content.

Transcript expression: Liver was snap-frozen in liquid nitrogen and chipped on dry ice. Frozen livers were homogenized in TriPure Isolation Reagent. Once equalized, RNA samples underwent reverse transcription (All-in-one RT Master Mix – ABM). qPCR was performed with BrightGreen Express reagent (ABM) and ran on the CFX384 Real-Time PCR system for 40 cycles. Relative transcript expression was calculated using the delta-delta Ct method[304], where genes of interest were normalized against the average Ct values of both Actb and Tbp, and shown relative to liver samples from male mice housed at T_S and fed a WD. Primer sequences can be found in **Table S1.1**.

Histology: Following cardiac perfusion, liver tissue was fixed in 30 mL of 10% neutral buffered formalin. After 24 hours of fixation, samples were placed in 70% ethanol and sent for processing at the University of Ottawa Louis Pelletier Histology Core Facility. Samples were paraffin-embedded, microtome sectioned and stained with H&E, Masson's Trichrome and Picrosirius red. Slides were scanned at 20X magnification on the Axio Scan Z1 Slide Scanner. NAFLD score was qualitatively and blindly determined from H&E-stained whole-section slides by a third-party pathologist. The micro- and macrovesicular steatosis area was quantified with ImageJ by

converting an ROI into a binary image followed by Watershed separation of lipid droplets. Particles were analyzed and vascular regions were excluded by circularity or manually. The cutoff between the two droplet sizes was $17.1e^3$ μm^2. Picrosirius red quantification was quantified from ROIs selected from the whole section slides using a trained pixel classifier on QuPath. From each section, 2-4 ROIs were selected to exclude large vascular regions that would skew the quantification.

Immunofluorescence: Paraffin-embedded sections were deparaffinized using a Leica ST5010 Autostainer XL, followed by heat-induced epitope retrieval with citric acid (pH 6.0). After blocking with donkey serum, slides were stained with F4/80 (1:75, Thermo Fisher – MA1-91124) and CLEC4F (1:200, R&D Systems– AF2784) overnight at 4˚C. The next day, sections were stained with secondary antibodies donkey anti-rat IgG Alexa Fluor Plus 647 (1:500, Thermo Fisher – A48272) and donkey anti-goat IgG Alexa Fluor 555 (1:500, Thermo Fisher – A21432) for 45 minutes at RT. Finally, sections were stained with DAPI (1:2000, Thermo Fisher – 62248) and mounted with Anti-Fade Fluorescence Mounting Medium (Abcam – ab104135). Once cured, the images were acquired on a Zeiss AxioImager Z1 epifluorescence microscope with a 20× or 63× oil immersion objective. For macrophage content quantification, QuPath was used to detect cells with an $F4/80^+$ stain at 20× magnification.

Statistics: GraphPad Prism software was used for all statistical analyses. Two-way ANOVA was performed to compare between CD- and WD-fed mice housed under T_N or T_S conditions, where a Šídák multiple comparisons test was performed to determine significant differences between house temperature/within dietary treatment (Figures 1, 2, 3 and S1), and between housing

temperature/within sex (Figure 4 and S2), except comparisons in figure 1A/B, O/P and Q/P, for which a repeated measures Two-way ANOVA was used with a Tukey's multiple comparisons test. Statistical outliers were identified in Figure 2E, Figure 4B and Figure S2A-B by the ROUT method with a Q value of 1% and are identified where applicable in the figure legends where each value represents the number of outliers identified and removed in the order of groups as they appear in the particular figure.

2.5 Results

T_N housing and WD feeding affect body weight, glucose tolerance and insulin sensitivity differently in male and female mice. To evaluate the effectiveness of T_N housing on the progression of MAFLD, we used male and female C57Bl/6J mice and began WD or control diet (CD) feeding at ~12 weeks of age. We acclimated T_N-housed mice for 2 weeks prior to initiating the diet. Over the course of the 16-week intervention, WD-T_N males gained significantly more weight compared to their WD-T_S counterparts (**Figure 2.1A**). No differences were observed in males fed a CD at either housing temperature. Moreover, there were no differences in the percentage of lean or fat mass between WD-fed groups. No changes between housing temperature were observed in females with respect to weight gain or percentage lean and fat mass (**Figure 2.1B**). Following 16 weeks of dietary intervention, 4 h-fasted blood glucose levels were consistently higher in WD-fed male and female mice compared to CD. Interestingly, when observing the effects of housing temperature in WD-fed mice, blood glucose levels were lower in male and female mice kept at T_N (**Figure 2.1C and F**). Basal insulin levels were higher with WD feeding compared to CD, and there were no significant temperature-dependent differences between any of the groups in either sex (**Figure 2.1D and G**). While similar patterns were observed with circulating levels of TG, total cholesterol

and HDL-cholesterol, LDL-cholesterol was significantly higher in WD-T_N females (**Figure 2.1E and 2.1H-N**). Finally, due to the important role of the gut microbiome in MAFLD pathology, we assessed intestinal permeability to interrogate whether there may be increased hepatic exposure to pro-inflammatory intestinal microbial products. There were no differences between WD-fed mice housed at T_S or T_N conditions in circulating levels of a fluorescently conjugated dextran substrate that was delivered via oral gavage (**Figure S2.1A**).

To assess the physiological response to glucose, we performed an intraperitoneal glucose and insulin tolerance test after 15 weeks of CD or WD feeding. No temperature-dependent differences were observed in CD-fed mice. However, male but not female WD-T_N mice appeared significantly more glucose tolerant compared to their T_S counterparts (**Figure 2.1O and 2.1P**). There were no differences in insulin sensitivity between housing temperatures in either CD or WD-fed mice (**Figure 2.1Q and 2.1R**).

Circulating liver enzymes and lipids are elevated in WD-T_N males. The induction of hepatic steatosis and progression along the continuum to a NASH-like phenotype is typically associated with a decrease in liver function. As a proxy measure of liver injury, we determined the circulating levels of ALT, aspartate transaminase (AST), alkaline phosphatase (ALP) and total bilirubin (TBIL). As expected, WD feeding raised ALT, AST and ALP levels and simultaneously reduced TBIL. Both ALT and AST levels were significantly elevated in WD-T_N males, with no other differences in circulating markers when compared to WD-T_S mice (**Figure 2.2A-B**). The weight of the liver, both absolute and relative to body weight, was higher in WD-fed mice relative to CD, independent of housing condition (**Figure 2.2C**). Similar results were observed in female mice,

though to a lesser extent (**Figure 2.2D**). Total liver TG but not total cholesterol was increased in WD-T_N males (**Figure 2.2E**), and there were no differences in female levels (**Figure 2.2E and F**).

T_N housing and WD feeding do not render mice more susceptible to NASH progression, independent of sex. We next sought to qualitatively score the level of steatosis, hepatic ballooning, inflammation, and fibrosis as indicators of the progression toward NASH. Blinded assessment of H&E-stained histological sections showed that WD-fed male mice had significantly worsened progression toward NASH; however, contrary to our hypothesis and despite WD-T_N males gaining more weight, this was independent of housing temperature (**Figure 2.3A, B and S2.1B**). Moreover, female WD-T_N mice remained protected from NASH induction compared to males (**Figure 2.3**), though compared to WD-T_S, female WD-T_N mice tended to have higher NAFLD activity scores (**Figure 2.3B**). There were also no differences in the frequency of micro- or macrovesicular steatosis between WD-fed groups (**Figure 2.3C**). To assess the development of fibrosis, Masson's trichrome and Picrosirius red staining revealed minimal collagen staining beyond the vascular regions in any of the WD-fed mice (**Figures 2.3D-E and S2.1C).**

T_N housing and WD feeding increase macrophage markers in the liver. To further validate and characterize the effect of WD feeding under different housing conditions, we determined the relative transcript levels of fibrotic, macrophage, cytokine and chemokine markers in the livers of male and female mice. Male, but not female, WD-T_N livers had significantly higher levels of *Col3a1* transcript compared to WD-T_S mice. However, no significant differences in *Col1a1* or *Col1a2* were observed. Female, but not male, WD-T_N livers had significantly higher levels of *Acta2* and *Timp1* transcript compared to WD-T_S mice (**Figure 2.4A**). There were no differences

in the transcript levels of cytokine or chemokine markers (**Figure S2.2A**). WD-T_N females had significantly increased levels of *Emr1* and *Cd9* transcript; however, there were no differences in the expression of other LAMs subset markers [122,124,126] (*Trem2*, *Gpnmb*) (**Figure 2.4B).** In keeping with this, we determined that there was a trend toward increased macrophage content in the livers of WD-T_N mice detected by F4/80$^+$ staining (**Figure 2.4C and D**), with no difference in HCLSs but an increased macrophage aggregates in female WD-T_N livers (**Figure 2.4E-G**). Finally, to follow up on the temperature-dependent differences in glucose metabolism, we observed no change in the expression of genes involved in gluconeogenesis (*Pepck, G6pc, Pgc1a*) (**Figure S2.2B**).

2.6 Discussion

Preclinical models have provided the foundation upon which much of our mechanistic understanding of fatty liver progression rests. Given the vast number of genetic and dietary/environmental instigators in mice, we sought to couple WD feeding with T_N housing conditions to potentially accelerate the onset and increase female susceptibility to diet-induced NASH. Contrary to our initial hypothesis, when C57Bl/6J mice were housed at T_N conditions and fed a WD for 16 weeks, there were only select differences in markers of NASH-induced fibrosis progression or severity in either sex. Moreover, while female mice remained mainly protected against diet-induced hepatic dysfunction, we observed partial susceptibility in females.

When exposed to a diet high in fat (60% kcal from fat) and housed at T_N, singly housed mice of both sexes experienced a significant induction of immune-mediated hepatic dysfunction[148]. This high-fat condition led to an increase in intestinal permeability and a microbe/TLR4/Th17-

dependent response in male C57Bl/6 mice, independent of changes in body weight or adiposity. In our study, male mice housed under T_N conditions and fed a WD were heavier than those housed at T_S, which is consistent with previous reports using a similar T_N-WD protocol[297]. Despite this, there were no changes in intestinal permeability or markers of hepatic inflammation. In comparison to CD-fed male mice, WD-feeding augmented the transcript levels of markers of inflammation; however, there were no changes due to housing temperature. Given the vast permutations of experimental conditions in the literature, it is extremely difficult to compare between studies. Recently, a NASH diet containing 40% kcal fat, 20% fructose and 0.02% cholesterol was coupled with T_N-like housing for 24 weeks to induce fibrosis[152]. Prior to this, many studies had used various dietary combinations containing high levels of fat and sugar (either as sucrose or fructose) and up to 2% cholesterol for up to 1 year[138,301,302,305–307]. To our knowledge, the most similar design that used a WD at 30°C, which included 0.3% cholesterol as compared to 0.2% in our study, demonstrated increased susceptibility of male C57Bl/6J mice to atherosclerosis following 24 weeks of diet[297]. Given that these mice are normally resistant to the initiation and progression of atherogenesis, these observations were attributed to increased inflammatory tone and elevated circulating cholesterol levels. No specific indicators of NASH progression were included.

There is a critical need to understand potential differences between how male and female mice progress toward fatty liver and NASH. While it is well known that female C57Bl/6 mice are more resistant to many of the effects of diet-induced obesity[308–310], we sought to directly compare the responses of male and female mice to T_N housing and WD feeding. Interestingly, T_N housing did not instigate further weight gain when paired with WD feeding in female mice, unlike their male

counterparts. However, there was a clear induction of weight gain in female mice fed a WD, independent of housing temperature and as reported previously[308]. Total and LDL-cholesterol rose significantly in WD-fed males, whereas in females, levels were not different compared to CD, but significantly increased LDL-cholesterol in response to T_N when fed a WD. There were few unexpected differences in hepatic lipid levels and markers of liver health, with WD feeding augmenting levels in both sexes as previously reported[138]. The increase in male WD-T_N levels of ALT and AST may have been driven by the increased adiposity. Despite this, there were no significant changes in NASH scoring between housing temperatures when comparing within biological sex. However, while female WD-T_N and WD-T_S were not statistically different, WD-T_N females tended to have more severe scoring, had significantly higher expression of macrophage-specific markers (*Emr1* and *Cd9* transcript and F4/80$^+$ cells) as well as significantly more macrophage aggregates in the liver. Increased susceptibility of fibrosis under WD-T_N was only observed at the transcriptional level (*Col3a1* for males and *Acta2*/*Timp1* for females), with no overt increased collagen deposition compared to CD-fed mice at either housing temperature. These observations were all independent of differential effects on total weight, unlike male mice. These results suggest strongly that while 16 weeks of WD-T_N conditions were not sufficient, divergence may occur soon after this time point. Recent studies have delineated multiple macrophage subsets in the hepatic MAFLD environment, including bone marrow-derived LAMs, defined in part by *Cd9* expression. Interestingly, while our manuscript was under consideration, a study was published that clearly demonstrates an increased inflammatory tone in livers of multiple mouse models of fatty liver housed under TN conditions[150].

Prior studies using a range of high fat-containing diets have demonstrated that glucose tolerance tends to improve in male mice housed at T_N conditions[302,305], although female data remains unavailable. Male WD-T_N were significantly more glucose tolerant compared to male mice housed at T_S, while there were no differences between housing temperatures in females. Interestingly, while markers of liver lipid metabolism and inflammation were indistinguishable between WD-T_S and WD-T_N mice, blood glucose levels after 4 h of fasting were significantly lower in both T_N-housed male and female mice. Serum insulin levels were also not different, and there were no significant changes in the transcript expression of gluconeogenic genes in the liver, although these measures were increased by WD feeding, independent of temperature. When C57Bl/6J mice were fed a diet high in fat (60% kcal from fat) and housed at T_N conditions for 12 weeks, there were no differences in glycemia or markers of glucose and insulin tolerance[302]. However, whether WD feeding and T_N housing indeed impair hepatic or peripheral insulin action requires further study.

There remain important considerations when interpreting our results, which first and foremost sought to use housing temperature as an external variable to augment fatty liver progression. We housed mice at approximately 29°C (28.5-29.5°C) and designated this as a T_N-like temperature[148,150,152,297], as opposed to 30°C or higher. Currently, there are discussions about the exact temperature of T_N, including whether this is a range or a point[311]. Moreover, the strain of the mouse must be considered[295,312]. Given the diversity of approaches, comparisons between T_N studies become challenging. Additionally, while cages were placed at either T_S or T_N conditions, mice were not singly housed. Despite the effect of huddling on elevating body temperature, mice are still considered cold-stressed when co-housed at 22°C. Moreover, as most fatty liver/NASH studies co-house littermates, we used this experimental paradigm to test our hypothesis. Co-

housing was also meant to minimize the social anxiety that affects singly housed mice and to enable reciprocal fecal microbiota transfer between mice (coprophagy)[313,314]. It would have been informative to track food intake and markers of energy expenditure, as has been done previously[301,315]. In male mice, T_N housing and WD feeding increased body weight, which may have stemmed from altered energy expenditure. However, this difference was inconsequential in the progression of hepatic steatosis and most markers of NASH. Moreover, while female mice tended to show higher severity on the NASH score, this occurred without changes in weight. Additionally, the importance of protein sources to the progression of diet-induced dysfunction has recently been highlighted[316]. Since our diet was strictly casein, better modeling of human consumption would be beneficial.

We also identified aspects of glucose homeostasis that were affected by WD feeding and T_N housing. It would be helpful to know whether glucose-stimulated insulin levels were altered in WD-T_N males to explain the increased rates of glucose clearance during the GTT. Moreover, whether these effects hold true after oral dosing of glucose or if performed under continuing T_N or T_S conditions (i.e., GTT and ITT assessments took place at T_S independent of housing condition) is also a question that remains unanswered. Mice began treatment at ~14 weeks of age, which is both older than conventionally seen but well short of modeling aged mice. Future study designs interrogating the relationship between diet-induced NASH progression, and T_N housing will do well to assess differences between sex, age and strain [151,317] in a longitudinal fashion. Finally, though 16 weeks was insufficient for T_N housing to completely exacerbate WD-induced progression toward NASH, we cannot rule out the potential for altered hepatic and/or circulating immune populations as well as transcriptional responses that may differentially prime the hepatic

metabolic and immune landscape for progression toward NASH[307,318], which are supported by the increased expression and content of macrophage markers in WD-T_N mice.

T_N housing has the potential to validate and clarify molecular and metabolic mechanisms that underpin normal and pathophysiology. Our study revealed that WD feeding coupled with T_N housing does not significantly exacerbate the progression of hepatic fibrosis and NASH-like pathologies. However, we present evidence that WD-T_N conditions for 16 weeks appear close to a potential "tipping point" and may serve well to tease out subtle genotype or drug effects of future work. Moving forward, studies that integrate a longer treatment time, the potential inclusion of dietary cholesterol (which is known to proportionally instigate hepatic fibrosis and stellate cell activation in mice), as well as fructose supplementation (to exacerbate lipogenesis) in conjunction with T_N housing will be necessary to provide a clearer translational model for interrogating mechanisms and testing potential therapies.

2.7 Figures

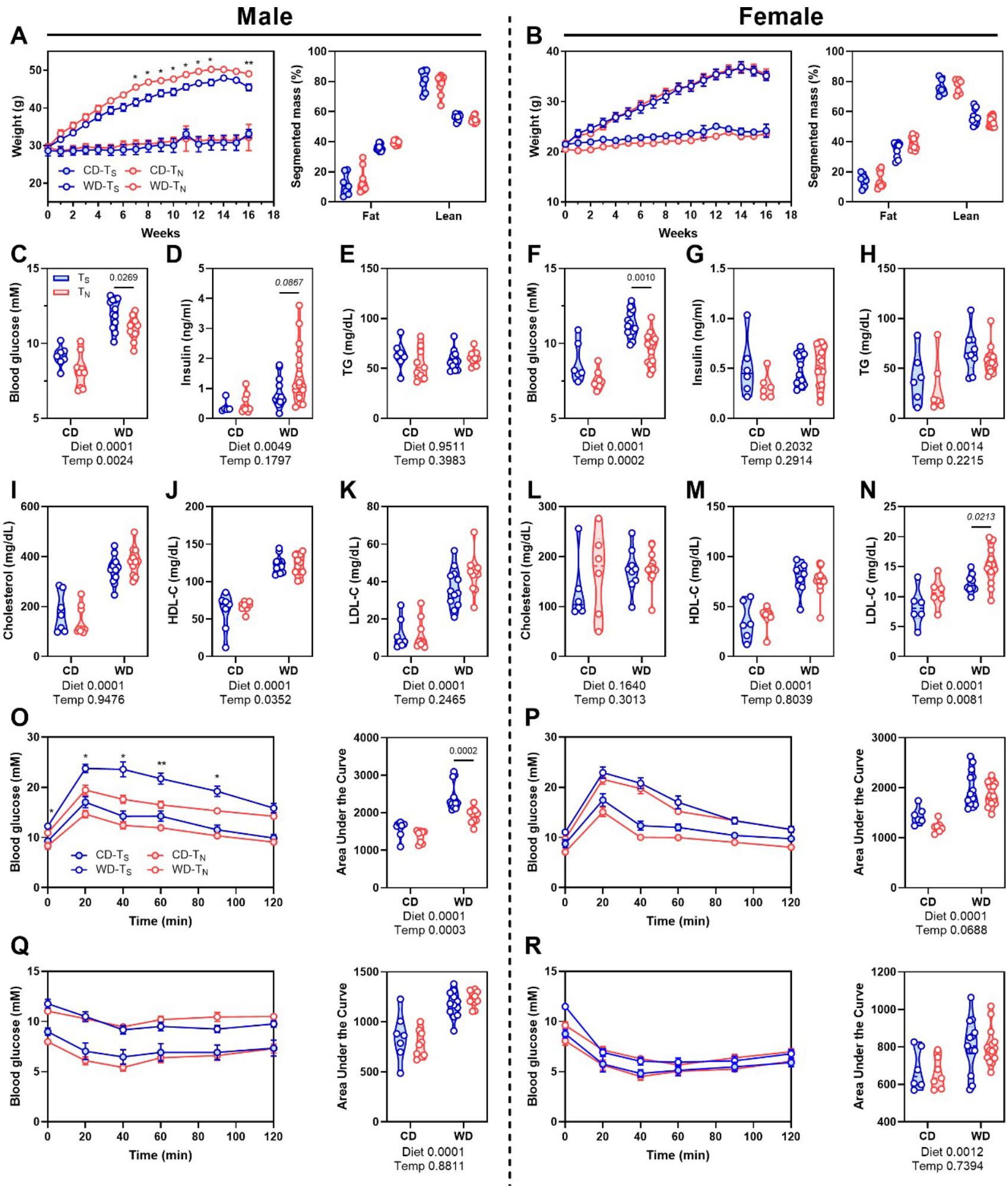

Figure 2.1. T_N housing and WD feeding have select effects in male and female mice. A/B) Male and female body weights, as well as the percentage of fat and lean mass for all groups, respectively. Mice were fasted for 4 h, and blood was collected for serum determination of (for male and female mice, respectively) C/F) blood glucose, D/G) insulin, E/H) TG, I/L) total cholesterol, J/M) HDL-cholesterol, K/N) LDL-cholesterol. O/P) Male and female IPGTT of WD-fed mice in response to 1.5 g/kg glucose. Q/R) Male and female ITT of WD-fed mice in response to 0.8 U/kg insulin, where the area under the curve is displayed. Data in A/B representing body weight, O/P indicating GTT and Q/R indicating ITT curves are shown as mean ± SEM and were analyzed by a Two-way repeated measures ANOVA with Tukey's test for multiple comparisons, where * and ** represent $p<0.05$ and $p<0.01$, respectively. Data shown in C-N were analyzed by 2-way ANOVA with a Šídák multiple comparisons test to determine significant differences within the diet and between housing temperatures. In C-R, lines between two groups indicate p-values calculated by multiple comparisons test and the text underneath the graphs indicates overall group effects (p-values) as calculated by two-way ANOVA. CD groups were comprised of 6-9 mice, whereas WD groups were comprised of 11-14 mice.

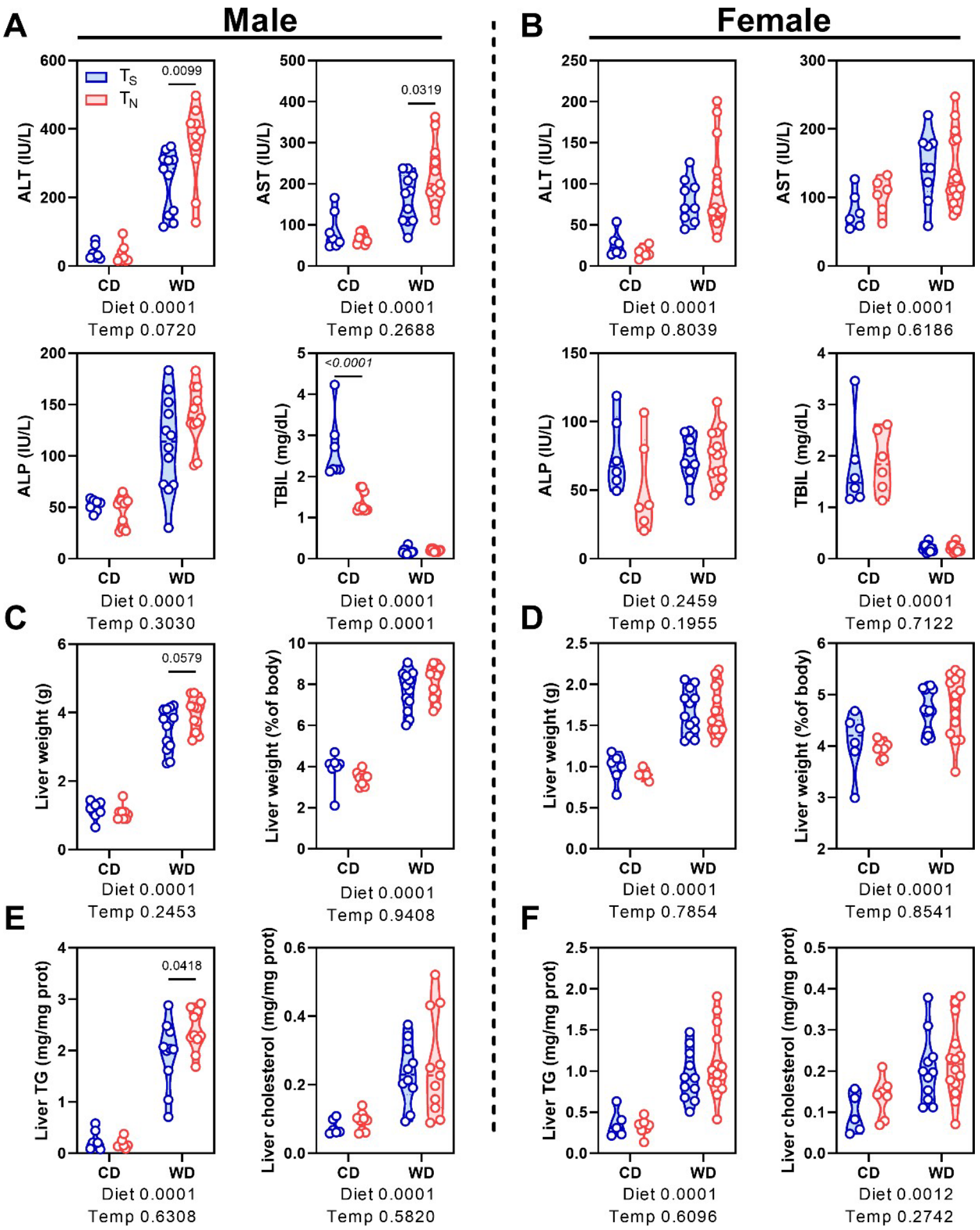

Figure 2.2. T_N housing and WD feeding do not alter liver enzyme or lipid levels. Serum determination of A) male and B) female ALT, AST, ALP activity and TBIL. C/D) Male and female liver weight in grams and as a percentage of the final body weight. E/F) Male and female liver TG and cholesterol levels. Data were analyzed by Two-way ANOVA with a Šídák multiple comparisons test to determine significant differences within the diet and between housing temperatures. Lines between two groups indicate p-values calculated by multiple comparisons test and the text underneath the graphs indicates overall group effects (p-values) as calculated by two-way ANOVA. CD groups were comprised of 6-9 mice (one liver from the female CD-T_S group was lost during the tissue harvest, leaving n=5 for that group for E and F), whereas WD groups were comprised of 11-14 mice. Outliers were as follows for E (0,1,0,0).

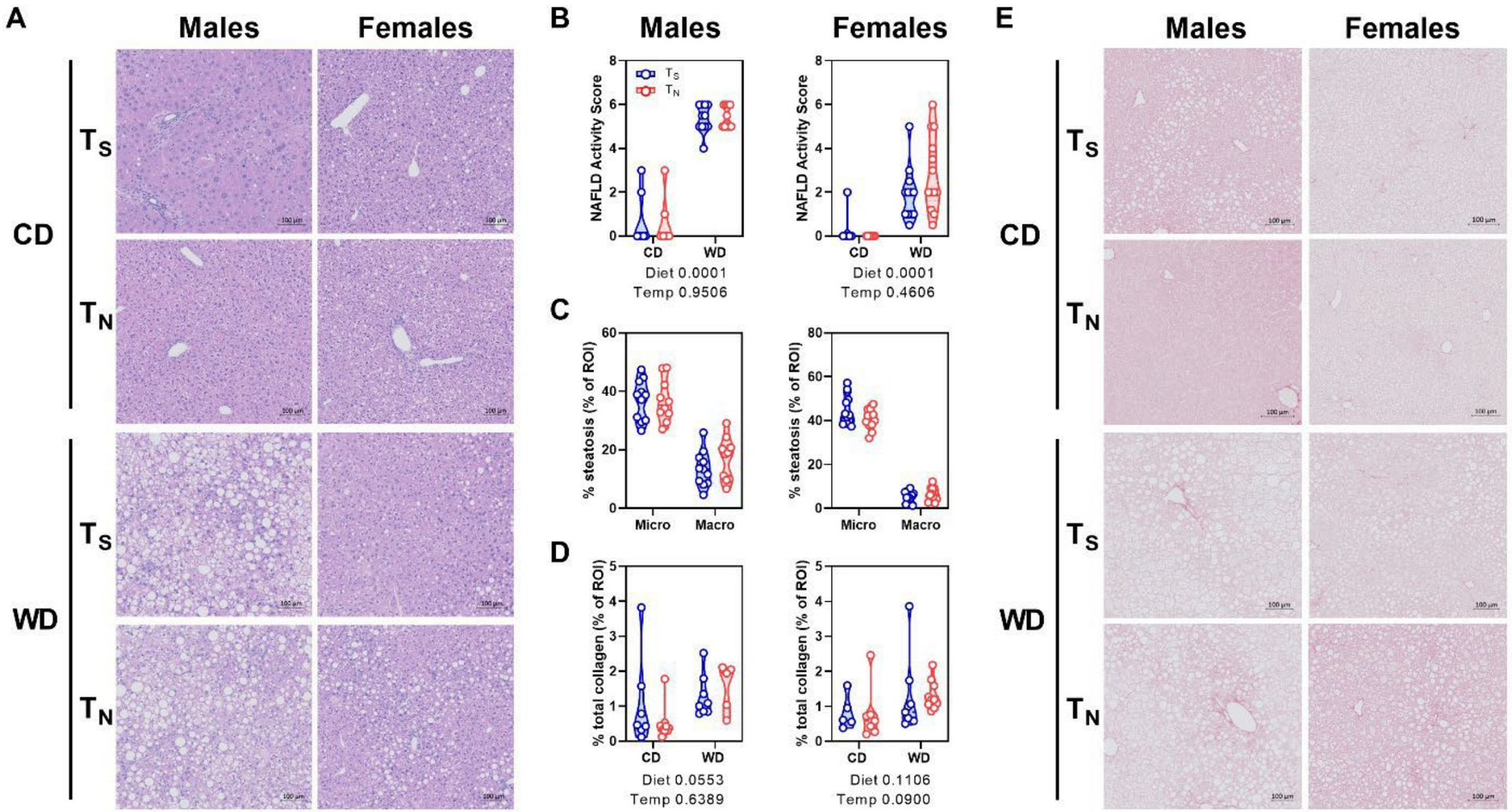

Figure 2.3. T_N housing does not exacerbate progression toward NASH beyond that observed with WD feeding. A) Representative H&E-stained images of the liver (scale bar is 100 µm). B) NAFLD activity score representing histological scoring of steatosis, ballooning and inflammation. C) Micro- (<17.1e^3 µm^2) and macrovesicular (>17.1e^3 µm^2) steatosis area as a percentage of the region of interest (ROI) for WD-fed males and females. D) Quantification of picrosirius red staining of total collagen as a percentage of ROI. E) Representative Picrosirius red stained images (scale bar is 100 µm). Data were analyzed by Two-way ANOVA with a Šídák multiple comparisons test to determine significant differences within the diet and between housing temperatures. In B and D, the text underneath the graphs indicates overall group effects (p-values) as calculated by two-way ANOVA. CD groups were comprised of 6-9 mice (one sample from the CD-TS female group was omitted due to sectioning error, leaving n=5 for this group in D), whereas WD groups were comprised of 11-14 mice.

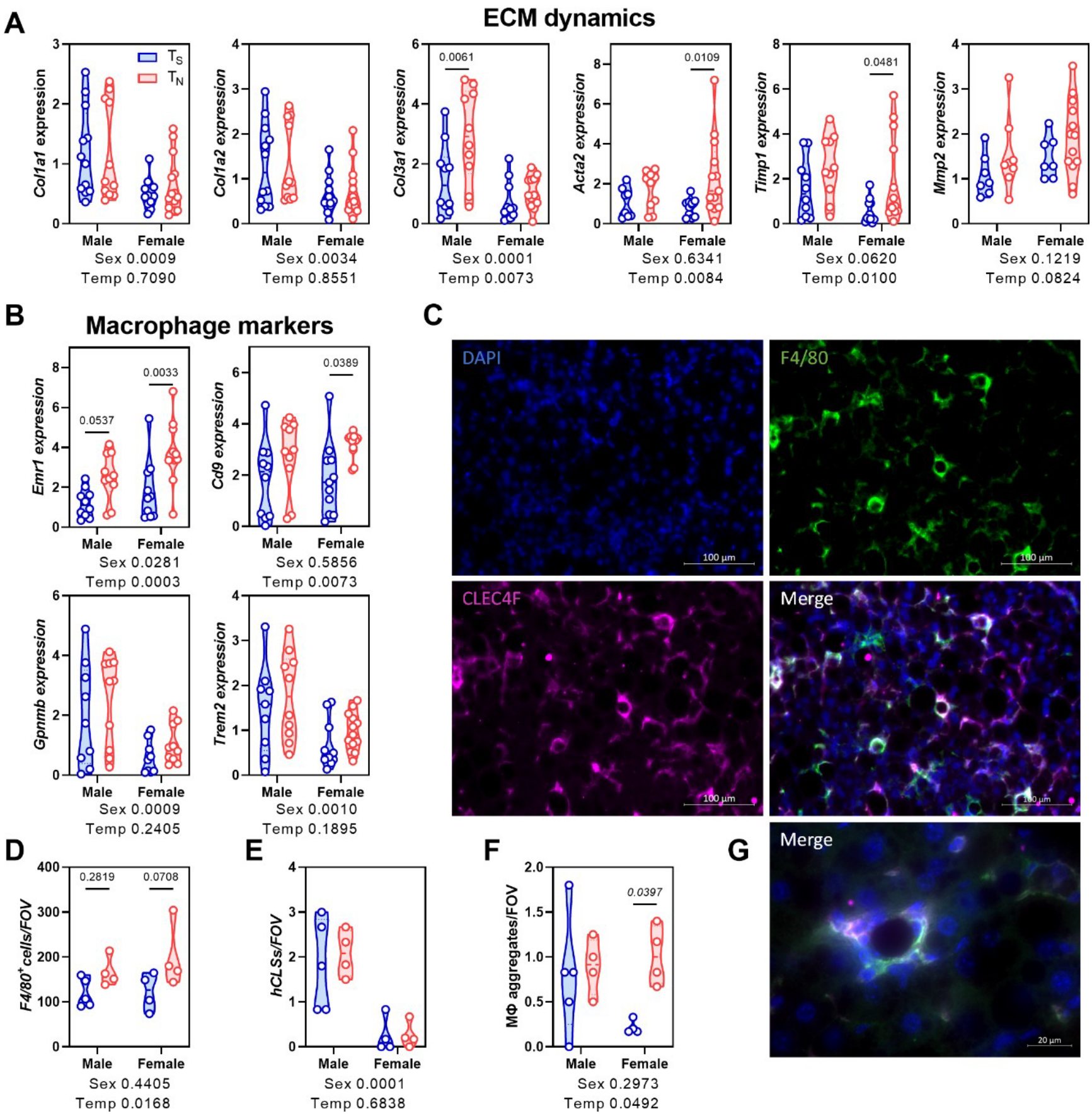

Figure 2.4. WD feeding changes select hepatic fibrosis transcripts and increases liver macrophage markers of WD-T_N mice. Hepatic mRNA transcript levels from WD-fed male and female mice. A) markers of extracellular matrix (ECM)-regulating transcripts (*Col1a1*, *Col1a2*, *Col3a1, Acta2, Timp1*, *Mmp2*), B) macrophage transcript markers (*Emr1*, *Cd9*, *Gpnmb*, *Trem2*). C) Representative immunofluorescence images of a WD-fed liver stained with DAPI, F4/80 and Clec4F. Quantification of D) $F4/80^+$ cells/field of view (FOV), E) HCLSs per field of view and F) hepatic macrophage aggregates/field of view for WD-fed liver sections. G) A representative image of HCLS staining. Transcript expression was normalized to the average expression of *ActB* and *Tbp* and shown relative to male WD-T_S mice. Data were analyzed by Two-way ANOVA with a Šídák multiple comparisons test to determine significant differences within sex and between housing temperatures. In A, B, and D-F, lines between two groups indicate p-values calculated by multiple comparisons test and the text underneath the graphs indicates overall group effects (p-values) as calculated by two-way ANOVA. Male and female WD groups were comprised of 6-14 mice (A and B). A subset of male and female mice was analyzed in D-F. Outliers were as follows for B: *Cd9* (0,2,0,0), *Gpnmb* (0,2,0,0), *Emr1* (1,1,0,0), *Trem2* (0,1,0,0).

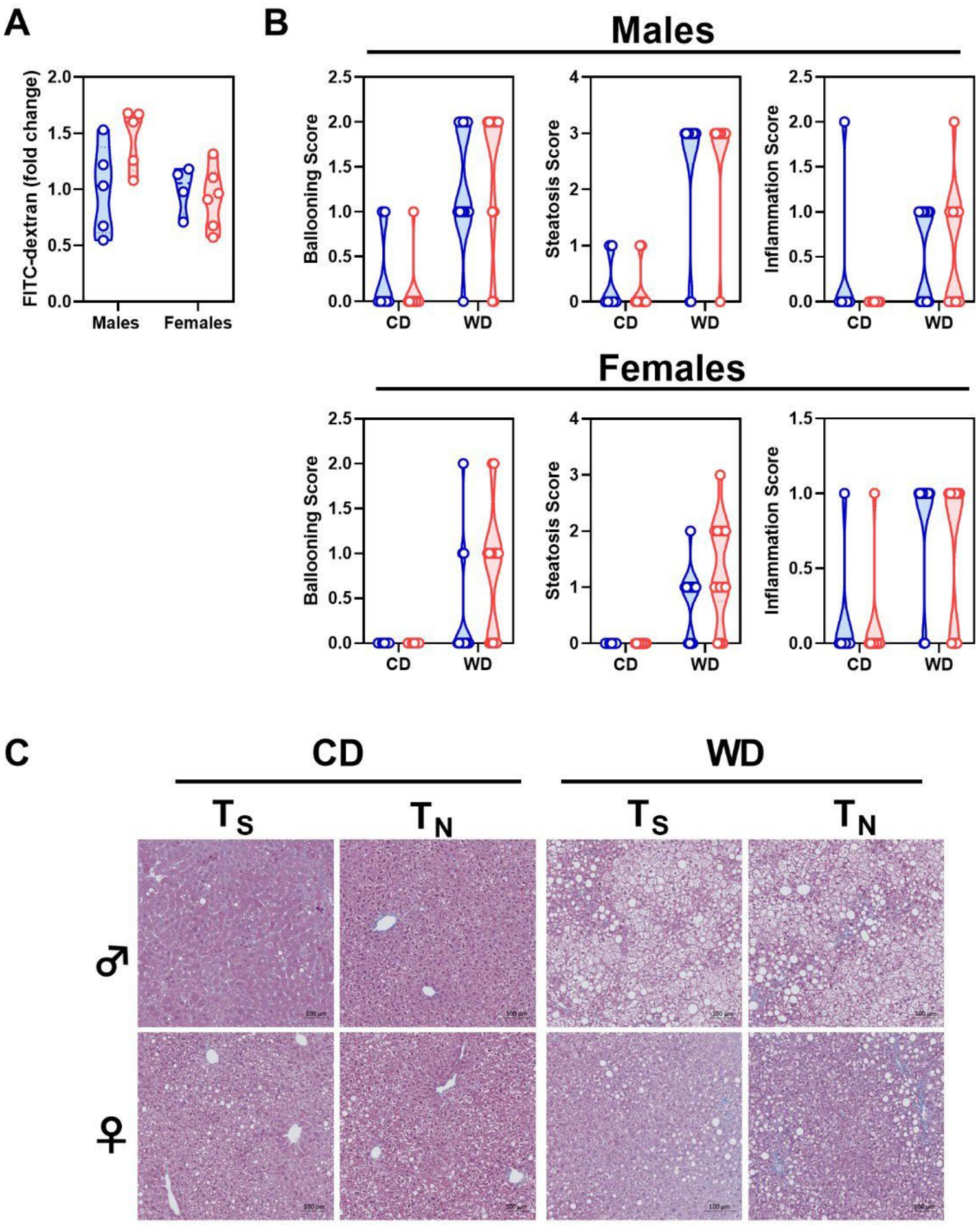

Supplemental Figure 2.1. T_N housing and WD feeding effects on gut permeability and hepatic fibrosis. A) Male and female intestinal permeability assessment of WD-fed mice fluorescence of FITC-dextran in serum. B) Male and female hepatocyte ballooning, steatosis and inflammation scores are shown individually and derived from Figure 3B. C) Representative Masson's Trichrome-stained images of the liver of male and female mice (scale bar is 100 µm). Data were analyzed by 2-way ANOVA with a Šídák multiple comparisons test to determine significant differences within sex and between housing temperatures (A). Data were analyzed by Two-way ANOVA with a Šídák multiple comparisons test to determine significant differences within diet and between housing temperatures (B). Data in A, male and female WD groups were comprised of 4-6 mice. Data in B, male and female CD groups were comprised of 6-7 mice, whereas male and female WD groups were comprised of 11-14 mice.

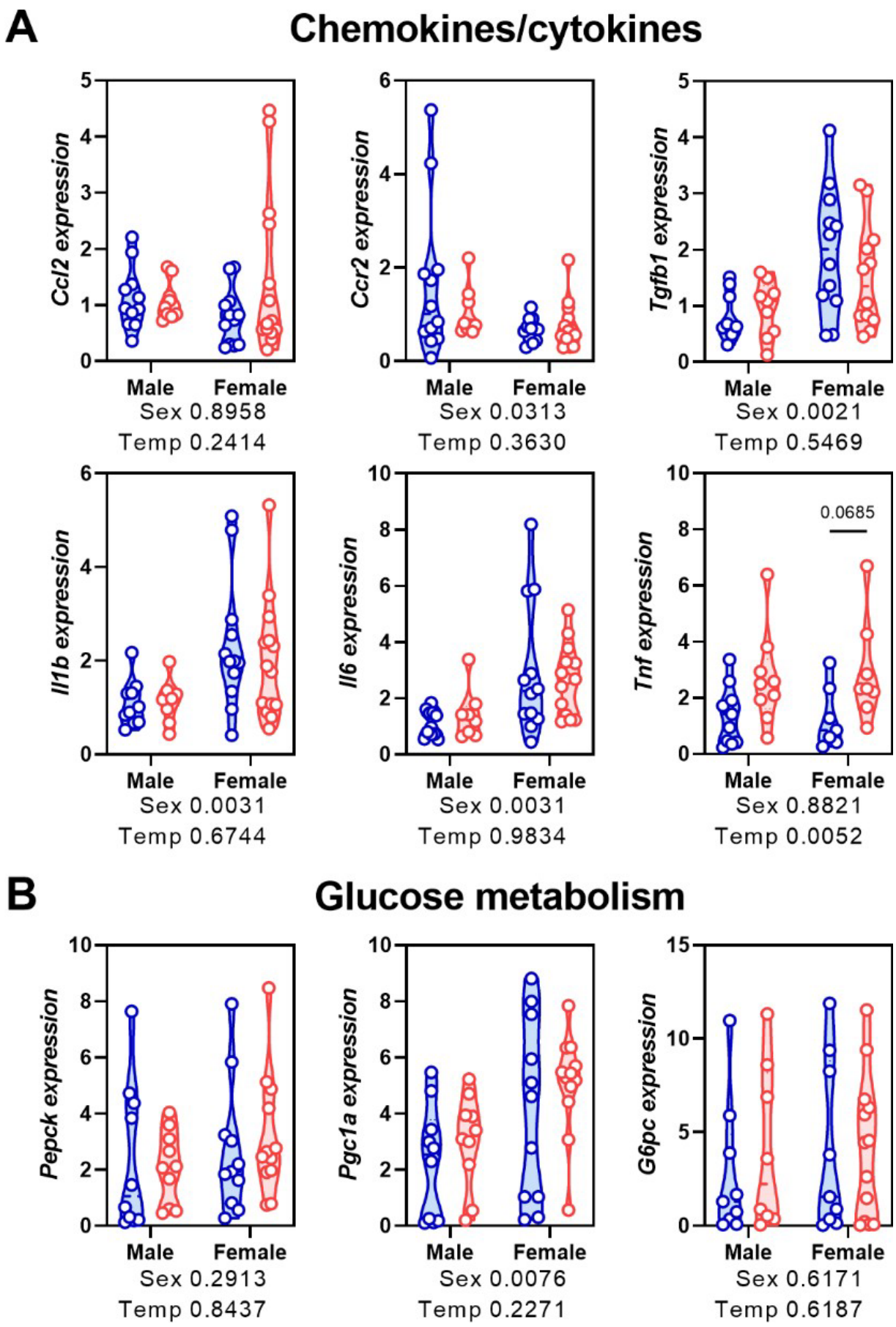

Supplemental Figure 2.2. T_N housing and WD feeding have little effect on liver inflammatory and gluconeogenic transcript expression. Hepatic mRNA transcript levels from WD-fed male and female mice. A) chemokine transcripts (*Ccl2*, *Ccr2*), cytokine transcripts (*Tgfb1*, *Il6*, *Il1b*, *Tnf*), and B) gluconeogenic transcripts (*Pepck*, *G6pc*, *Pgc1a*). Transcript expression was normalized to the average expression of *ActB* and *Tbp* and shown relative to male T_S-WD-fed mice. Data were analyzed by Two-way ANOVA with a Šídák multiple comparisons test to determine significant differences within sex and between housing temperatures. Lines between two groups indicate p-values calculated by multiple comparisons test and the text underneath the graphs indicates overall group effects (p-values) as calculated by two-way ANOVA. Male and female WD groups were comprised of 6-14 mice. Outliers were as follows for A; *Ccl2* (0,0,0,1) *Ccr2* (0,1,0,2), *Tgfb1* (0,1,2,0), *Tnf* (1,0,0,0), B; *Pepck* (0,1,0,0), *G6pc* (0,1,0,0), *Pgc1a* (0,1,0,0).

Table S2.1. Primer sequences

Gene	Forward primer	Reverse primer
Actb	GGCTGTATTCCCCTCCATCG	CCAGTTGGTAACAATGCCATGT
Tbp	GCTCTGGAATTGTACCGCAG	CTGGCTCATAGCTCTTGGCTC
Emr1	GCATCATGGCATACCTGTTC	GAGCTAAGGTCAGTCTTCCT
Trem2	CTGGAACCGTCACCATCACTC	CGAAACTCGATGACTCCTCGG
Cd9	TGCTGGGATTGTTCTTCGGG	GCTTTGAGTGTTTCCCGCTG
Gpnmb	GAGCACAACCAATTACGTGGCT	GGTGATATTGGAACCCACCAGA
Col1a1	GCTCCTCTTAGGGGCCACT	CCACGTCTCACCATTGGGG
Col1a2	GTAACTTCGTGCCTAGCAACA	CCTTTGTCAGAATACTGAGCAGC
Col3a1	TCTGGAAGCCAGAACCATGT	AATGGGATCTCTGGGTTGGG
Acta2	GTCCCAGACATCAGGGAGTAA	TCGGATACTTCAGCGTCAGGA
Timp1	TCTTGGTTCCCTGGCGTACTCT	GTGAGTGTCACTCTCCAGTTTGC
Mmp2	CAAGTTCCCCGGCGATGTC	TTCTGGTCAAGGTCACCTGTC
Il6	TAGTCCTTCCTACCCCAATTTCC	TTGGTCCTTAGCCACTCCTTC
Il1b	GCAACTGTTCCTGAACTCAACT	ATCTTTTGGGGTCCGTCAACT
Tgfb1	CTCCCGTGGCTTCTAGTGC	GCCTTAGTTTGGACAGGATCTG
Ccr2	ATCCACGGCATACTATCAACATC	CAAGGCTCACCATCATCGTAG
Ccl2	TTAAAAACCTGGATCGGAACCAA	GCATTAGCTTCAGATTTACGGGT
Pepck	GTGCTGGAGTGGATGTTCGG	CTGGCTGATTCTCTGTTTCAGG
G6pc	ACTGTGGGCATCAATCTCCTC	CGGGACAGACAGACGTTCAGC
Pgc1a	ATACCGCAAAGAGCACGAGAAG	CTCAAGAGCAGCGAAAGCGTCACAG

2.8 Acknowledgments

The authors would like to thank the University of Ottawa Louise Pelletier Histology Core Facility for the processing, staining and scanning of the liver tissues, as well as Dr. Manijeh Daneshmand for the pathological scoring of liver sections. BioRender was used to create the graphical abstract (publication license MR25AFBM7S).

2.9 Funding

This research was funded by project grants from the Canadian Institutes of Health Research (CIHR) (PJT148634 to M.D.F) and a CIHR New Investigator award (MSH141981 to M.D.F.), a uOttawa Faculty of Medicine Translational Research Grant (M.D.F), a Diabetes Canada (OG-3-21-5591) and a Heart and Stroke Foundation of Canada New Investigator award to E.E.M. J.R.C.N and C.P. were supported by Ontario Graduate Scholarships, T.K.T.S was supported by a CIHR Vanier Scholarship and N.A.T. received a University of Ottawa Heart Institute Cardiac Endowment scholarship.

Conflict of Interest statement: The authors have no conflict of interest to declare.

Chapter 3: Myeloid AMPK is dispensable for and low-dose metformin does not improve diet-induced NASH in male and female mice

3.1 Preface: This chapter is under review in the Journal of Lipid Research.

Julia R.C. Nunes[1], Conor O'Dwyer[1], Peyman Ghorbani[1], Tyler K.T. Smith[1], Samarth Chauhan[1], Victoria Robert-Gostlin[1], Benoit Viollet[2], Marc Foretz[2], Morgan D. Fullerton[1,3]*

[1] Department of Biochemistry, Microbiology and Immunology, Faculty of Medicine, Centre for Infection, Immunity and Inflammation, Ottawa Institute of Systems Biology, University of Ottawa, Ottawa, ON, Canada

[2] Université Paris cité, CNRS, Inserm, Institut Cochin, Paris, France

Centre for Catalysis Research and Innovation, University of Ottawa, Ottawa, ON, Canada

Contributions

Author Contributions: J.R.C.N. and M.D.F. conceived and planned the study. J.R.C.N., T.K.T.S., P.G., C.O., S.C. and V.R.G. performed the experiments and testing. B.V. and M.F. provided experimental mouse models. M.D.F. provided funding. J.R.C.N. and M.D.F. wrote the manuscript. All authors edited the manuscript and provided comments. M.D.F. is the guarantor of this work and, as such, has full access to all the data in the study and takes responsibility for the integrity of the data and the accuracy of the analysis.

3.2 Abstract

Metabolic programming underpins the inflammatory processes of immune cells. In the context of chronic liver disease, liver macrophage activation and response to hepatocellular damage is dependent on profound metabolic changes. Here, we sought to identify the role of an important metabolic regulator, AMPK, specifically within myeloid cells during the progression of NASH and whether treatment with low-dose metformin, a first-line therapy for diabetes and activator of AMPK, would be effective against disease progression. Male and female Flox control and MacKO mice were fed a low-fat control or a choline-deficient, amino acid defined 45% Kcal HFD (CDAHFD) for 8 weeks, where metformin was introduced in the drinking water (50 mg/kg/day) at 4 weeks. In male mice, CDAHFD-feeding induced a NASH-like phenotype; however, disruption of myeloid AMPK signaling did not affect markers of hepatic steatosis or fibrosis. While metformin treatment lowered random-fed blood glucose levels, there was no effect of metformin treatment on any index of NASH investigated. Upon CDAHFD-feeding, female mice developed hepatic steatosis and fibrosis, though to a lesser extent than males; however, no differences were observed between Flox and MacKO groups, with or without metformin. These results suggest that basal AMPK signaling in myeloid cells, both liver-resident and infiltrating, are dispensable during CDAHFD-induced NASH progression in male and female mice.

3.3 Introduction

MAFLD captures a spectrum of diseases from simple steatosis through to NASH[71]. A manifestation of metabolic syndrome with causal ties to obesity and diabetes, the incidence of MAFLD is projected to affect over 30% of adults by 2030[72]. While simple steatosis is considered relatively benign, lipotoxic species can accumulate in a subset of individuals, resulting in

hepatocellular death and the onset of inflammation and fibrosis (i.e., NASH). In response to hepatic damage signals, liver-residential macrophages called KCs secret signals that recruit monocytes as well as other immune mediators. KCs also mediate the activation of HSCs for the production of collagen, facilitating fibrogenesis[72,292]. In recent years, the nuanced complexities of the heterogeneity of the hepatic macrophage landscape have become clearer[319]. With the identification of specific macrophage subsets, many unanswered questions remain as to the plasticity of these immune populations, their activation state, and their associated metabolic programming and crosstalk.

Metabolic programming in response to nutrient and energy availability underpins the function of all cells. AMPK is a heterotrimeric serine/threonine kinase that signals to promote catabolic pathways and suppresses anabolic programs. In the context of metabolic dysfunction, there is extensive evidence of the protective effect of hepatocyte AMPK in both gain- and loss-of-function models[212,215,277,278]. In recent years, with the use of *in vivo* models of point mutations that specifically interrogate single targets, we and others have begun to dissect the role of various AMPK signaling axes[212,216]. With an appreciation for the role of hepatocyte-specific AMPK and an understanding of the beneficial effects of activating AMPK in the liver niche, the contribution of the immune compartment in the onset and progression of MAFLD and NASH remains unclear.

In recent years, there have been concerted efforts to generate clinically relevant pharmacological activators of AMPK and to repurpose/use existing drugs to combat various chronic metabolic disorders, including MAFLD and NASH[199,212,213,215,273,320,321]. Biguanide metformin, which remains one of the most widely prescribed drugs worldwide, has long been a first-line defence in

the treatment of IR and type 2 diabetes and activates AMPK signaling in the liver. While preclinical models have illuminated several potential mechanisms driving several of the beneficial effects of metformin[276], dose, route of administration, and physiological readout are the main considerations. In the context of NASH progression, there is some clinical evidence that metformin administration is associated with improved prognosis[322–325].

The liver exists as a hierarchical structured organ where spatial cellular orientation provides specialized function[326]. Understanding of how metabolic programs within these cellular compartments affect and are affected by steatosis and NASH continues to grow. Without AMPK signaling in the hematopoietic compartment during diet-induced obesity, a generalized pro-inflammatory program led to hepatic IR in the absence of worsened steatosis[258]. However, this approach failed to capture the importance of AMPK signaling in the context of liver-resident and infiltrating macrophages during disease onset and progression[319], and few studies have specifically interrogated AMPK signaling, regardless of cell type, in the context of steatosis progression toward NASH[274,327]. Few preclinical models fully capture the translational aspects of human NASH. However, to circumvent the severity and complications that accompany a traditional MCD, a diet that is deficient for choline and with restricted levels of methionine in conjunction with high-fat content, CDAHFD has been demonstrated to augment progression to NASH[328]. Using this and other dietary models, hepatocyte-specific AMPK has been shown to act directly on Caspase-6 to reduce its activity and suppress NASH-induced hepatocellular damage[281]. Given the role of myeloid AMPK signaling in modulating macrophage polarization in the context of adipose tissue inflammation[258], skeletal muscle regeneration [256,257] and atherosclerosis[263,264,267,268], we sought to clarify if AMPK signaling in resident and infiltrating liver macrophages was protective against

diet-induced NASH. In male and female mice, CDAHFD induced significant fibrosis and worsened circulating levels of liver injury markers. However, these parameters were unaffected by the disruption of myeloid AMPK activity as well as systemic treatment with a clinically relevant dosing regime of metformin.

3.4 Material and Methods

Mice: All mice used in this study were on a C57Bl/6J background. Mice were fed a standard chow (Teklad Global 18% Protein Rodent Chow Diet T.2018.15 – Envigo/Inotivco) prior to dietary intervention and housed in a barrier facility with a 12-light/12-hour dark cycle (7 pm-7 am dark). Generation of *Prkaa1*$^{fl/fl}$ and *Prkaa2*$^{fl/fl}$ mice have been previously described[215,329]. Double *Prkaa1/2*$^{fl/fl}$ mice (referred to as Flox) were crossed with hemizygous Lysozyme M Cre [330] (LysM-Cre) positive mice (referred to as MacKO). Flox (Cre negative) and MacKO (Cre positive) male and female mice (11-13 weeks old) were fed a macronutrient complete low-fat control diet (L-amino acid diet with 10 kcal% fat with normal methionine and choline or low-fat diet (LFD)– Research diets A06071322) or a choline-deficient, methionine-defined high fat (L-amino acid diet with 45 kcal% fat with 0.1% methionine and no added choline or CDAHFD – Research diets A06071309) for 8 weeks. Metformin (Sigma – cat. 317240) was administered in the drinking water 4 weeks into the dietary intervention at a dose of 50 mg/kg/day and replaced every 3 days (water intake was measured over 24 h, and metformin stocks were diluted appropriately). Random blood glucose was measured with a glucometer prior to the tissue harvest. All animal protocols were approved by the uOttawa Animal Care Committee (BMIe3744).

Serum and liver lysates assay: Terminal blood was collected via cardiac puncture of the left ventricle and placed on ice. Serum was collected from clotted blood by centrifugation. Serum ALT, AST, ALP, TBIL, TG, total cholesterol, as well as HDL- and LDL-cholesterol were measured using the Beckman Coulter AU480 clinical chemistry analyzer at the Pathology core at the Toronto Centre for Phenogenomics. Liver was snap-frozen in liquid nitrogen and chipped on dry ice for analysis. Liver lipids were extracted using a Bligh and Dyer lipid extraction[303], and total protein was quantified using a bicinchoninic acid assay as per the manufacturer's instructions (Fisher–Cat. PI-23225). Liver cholesterol and TG were quantified from the lipid fraction with colorimetric kits (L-Type TG M – Fujifilm Wako, Infinity Cholesterol Liquid Stable Reagent – Thermo 163 Fisher) followed by normalization to total protein level in the liver.

Histology: Intact livers were perfused with PBS via the left ventricle and fixed in 30 mL of 10% neutral buffered formalin for 24 hours. Following fixation, samples were transferred to 70% ethanol and processed at the University of Ottawa Louis Pelletier Histology Core Facility. Samples were paraffin-embedded, microtome sectioned and stained with H&E, Masson's Trichrome and Picrosirius Red. Quantification of total collagen was determined by whole-section Picrosirius red staining using a trained pixel classifier from QuPath[331]. From each section, 2-4 ROIs were selected to exclude large, vascularized regions that would skew quantification.

Transcript expression: PBS-perfused snap frozen livers were chipped on dry ice and homogenized in TriPure Isolation Reagent for RNA extraction (Sigma – cat. 11667165001) as per the manufacturer's instructions. RNA was analyzed for 260/280 purity (~2.0), equalized and reverse transcribed (All-in-one RT Master Mix – ABM). Real-time qPCR was performed with BlasTaq

Probe 2X qPCR Master Mix and run on Qiagen Rotor-Gene Q 2plex HRM instrument. Relative transcript expression was determined using the delta-delta Ct method[304], where the average Ct of the gene of interest was normalized to that of *Actb* and *Hprt* and shown relative to mice fed the LFD. Primer sequences are available in Table S1.

Flow cytometry: Remaining PBS-perfused livers were gently minced in 10 mL digest buffer composed of complete DMEM (Wisent – 3190005-CL with 10% FBS, 1% penicillin-streptomycin) with 0.5 mg/mL collagenase IV (Millipore Sigma – C5138) and 50 U/mL DNase I (Millipore Sigma – 1010459001). Once all tissues were collected, liver digests were allowed to warm to 37 °C for 5 minutes, followed by shaking incubation for 20 minutes at 200 rpm. Following the incubation, liver digests were diluted with 25 mL of cold complete DMEM and passed through a 100 µM cell strainer. Hepatic immune cells were enriched by a series of 50 x g centrifugation for depletion of hepatocytes[332]. Finally, immune cells were pelleted at 500 x g centrifugation for 5 minutes and collected for the following stain on ice; 30 minutes 1:250 Fc receptor block and 1:500 Live/dead blue, 20 minutes primary antibody stain (1:400 CD45.2-PerCP-Cy5.5, 1:100 F4/80-BV711, 1:600 CD11b- APC-eFluor 780, 1:400 TIM4-Alexa Fluor 647, 1:200 VSIG4-PE), and 15 minutes fixation with 4% paraformaldehyde. All samples were acquired on the Cytek® Aurora 5L UV-V-B-YG-R with preset optimized voltages.

Statistics: GraphPad Prism software (version 9.5.1) was used for all statistical analysis. Two-way ANOVA was performed for intra-sex comparisons between LFD, CDAHFD or CDAHFD+Met, where a Tukey's Multiple comparisons test was used to interrogate genotype differences within treatment. Statistical outliers were identified by the ROUT method with a Q value of 1%.

3.5 Results

Deletion of myeloid AMPK and systemic metformin do not influence hepatic or circulating lipids.

The protective effect of hepatocyte AMPK against MAFLD progression has been demonstrated in genetic and pharmacological studies[171,333]. To investigate the significance of AMPK in all bone marrow-derived and tissue-resident myeloid cells, we used male and female Flox and MacKO mice and induced NASH over the course of 8 weeks using a CDAHFD, which is known to produce hepatic steatosis, inflammation and F2 fibrosis[142]. Moreover, we also sought to determine whether a low but clinically relevant dosing regime of metformin could mitigate NASH progression in this model and subsequently, whether myeloid-specific AMPK signaling was involved. As expected, compared to LFD-fed mice, CDAHFD-fed males maintained their body weight (**Figure S3.1A**). In contrast, CDAHFD-fed females gained weight similar to LFD controls (**Figure S3.1B**). There were no differences in weight among male mice, whereas female MacKO mice were heavier than control Flox mice after 8 weeks of CDAHFD feeding (**Figure 3.1A** and **G**). Numerous models of MAFLD/NASH, including a version of CDAHFD, have observed reduced AMPK activity in the liver homogenate[215,281]. To address this general suppression, we reactivated AMPK by introducing metformin at a dose of 50 mg/kg/day administered in the drinking water in the latter 4 weeks of the study. Intervention with metformin did not affect body weight in any group (**Figure 3.1A** and **G)** but lowered random blood glucose in euglycemic CDAHFD-fed male mice independent of genotype (**Figure 3.1B**); however, this effect was not reproduced in females (**Figure 3.1H**). Although the CDAHFD model does not induce obesity or hyperglycemia, liver weight, as a proxy for hepatic steatosis, was increased in both males and females independent of myeloid AMPK or metformin treatment (**Figure 3.1C** and **I**). This was corroborated by the hepatic macro- and micro-vesicular steatosis observed in both male and female mice, albeit to a larger degree in males

(**Figure 3.1D** and **J**). Moreover, while levels were significantly induced by the CDAHFD, there were no differences in total hepatic cholesterol and TG content between genotypes or with metformin treatment (**Figure 3.1E** and **K**). One of the mechanisms by which CDAHFD expedites NASH progression is the disruption of lipoprotein production and secretion, as choline is critical for this pathway[328]. As expected, compared to control-fed mice, CDAHFD-fed mice had lower circulating total and LDL- and HDL-cholesterol (**Figure 3.1F** and **L**), while there were no differences in circulating levels of TG across all groups. Overall, neither deletion of myeloid AMPK nor systemic metformin treatment influenced markers of hepatic steatosis or the circulating lipid profile.

Hepatic fibrosis and markers of liver injury are unchanged by myeloid AMPK disruption or metformin treatment. As expected, feeding mice a CDAHFD for 8 weeks resulted in hepatic fibrosis as measured by Picrosirius red and Masson's Trichrome staining, though primarily in male mice (**Figure 3.2A** and **G** and **S3.1**). Quantification of total collagen (Picrosirius red) revealed that myeloid AMPK activity did not influence the degree of hepatic fibrosis in male or female mice at this point in the diet (**Figure 3.2B** and **H**). At the transcriptional level, there were also no differences in the expression of collagen peptide transcripts (*Col3a1, Col1a1*) or markers of hepatic stellate cell activation (*Acta2*) (**Figure 3.2C-E** and **I-K**). Moreover, there were no effects of systemic metformin treatment on markers of hepatic fibrosis. The circulating levels of markers that indicate liver injury were generally increased in response to the CDAHFD, again with a more profound effect observed in males compared to females. There were no changes attributable to myeloid AMPK or metformin treatment (**Figure 3.2F** and **L**).

Deletion of myeloid AMPK or metformin treatment does not affect markers of hepatic inflammation. Although myeloid AMPK signaling and systemic metformin treatment were insufficient to modulate hepatic steatosis and fibrosis, we were interested in potential differences in markers of macrophage infiltration and inflammatory signaling. In the setting of NASH, bone marrow-derived monocytes differentiate into different macrophage subsets, including Trem2^{+} LAMs that can form HCLSs[122,124–126]. In agreement with this, we observed increased transcript expression of *Emr1* and *Trem2* in CDAHFD males (**Figure 3.3A**), while only Trem2 expression was increased in female mice (**Figure 3.3D**). This is suggestive of high macrophage content in the liver derived from infiltrating monocytes, though it was unaffected by the presence of myeloid AMPK or systemic metformin. Moreover, there was an augmented expression of monocyte chemokine *Ccl2*, which may signify higher monocyte infiltration in CDAHFD-fed males (**Figure 3.3B**). Finally, we observed a robust increase in the expression of *Tnfa* in CDAHFD-fed males, though not *Il1b*. However, none of these transcriptional responses were influenced by myeloid AMPK or systemic metformin treatment (**Figure 3.3C**). In line with our previous observations, the transcriptional response in CDAHFD-fed females was less drastic compared to males and showed no dependence on myeloid AMPK signaling (**Figure 3.3D-F**).

3.6 Discussion

There is extensive evidence of the protective effects of activating hepatocyte-specific or hepatocellular AMPK activity in various dietary models of MAFLD[171,333]. Recently, our understanding of this role was extended to include limiting cell death through the inhibition of Caspase 6[281]. While many studies focused on the role of AMPK in hepatocytes specifically or in the overall liver environment, few have assessed the importance of AMPK signaling within the

hepatic immune compartment. Deletion of the AMPK β1 subunit from the hematopoietic compartment worsens liver inflammation and increases hepatic immune infiltration in male mice fed an HFD[258]. In contrast, LysM-mediated deletion of the AMPKα1 subunit was shown to diminish monocyte recruitment and macrophage infiltration under high-fat feeding conditions, which was accompanied by worsened steatosis and IR in a mix of male and female mice[268]. KCs are key players in the initiation of inflammation, immune infiltration as well as communication with damaged hepatocytes and activation of HSCs[319]. However, NASH macrophage populations are more heterogeneous than the simple distinction made between tissue-resident and infiltrating macrophages. KCs can be segmented by their expression of ESAM and NASH-induced expression of CD36, which plays an important role in liver oxidative stress[117]. Infiltrating macrophages that arise during NASH can also be subdivided into LAMs and macrophages that repopulate the KC niche (MoKCs)[122,124,126]. Given the complex heterogeneity of hepatic macrophages during NASH, we sought to address AMPK expressed in all macrophages present in the NASH hepatic environment.

There are continuing efforts to develop a translationally relevant mouse model to mirror human NASH. We and others have characterized the effect of various dietary interventions coupled with thermoneutral housing (~29 °C) to promote the progression toward hepatic fibrosis[148–151]. With and without the effect of T_N, greater than 16 weeks were necessary. To accelerate fibrogenesis, we chose to introduce a CDAHFD, which produces F2 fibrosis after 8 weeks. As expected, we observed decreased lipoprotein secretion when compared to LFD-fed mice. This effect is mainly mediated by choline deficiency, which results in a high degree of steatosis in combination with a high fat content[142]. Moreover, in contrast to an MCD, the mice do not experience weight loss or a

change in blood glucose. Importantly, our results confirm that female C57Bl/6J mice remain sensitive to a degree of NASH induction; however, this was not observed to the same extent as in male mice. Our data suggest that removing AMPK signaling in myeloid cells has little consequence on the degree of steatosis, inflammation or fibrosis in male or female mice. This aligns with previous work that showed that whole-body deletion of AMPKα1 in female mice failed to affect CCl_4-induced hepatic fibrosis[282]. However, it is important to consider that these observations may be specific to the strain of mice (C57Bl/6J), dietary intervention (CDAHFD) and timing (8 weeks) used in this study. We were able to confirm KC depletion and replacement by MoKCs (**Supplemental Figure S3.3**); therefore, we cannot rule out the potential importance of AMPK signaling in KCs at earlier stages of this NASH model[118].

Our goal was to assess the importance of AMPK in liver macrophages during NASH progression. To target AMPK signaling specifically, we chose to use the *LysM* promoter for the expression of *Cre*. Our model makes use of a double deletion of both catalytic subunits of AMPK (*Prkaa1* and *Prkaa2*). While the α1 subunit is predominantly expressed in immune subsets[334], we reasoned that dual deletion would ensure complete disruption of AMPK signaling in LysM-expressing cells. To this end, monocytes and differentiated macrophages represent the majority of cells that undergo LysM-mediated recombination and AMPKα1/α2 deletion; however, we cannot rule out the potential targeting of granulocytes such as neutrophils[335]. Neutrophils not only contribute to fibrogenesis indirectly, but infiltration of this population also significantly contributes to the production of inflammatory cytokines[38]. Therefore, AMPK deletion in granulocytes may play a confounding role in our interpretation of the effect of macrophage AMPK-mediated inflammation and crosstalk in NASH. Despite these caveats, LysM-mediated recombination has been shown to

be high for both KCs and MoKCs[336]. However, *Cre* recombination efficiency may not be equal amongst different macrophage subsets within the hepatic environment, both under normal conditions and NASH[336]. We have previously validated the deletion of AMPK signaling in thioglycolate-induced peritoneal macrophages, which represent recently differentiated monocytes and residential peritoneal macrophages [257,267]. However, there may be residual AMPK expression in infiltrating macrophage subsets such as LAMs, a macrophage population that forms HCLSs, a key histological feature of NASH[122,124,126].

Numerous studies have reported reduced liver AMPK activity (representing the liver environment, not just hepatocytes) in various dietary models of MAFLD and NASH[215,281]. We chose to introduce the systemic delivery of metformin for the reactivation of AMPK. Metformin represents the historical first-line defence in the treatment of type 2 diabetes (among other chronic conditions) and has a storied history, given the initial observations that it activates AMPK[276,337]. While the AMPK-activating and therapeutic mechanisms of AMPK remain to be fully understood (or demonstrated clinically in certain contexts), preclinical studies have shown consistent reductions in hepatic steatosis in HFD-fed mice through AMPK-dependent and independent mechanisms[276]. However, its efficacy in preventing/ameliorating the progression of NASH is less clear. Given the importance of appropriate dose and delivery of metformin in preclinical studies, and since renal expression of organic cation transporters is known to be down-regulated by choline deficiency[338] (potentially increasing local and circulating levels of metformin), we chose continuous oral delivery of a low dose of metformin in the drinking water. While it was recently reported that low-dose metformin activates lysosomal AMPK via the PEN2-ATP6AP1 axis, thereby reducing hepatic steatosis in an HFD model[208], we observed no difference in hepatic lipids in the CDAHFD-

fed mice. Interestingly, metformin intervention after 4 weeks of NASH progression also had no impact on markers of fibrosis or liver injury in the CDAHFD model. It remains possible that the localized dose of metformin delivered to the liver (all cell types) was insufficient for the activation of liver macrophage AMPK, and metformin is not able to attenuate markers of NASH progression in the CDAHFD model, which has been demonstrated previously at a higher dose in MCD-fed mice[339–341]. Moreover, the expression of transporters responsible for metformin uptake in immune cells is unknown, and failure to activate AMPK in T cells *in vivo* has been observed[342]. It may also be plausible that preventative treatment (at the onset of dietary intervention) may target a larger population of KCs prior to their NASH-induced depletion[118].

To our knowledge, this is the first investigation into the role of myeloid-specific AMPK signaling during the onset and progression of NASH and chronic low-grade inflammation in the liver. We recognize that characterization of the hepatic macrophage populations between LFD and CDAHFD, as well as with and without AMPK signaling, would have added to our overall understanding as we cannot rule out the potential that frequencies of resident KCs and infiltrating MoKCs macrophages may be different. We also acknowledge that there may be effects of hepatic macrophage AMPK signaling that are not captured here that would be observed under a different experimental paradigm. The use of a KC-specific Cre system (*Clec4f*) would restrict the deletion of AMPK to resident KCs and MoKCs that experience an induction of *Clec4f* expression[121]. However, given the NASH-induced death and disappearance of embryonically derived KC[118], future studies warrant longitudinal analysis of KC metabolism and activation under a NASH-induced diet, as there may be key differences during the onset and progression with this model. Finally, earlier intervention with a specific and direct AMPK activator like PXL770[274], whether

delivered systemically or packaged for cell-specific delivery or constitutive/inducible genetic activation, may also prime KCs prior to the release of hepatic DAMPs that appear upon the onset of NASH induction.

AMPK signaling governs several metabolic pathways across cell types and circumstances. Macrophage AMPK maintains physiological homeostasis by regulating lipid metabolism and inflammatory signaling. However, when fed a CDAHFD, myeloid AMPK does not impact NASH progression in male or female mice, and low-dose metformin treatment failed to improve markers of hepatic fibrosis and inflammation. While endogenous signaling may be dispensable, whether AMPK signaling can be leveraged to reprogram resident and infiltrating macrophages to improve NASH prognosis remains to be tested but may represent an additive therapeutic benefit.

3.7 Figures

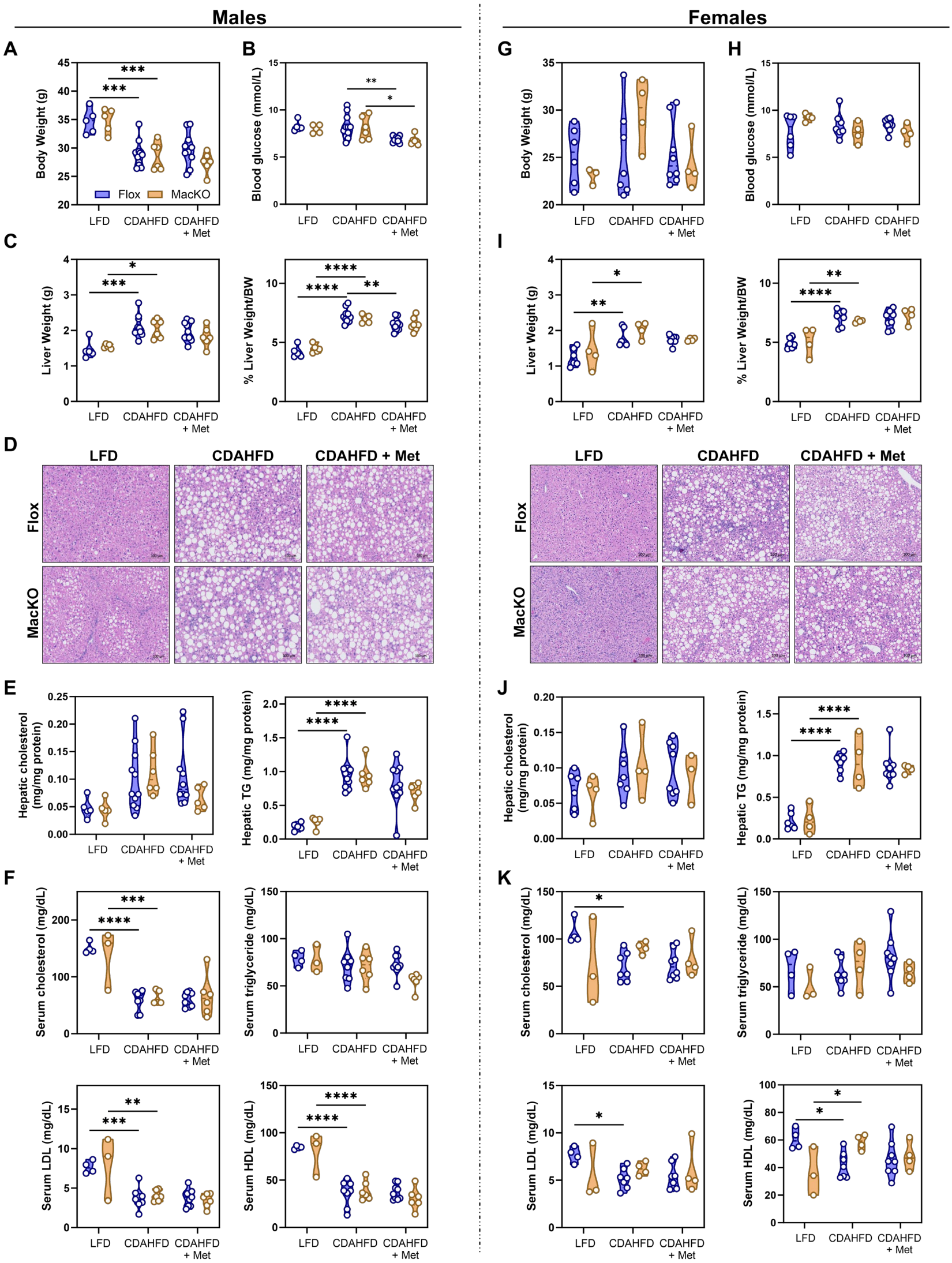

Figure 3.1. Myeloid AMPK signaling and metformin intervention does not influence hepatic steatosis or circulating lipids. A/G) Final body weights of male and female control Flox and MacKO mice on a LFD, CDAHFD or CDAHFD + 50 mg/kg/d metformin, B/H) random blood glucose at week 8 of male and female control (Flox) and MacKO mice C/I) liver weight (g) and liver weight expressed as a percentage of body weight (%) D/J) representative H&E-stained liver sections (20x magnification, 100 µM scale bar), E/K) hepatic cholesterol and TG normalized to total protein F/L) serum total cholesterol, total TG, LDL-cholesterol and HDL-cholesterol. Data were analyzed by Two-way ANOVA with Tukey's test for multiple comparisons where *,**,*** and **** represent $p<0.05$,$p<0.01$, $p<0.001$ and $p<0.0001$, respectively. LFD groups comprised 3-5 mice, and CDAHFD groups comprised 5-11 mice.

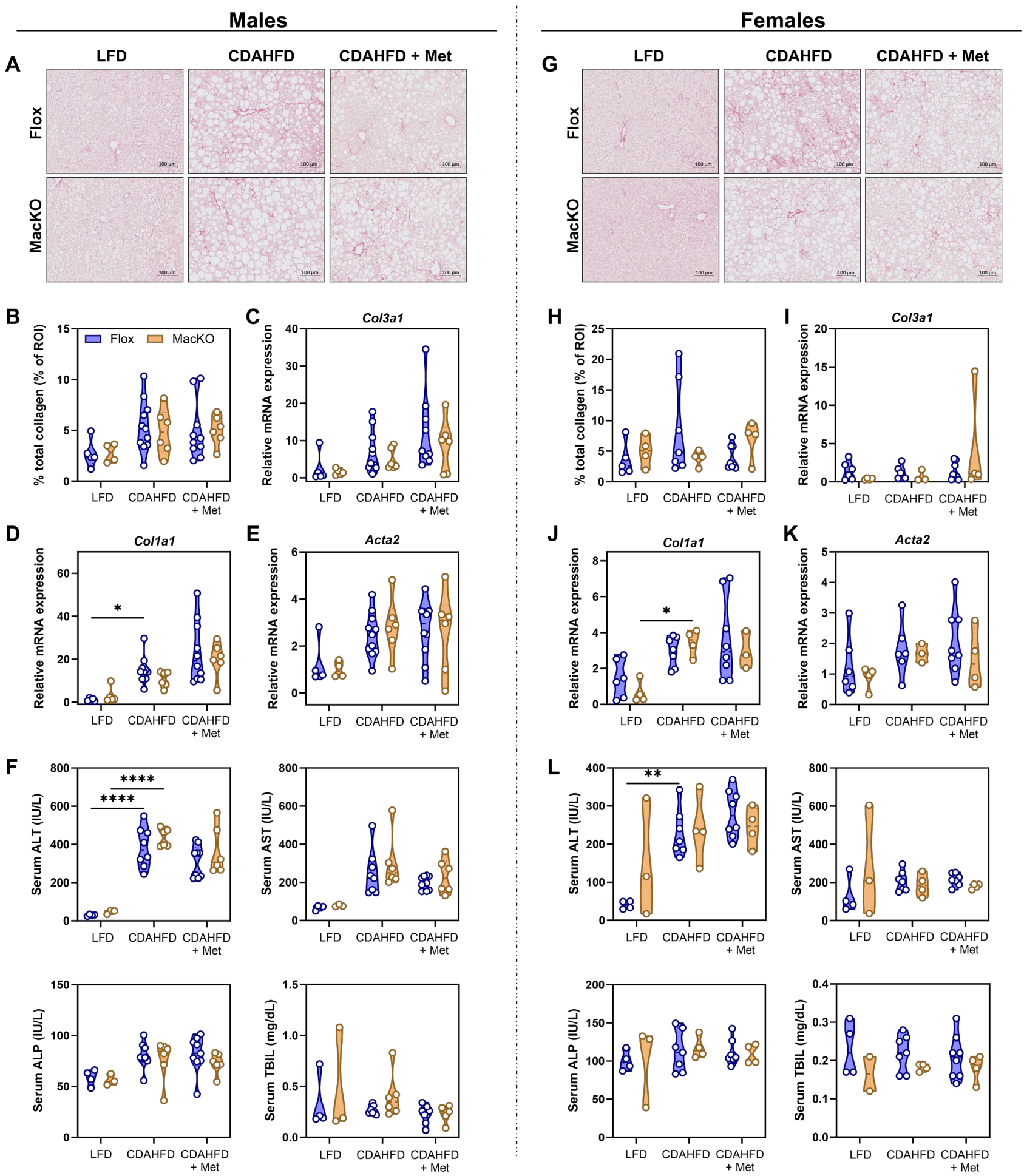

Figure 3.2. Myeloid AMPK signaling and metformin intervention does not influence hepatic fibrosis or circulating liver enzymes. A/G) Representative Picrosirius Red-stained liver sections (20x magnification, 100 µM scale bar) of male and female control Flox and MacKO mice on a LFD, CDAHFD or CDAHFD + 50 mg/kg/d metformin, B/H) total collagen quantification of Picrosirius red, C-E/I-K) Hepatic mRNA transcript levels of markers of extracellular matrix-regulating transcripts (*Col3a1*, *Col1a1*, *Acta2*), F/L) serum levels of liver injury markers (ALT, AST, ALP and TBIL). Transcript expression was normalized to the average expression of *Actb* and *Hprt* and shown relative to LFD-fed Flox mice. Data were analyzed by Two-way ANOVA with Tukey's test for multiple comparisons where *,** and **** represent $p<0.05$, $p<0.01$ and $p<0.0001$, respectively. LFD groups comprised 3-5 mice, and CDAHFD groups comprised 5-11 mice.

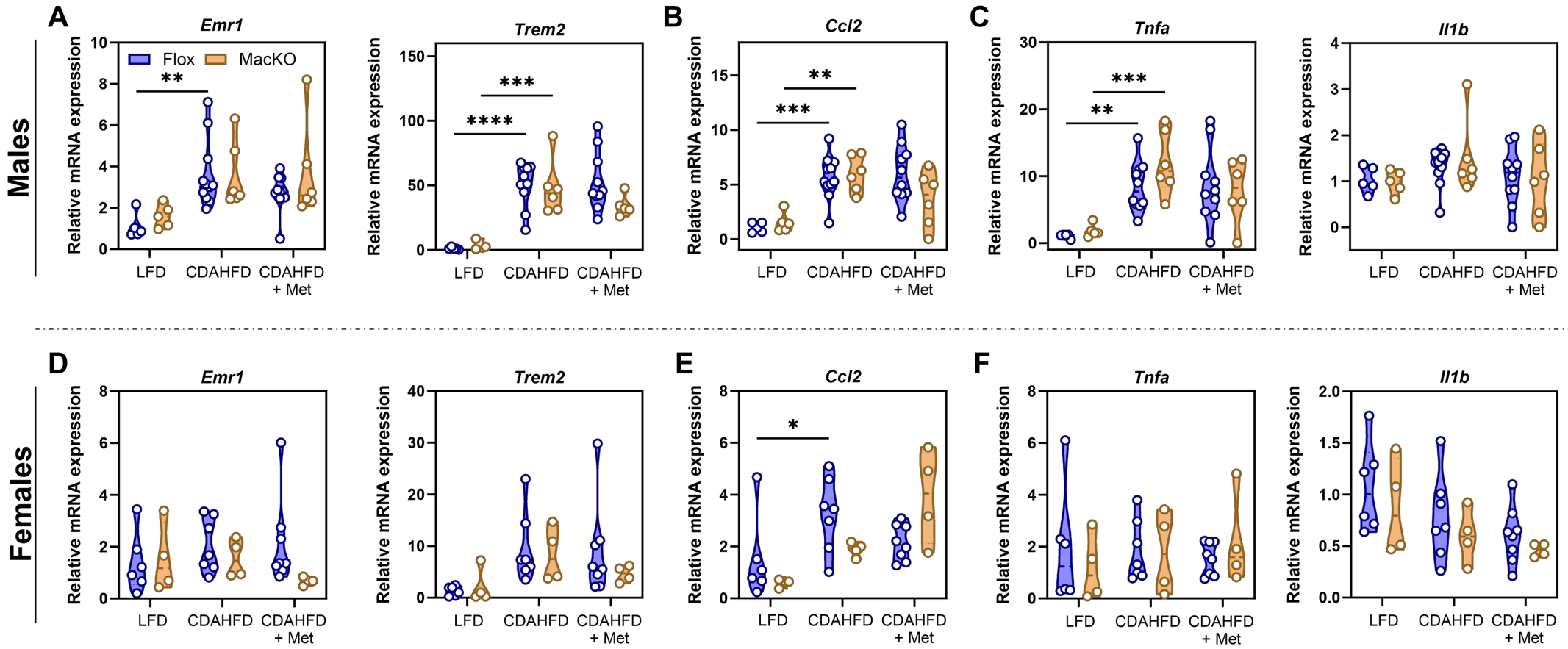

Figure 3.3. Myeloid AMPK signaling and metformin intervention do not affect markers of hepatic inflammation. A/D) Hepatic mRNA transcript levels of macrophages markers (*Emr1*, *Trem2*) from male and female control Flox and MacKO mice on a LFD, CDAHFD or CDAHFD + 50 mg/kg/d metformin, B/E) the marker of monocyte recruitment (*Ccl2*) and C/F) inflammatory cytokines (*Tnf*, *Il1b*). Transcript expression was normalized to the average expression of *Actb* and *Hprt* and shown relative to LFD-fed Flox mice. Data were analyzed by Two-way ANOVA with Tukey's test for multiple comparisons where *, **, ***, **** represent $p<0.05$, $p<0.01$, $p<0.001$ and $p<0.0001$, respectively. LFD groups comprised 5 mice, and CDAHFD groups comprised 5-11 mice.

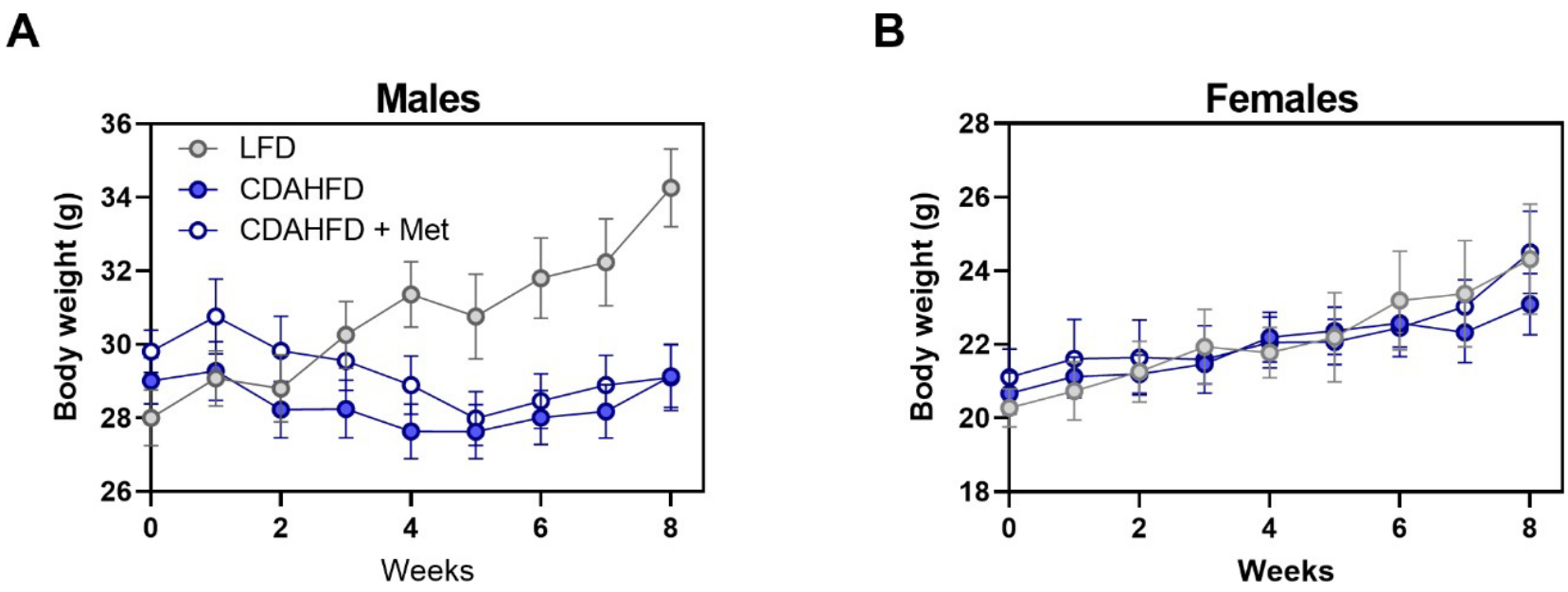

Supplemental Figure 3.1. CDAHFD does not induce weight loss in male or female mice. Weekly body weights of Flox and MacKO (combined) male and female mice fed an LFD, CDAHFD or CDAHFD with 50 mg/kg/d metformin treatment in the drinking water at week 4.

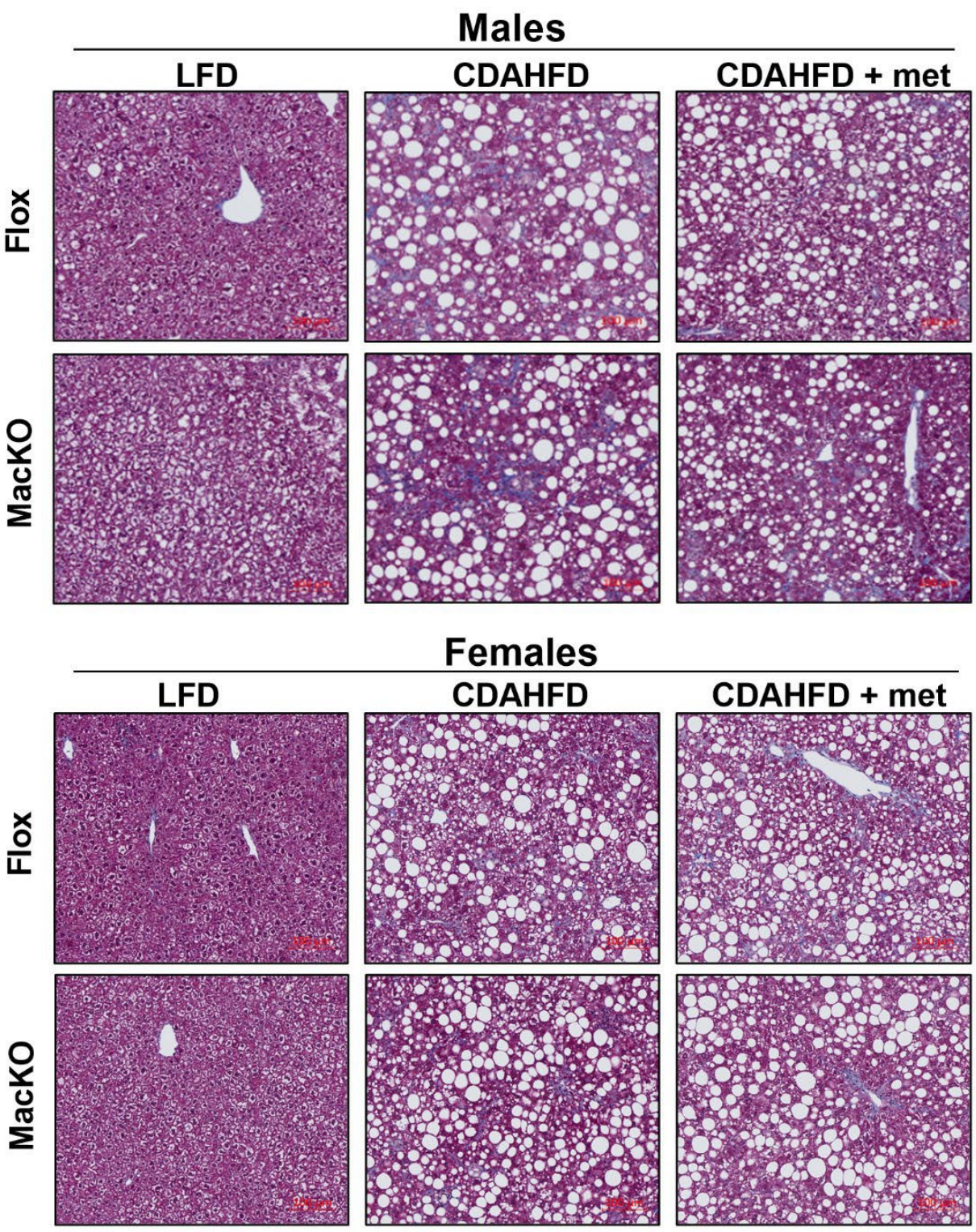

Supplemental Figure 3.2. Myeloid AMPK signaling and metformin intervention does not influence hepatic fibrosis. A) Representative Masson's Trichrome-stained liver sections (20x magnification, 100 μM scale bar) of male and control Flox and MacKO mice on a LFD, CDAHFD or CDAHFD + 50 mg/kg/d metformin.

Representative LFD liver

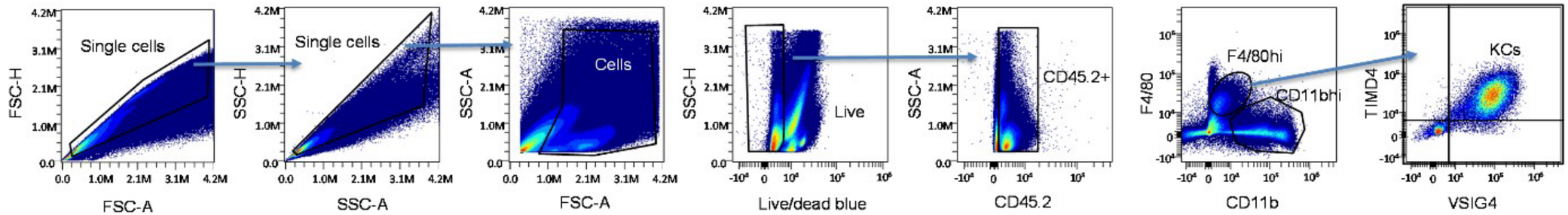

Representative CDAHFD liver

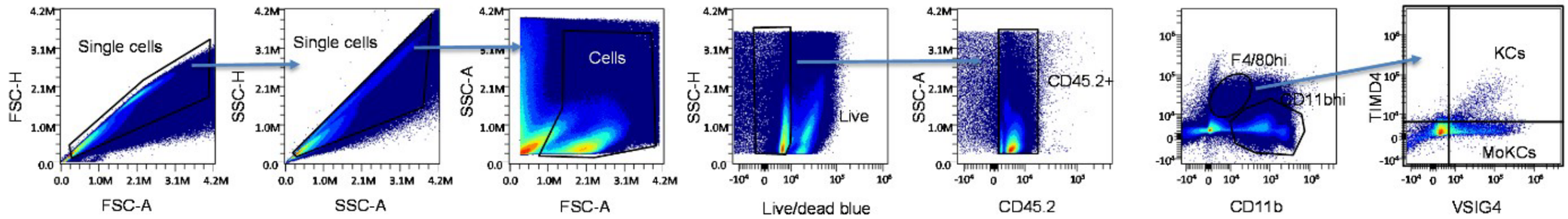

Supplemental Figure 3.3. Resident macrophage populations disappear after a CDAHFD. Representative hepatic immune flow plots of male mice fed an LFD or CDAHFD. Gating strategy showing KCs ($TIM4^{+}$ $VSIG4^{+}$) and MoKCs ($TIM4^{-}$ $VSIG4^{+}$) from $F4/80^{hi}$ $CD11b^{lo}$ $CD45^{+}$ live single cells

Table S3.1. – Primer sequences

Gene	Forward primer	Reverse primer
Col3a1	TCTGGAAGCCAGAACCATGT	AATGGGATCTCTGGGTTGGG
Col1a1	GCTCCTCTTAGGGGCCACT	CACGTCTCACCATTGGGG
Acta2	GTCCCAGACATCAGGGAGTAA	TCGGATACTTCAGCGTCAGGA
Emr1	GCATCATGGCATACCTGTTC	GAGCTAAGGTCAGTCTTCCT
Trem2	CTGGAACCGTCACCATCACTC	CGAAACTCGATGACTCCTCGG
Ccl2	TTAAAAACCTGGATCGGAACCAA	GCATTAGCTTCAGATTTACGGGT
Tnf	CCCTCACACTCAGATCATCTTCT	GCTACGACGTGGGCTACAG
Il1b	GCAACTGTTCCTGAACTCAACT	ATCTTTTGGGGTCCGTCAACT
Actb	GGCTGTATTCCCCTCCATGG	CCAGTTGGTAACAATGCCATGT
Hprt	TCAGTCAACGGGGGACATAAA	GGGGCTGTACTGCTTAACCAG

3.8 Acknowledgments

The authors would like to thank the University of Ottawa Louise Pelletier Histology Core Facility for the processing, staining, and scanning of the liver tissues, as well as Dr. Vera Tang and the Faculty of Medicine Flow Cytometry and Virometry Core Facility (RRID: SCR_023306).

3.9 Funding

This research was funded by project grants from the Canadian Institutes of Health Research (CIHR) (PJT148634 to M.D.F) and a uOttawa Faculty of Medicine Translational Research Grant (M.D.F). J.R.C.N was supported by Ontario Graduate Scholarships, and T.K.T.S was supported by a CIHR Vanier Scholarship.

Conflict of Interest statement: The Authors have no conflict of interest to declare.

Chapter 4: Macrophage and hepatocyte AMPK signaling do not influence acetaminophen-induced liver injury.

4.1 Preface: This chapter is ready to be submitted.

Julia R.C. Nunes[1,2], Tyler K.T. Smith[1,2], Conor O'Dwyer[1,2], Peyman Ghorbani[1,2], Victoria Robert-Gostlin[1,2], Ciara Pember[1,2], Alexia Cabrera Brutus[1,2], Rama El Hakim[1,2], Suresh Gadde[3], Benoit Viollet[4,5], Marc Foretz[4,5], Morgan D. Fullerton[1,2]

[1]University of Ottawa Centre for Infection, Immunity, and Inflammation

[2]University of Ottawa Department of Biochemistry, Microbiology, and Immunology

[3]University of Ottawa Department of Cellular and Molecular Medicine

[4]Institut Cochin, Paris, France

[5]Université Paris Descartes, Sorbonne Paris Cité, Paris, France.

Contributions

Author Contributions: J.R.C.N. and M.D.F. conceived and planned the study. J.R.C.N., T.K.T.S., P.G., C.O., C.P., V.R.G., A.C.B. and R.E.H. performed the experiments and testing. B.V. and M.F. provided experimental mouse models. S.G. provided the NPs. M.D.F. provided funding. J.R.C.N. and M.D.F. wrote the manuscript. All authors edited the manuscript and provided comments. M.D.F. is the guarantor of this work and, as such, has full access to all the data in the study and takes responsibility for the integrity of the data and the accuracy of the analysis.

4.2 Abstract

Drug-induced liver injury from APAP overdose represents the leading cause of ALF in developed nations. To date, the antioxidant NAC is the sole first-line treatment for APAP overdose; however, it is only effective at the early stages of poisoning. In the liver, toxicity drives oxidative stress and mitochondrial dysfunction that leads to hepatocellular necrosis. Resident macrophages (KCs) respond to hepatic damage and initiate an inflammatory cascade of events, including the recruitment of monocytes and neutrophils. Given the central importance of metabolic programs in regulating the hepatic immune environment/responses, we sought to uncover the role of AMPK in AILI. We first aimed to assess whether systemic activation of AMPK with MK-8722 could influence the damage and immune activation seen during APAP overdose. Secondly, we spatially interrogated the importance of AMPK in hepatocytes (deletion mediated by Alb-CreERT2) or myeloid cells (deletion driven by LysM-Cre). Finally, while myeloid AMPK deletion had minimal effect on hepatic necrosis or circulating markers of liver injury, we next aimed to specifically target resident macrophages with NPs encapsulated with MK-8722. While we were able to specifically target KCs as early as 2 hours, activation of hepatic macrophage AMPK did not alter necrosis or immune infiltration. Overall, these results suggest hepatic AMPK signaling does not influence AILI.

4.3 Introduction

APAP is a widely used over-the-counter analgesic drug and a leading cause of acute liver injury when overdosed[40,41]. Those who suffer from chronic liver diseases like MAFLD are considered especially vulnerable (even taking the recommended doses)[42,43]. The majority of APAP is metabolized by hepatic glucuronidation and sulfation or excreted in the urine[41,44]. The remaining

APAP is converted to NAPQI via CYP450 in the liver[45]. This highly toxic metabolite is very quickly scavenged by GSH; however, during overdose, NAPQI can accumulate, leading to hepatic necrosis. Currently, NAC, a precursor of GSH, is the only clinically used treatment; however, this antioxidant is not without limitations and side effects. This treatment is only effective during the early stages of injury and only effective at high doses due to its low bioavailability. Adverse effects of NAC include allergic reactions, bronchospasm and potentially full liver failure resulting in death. Moreover, if the therapeutic window is missed, liver transplantation is the only viable option[46].

Hepatic necrosis is the culmination of several types of cellular stress. The accumulation of NAPQI leads to the formation of APAP adducts via interactions with protein sulfhydryl groups[47]. NAPQI induces mitochondrial oxidative stress and mitochondrial permeability transition pore opening and subsequent DNA fragmentation, resulting in hepatocellular necrosis and a massive release of DAMPs. Hepatic DAMPs, such as nuclear and mitochondrial DNA, HMGB1 and ATP, are recognized by residential macrophages called KCs through TLRs[35,343,344]. KCs and other hepatic immune populations secrete proinflammatory cytokines for the recruitment of monocytes and neutrophils. While many studies have investigated the roles of myeloid populations using selective depletion or neutralizing antibodies, their relative importance seems to be dependent on the stage of injury[344]. Overall, immune-mediated signaling that aggravates cellular injury early is necessary for the clearance of cell debris and hepatic regeneration during the resolution stage.

AMPK is serine/threonine kinase and a master metabolic regulator. Through its ability to sense energy nucleotides and nutrients, AMPK suppresses anabolic and upregulates catabolic pathways

in response to low cellular ATP and nutrient deprivation[171]. It has been established that AMPK modulates aspects of macrophage polarization and metabolism[246–251]. Briefly, macrophage AMPK activity is suppressed by proinflammatory stimuli like LPS[246]. This aligns with the drastic increase of proinflammatory mediators when AMPK signaling is abolished. On the other hand, activation of AMPK skews macrophages toward an anti-inflammatory phenotype[256,257]. In the setting of acute injury, myeloid AMPK deficiency impaired both lung and skeletal muscle repair and regeneration through the proinflammatory skewing of macrophages[256,257]. Recently, in a model of liver ischemia and reperfusion, AMPK was found to blunt hepatic necroptosis and inflammation through phosphorylation and inhibition of RIPK1[259]. In addition to acute injury models, a vast body of literature demonstrates the importance of macrophage AMPK signaling during chronic low-grade inflammation of atherosclerosis, obesity and fatty liver disease[171,333].

In response to APAP overdose, AMPK activity is suppressed. The use of a broad-spectrum inhibitor of protein kinase C suggested that protein kinase C activation may be at least in part responsible for this suppression[345]. However, AMPK activation with metformin and a wide range of polyphenols (amongst other compounds) have proven to be beneficial against APAP-induced necrosis[346–352]. Moreover, A-769662, which is one of the first discovered allosteric and direct activators of AMPK, when delivered as a priming dose, was shown to attenuate hepatic necrosis 6 hours post-APAP overdose[353]. AMPK activation resulted in increased ATP production through glycolysis, thereby compensating for ATP depletion that occurs during APAP-induced mitochondrial stress.

The beneficial effect of AMPK signaling on APAP-induced injury was observed early in the cellular response, and questions remain as to the effect of AMPK during peak injury. To address this knowledge gap, we used systemic and targeted delivery of a second-generation allosteric AMPK activator in combination with models of hepatic and myeloid-specific AMPK deletion. Both basal AMPK in the hepatocellular and myeloid compartments did not affect AILI or the hepatic immune populations. Systemic activation of direct pan-AMPK activator MK-8722[199] , as well as NP-mediated targeting of KC AMPK, were equally ineffective against AILI.

4.4 Material and Methods

Mice: All mice used in this study were male mice on C57Bl/6J background and 7-13 weeks old at the time of APAP injection. All mice were fed a standard chow (Teklad Global 18% Protein Rodent Chow Diet T.2018.15 – Envigo/Inotivco) and housed in a barrier facility with a 12-light/12-hour dark cycle (7 pm-7 am dark). C57Bl/6J mice were obtained from Jackson Laboratory (000664) and subsequently maintained at the University of Ottawa. Generation of *Prkaa1*$^{fl/fl}$ and *Prkaa2*$^{fl/fl}$ mice have been previously described[215,329]. For deletion of AMPK in myeloid cells, double *Prkaa1/2*$^{fl/fl}$ mice (referred to as Flox) were crossed with mice that were hemizygous for Cre recombinase under the control of the Lysozyme M promoter[330] (LysM-Cre and referred to as MacKO). For hepatocyte-specific AMPK deletion, double *Prkaa1/2*$^{fl/fl}$ mice were crossed to Albumin Cre-ERT2 (Alb-Cre) positive mice (referred to as HepKO)[215]. HepKO (including Flox controls) received 1 mg of tamoxifen (in 10% ethanol and 90% sunflower oil) via *i.p.* injection for 5 consecutive days and left to recover for two weeks prior to experiments. MacKO and associated Flox control mice that were directly compared to HepKO also received tamoxifen. All animal protocols were approved by the uOttawa Animal Care Committee (BMIe3742).

Mild AILI and AMPK Activation: Overdose was achieved by fasting for 12 hours (3 hours after the start of the dark cycle – 10 pm to 10 am) to normalize hepatic GSH across biological replicates[354]. The following day, mice were injected with 300 mg/kg i.p. of APAP (15 mg/mL in sterile 0.9% saline kept at 25°C), and food was replaced. Mice were monitored for clinical endpoints for 8 hours post-injection. The AMPK activator, MK-8722, was provided by Merck. Systemic administration of 10 mg/kg MK-8722 (0.25% methylcellulose, 5% Tween80, 0.02% SDS in sterile water[199]) was delivered *i.p.*, 1 hour prior to APAP injection. Targeted administration of MK8722 (3 mg/kg packaged in PLGA-PEG NP or empty NP and resuspended in saline) was delivered via the tail vein directly after injection of APAP. All cohorts injected with PLGA-PEG NP received the same amount of polymer between empty NPs and NP-MK8722.

Generation of PLGA-PEG NPs: All NPs were synthesized via the nanoprecipitation method[355]. NP-MK8722: PLGA 10K -PEG 5K solution was prepared in acetonitrile at 10 mg/mL concentration. MK-8722 solution was prepared at 1mg/mL concentration in acetonitrile. For NP development, desired amounts of PLGA-PEG and MK-8722 solutions are mixed at a 10:1 w/w ratio and added dropwise to nuclease-free (or DI) stirring water while maintaining a 10:1 v/v ratio of water to organic solvent. NPs were stirred at room temperature for 4-5 hours and filtered sequentially through sterile 0.45 μM syringe filters. The NPs were collected and purified by centrifugation using microsep advance centrifugal devices (Pall, MWCO 100kDa). The concentrated NPs were washed twice with deionized water and resuspended in H_2O or PBS. Empty-NPs: NPs without MK-8722 were prepared similarly by replacing the MK-8722 solution with acetonitrile. NP-Alexa Fluor A50: Alexa 750-conjugated PLGA polymer solutions were

prepared in acetonitrile at 10mg/ml. For Alexa-750-NPs, a 1-2:10 w/w ratio of Alexa Fluor 750-PLGA and PLGA-PEG solutions were mixed and added dropwise to water (10:1 v/v ratio of water to organic solvent) and stirred in the dark for 4-5 hours. The NPs were concentrated and purified by centrifugation using microsep advance centrifugal devices (Pall, MWCO 100 kDa). The concentrated NPs were washed twice with deionized water and resuspended in H_2O or PBS. Size measurements of all NPs were performed using ZetaView based on the nanoparticle tracking analysis technique[356]. To measure their sizes, 10-20 µL of concentrated NPs were diluted in 10-20 mL of water or PBS. MK-8722 concentrations in the NPs were measured by HPLC. For this, a calibration curve was prepared by using different concentrations of MK-8722 in (1:1 acetonitrile: H_2O) in HPLC. MK-8722 was eluted using the C18 column with acetonitrile: H_2O mobile phage with a gradient. For MK-8722 concentration in the NPs, 80-100 µL of NPs were dissolved in 1:1 acetonitrile: H_2O and vortexed for 30-40 mins to break down the NPs before injecting them for HPLC.

Histology: Intact livers were perfused with PBS via the left ventricle and fixed in 30 mL of 10% neutral buffered formalin for 24 hours. Following fixation, samples were transferred to 70% ethanol and processed at the University of Ottawa Louis Pelletier Histology Core Facility. Samples were paraffin-embedded, microtome sectioned and stained with H&E. Quantification of necrosis was determined by whole-section H&E staining and expressed as % necrotic area using QuPath[331].

Serum and liver lysates assay: Terminal blood was collected via cardiac puncture of the left ventricle and placed on ice. Serum was collected from clotted blood by centrifugation. The perfused liver was snap-frozen in liquid nitrogen and chipped on dry ice for analysis. Serum ALT,

AST and ALP were measured using the Beckman Coulter AU480 clinical chemistry analyzer at the Pathology core at the Toronto Centre for Phenogenomics.

Flow cytometry analysis: The remaining perfused liver (after collection for histology and snap-frozen samples) was weighed for cell count normalization. Tissues were gently minced in 10 mL digest buffer composed of complete DMEM (Wisent – 3190005-CL with 10% FBS, 1% penicillin-streptomycin) with 0.5 mg/mL collagenase IV (Millipore Sigma – C5138) and 50 U/mL DNase I (Millipore Sigma – 1010459001) and submerged in ice. Following 5 minutes of warming at 37 °C, liver digests were incubated and shaken at 200 rpm for 20 minutes. Following the incubation, digests were submerged in ice and digest buffer was diluted with 10 mL of cold complete DMEM. In the 4 °C room, digested livers were passed and plunged through a 100 μm cell strainer with an additional 15 mL of cold complete DMEM. Initial enrichment of hepatic NPCs was achieved via 50 x g centrifugation for 5 minutes, and collection of the supernatant and pelleted hepatocytes was discarded. NPCs were then pelleted at 500 x g centrifugation for 5 minutes and resuspended in 5 mL of 28% Opti-Prep (16.8% iodixanol, Fisher – NC1339550) prepared in 1% FBS and 5 mM EDTA (gradient solution). Gradients were prepared with 2 mL of basal DMEM overlay and gentle layering of resuspended NPCs using a Pasteur pipette placed at the bottom of the 15 mL conical tube[357]. Gradients were then centrifuged at 1500 x g for 25 minutes with the deceleration brake removed. NPCs were collected between both phases and washed with PBS prior to staining for flow. Blood was collected with 10 μL of 0.5 M EDTA and kept on ice until ready until the end of the tissue harvest. Blood was diluted in 9 mL of RBC lysis buffer and incubated for 10 minutes at RT then placed on ice. Blood leukocytes were pelleted at 500 x g centrifugation and resuspended in 1% FBS PBS, followed by flow staining (**see Table S4.1**). All samples were acquired on the

Cytek® Aurora 5L UV-V-B-YG-R with preset optimized voltages. For the localization of NP-A750, we repeated the same protocol apart from the tissue digestion. To ensure hepatocyte viability, mice were first perfused through the vena cava with a HEPEs buffer containing EDTA (pH 7.4) followed by another HEPEs buffer (pH 7.6 with $CaCl_2$) with 0.5 mg/mL collagenase IV (Millipore Sigma – C5138).

Statistics: GraphPad Prism software (version 9.5.1) was used for all statistical analysis. Data from Figure 4.1 was analyzed by one-way ANOVA with Dunnett's test for multiple comparisons of Flox vs. MacKO or HepKO. Data from Figure 4.2 and S4.3 was analyzed by unpaired two-tailed t-test. Data from Figure 4.4, S4.1 and S4.2 were analyzed by two-way ANOVA with comparisons where a Tukey's Multiple comparisons test. Statistical outliers were identified by the ROUT method with a Q value of 1%.

4.5 Results

Basal hepatocellular and macrophage AMPK do not influence APAP-induced necrosis and immune infiltration. There exists an extensive body of literature on the implications of hepatocellular AMPK deficiency and activation[171,333]. Mostly in the context of lipid homeostasis, AMPK activation reduces hepatic steatosis. In the realm of NASH-induced hepatocellular death, AMPK phosphorylates and inhibits pro-apoptotic Caspase-6[281]. Recently, it was found that hepatic AMPK also modulates acute metabolic stress-induced apoptosis and inflammation through inhibition of RIPK1[259]. To address whether AMPK regulation of different hepatic compartments could affect APAP-induced injury, we examined APAP overdose in male Flox, MacKO or HepDKO mice. Following 24 hours of APAP overdose, there was clear evidence of hepatic

necrosis as indicated by the absence of hematoxylin stain (DNA fragmentation), immune infiltration and coagulation (**Figure 4.1A**)[354]. Quantification of % necrotic area showed that AMPK deficiency in either the myeloid cells or hepatocytes had no effect, a result that was corroborated with the quantification of circulating liver enzymes (**Figure 4.1B**). Moreover, when assessing the resolution phase of AILI (48 h), macrophage AMPK signaling seemed to play no role (**Figure S4.1A, B**). Although hepatic AMPK signaling was insufficient to influence liver injury, we were interested in whether AMPK deficiency could influence the immune response elicited by APAP overdose. As expected, in response to the release of hepatic DAMPs, there was significant immune infiltration (compared to saline–hashed line) of primarily monocytes and neutrophils, populations that also predominated in the blood (**Figure 4.1C, D**). Regarding the residential macrophage population, we observed an increase in the total number of KCs (**Figure 4.1C**). In contrast to the reported literature[343], within this timeframe, this is most likely due to localized proliferation. Despite the striking immune response, we observed no differences in immune infiltration or KC population number between genotypes.

Systemic AMPK activation does not protect against hepatic necrosis. Several studies have reported the protective effect of indirect activators of AMPK, including a variety of polyphenols and metformin[346,348,351,352]. To our knowledge, the only allosteric activator tested has been A-769662. Specifically, following a 6-hour overdose, A-769662 pretreatment replenished cellular ATP, thereby protecting against hepatic necrosis[353]. To expand on the findings of Hwang *et al.* (2015) and address the crosstalk of dying hepatocytes with the immune system, we assessed AMPK activation following 24-hour overdose. Similar to A-769662 dosing, WT mice were pretreated with a direct allosteric activator MK-8722 (10 mg/kg) 1 hour prior to APAP overdose. Following

24 hours of injury, hepatic necrosis and serum liver enzymes were quantified, and we concluded that systemic priming of AMPK did not ameliorate AILI (**Figure 4.2A-C**).

PLGA-PEG NPs target hepatic macrophages. Given that systemic delivery of MK-8722 did not alter APAP-induced injury, we questioned whether targeting hepatic macrophages could accelerate liver repair. NPs have been gaining traction as an efficient and modular drug delivery system. PLGA-PEG NPs serve as an inert vehicle for the packaging of different compounds[358,359]. Moreover, while the target of specific tissues and tumours may be challenging, NPs typically accumulate in the liver[360,361]. To validate that our PLGA-PEG NPs were localized to the liver, we injected NP-A750 through the tail vein and assessed fluorescence. As expected, intra-vital imaging showed that NPs accumulate in the liver as early as 2 hours with evidence of localization to the kidneys. Importantly, fluorescence is still detected exclusively in the liver 24 hours later (**Figure 4.3A**). Size distribution measured by the ZetaView confirmed that the PLGA-PEG NPs were approximately 100 nm in diameter[362]. Given the localization of KCs in the liver sinusoids and the size of the particles, their accumulation in hepatic macrophages is expected. Flow cytometry confirmed that the fluorescence detected in the whole liver tissue after 2- and 24-hours post NP-A750 injection was due to the NP accumulation in KCs (**Figure 4.3B**). Finally, we confirmed that empty NPs were truly inert and did not influence hepatic necrosis and liver enzymes in both Flox and MacKO mice (**Figure S4.2**).

Targeted activation of KC AMPK does not alter necrosis or immune infiltration. Since we confirmed the targeting of hepatic macrophages, we looked to package and deliver MK-8722 in PLGA-PEG NPs. Flox and MacKO mice were injected with 300 mg/kg APAP following a 12-

hour overnight fast. Immediately following APAP, 3 mg/kg MK-8722 encapsulated in PLGA-PEG NPs was administered via the tail vein. Quantification of hepatic necrosis revealed that targeted activation did not influence liver injury in either Flox or MacKO mice (**Figure 4.4A, B**). This was also reflected in the levels of serum ALT and AST (**Figure 4.4C**). Assessment of hepatic infiltration of monocytes and neutrophils and the frequencies present in circulation were only influenced by AILI (**Figure 4.4D, E**), and the KC populations were also unaffected (**Figure 4.4D**). We did observe, however, that NP-MK8722 treatment (relative to empty NPs) in MacKO mice unexpectedly increased hepatic neutrophil infiltration, highlighting the possible leakage of MK-8722 and activation of AMPK in non-myeloid cell populations (**Figure 4.4D**).

4.6 Discussion

While histologically, AILI displays features of oncotic necrosis (cellular swelling) and karyolysis (dissolution of nuclear material), the death signaling pathways have been classified as a type of programmed necrosis with some features of apoptosis and necroptosis[363,364]. These mechanisms include translocation of BCL2-associated X to mitochondria and cytochrome C release, as well as induction of RIPKs [365,366]. Despite the APAP induction of RIPK1, Iorga *et al.* (2021) determined with a hepatocyte-specific RIPK1 kinase-dead (RIPK D138N) and knockout, that it was not the kinase activity of RIPK1 that was important, but that RIPK1 serves as a platform for A20 scavenging and upregulation of ASK-mediated phosphorylation of JNK[367]. Taking this into consideration, it is unlikely that hepatocyte AMPK mediates APAP-induced cell death through inhibition of RIPK1 activity. However, it is possible that myeloid AMPK-RIPK1 signaling may be important. In a model of apoptosis like liver ischemia-reperfusion, it is possible that we would observe a higher degree of cell death and more immune infiltration in our AMPK HepKO mice[259].

Similarly, given the mechanisms of APAP-induced hepatocellular death, the AMPK-Caspase 6 pathway observed in a mouse model of NASH should not be relevant in our model[281]. Overall, we observed that hepatocyte AMPK deficiency did not modulate hepatic necrosis and, therefore, did not influence immune infiltration.

In response to hepatic DAMPS, KCs are activated and responsible for the recruitment of various immune mediators like neutrophils and monocytes. Here, we show that macrophage AMPK deficiency does not modulate hepatic necrosis or immune infiltration 24 hours post-APAP. Several studies have attempted to decipher whether KCs play a protective role in APAP overdose, though no consensus has emerged[49–55]. Similarly, blocking neutrophil infiltration has been shown to both aggravate and attenuate hepatic necrosis[58–61]. Proinflammatory monocytes, on the other hand, aggravate liver injury early on, but their macrophage descendants are also necessary for phagocytosis during the resolution phase[50,54,62–64,66]. Our model results in the complete deletion of both catalytic subunits of AMPK (α1 and α2) in LysM-expressing cells. While this predominantly affects monocytes and macrophages, potential AMPK deficiency in neutrophils should be considered as a potential caveat[368]. Moreover, given the conflicting evidence as to the role of KCs and neutrophils in APAP overdose, it is not possible to discern how AMPK deletion in specific myeloid populations may influence injury. Nevertheless, assessment of the role of KC-specific AMPK in the initiation of inflammation warrants investigation.

Most *in vitro* studies looking at macrophage AMPK signaling and immunometabolism have used LPS for TLR4 stimulation[246,248,250]. In the realm of metabolic syndrome and associated diseases (atherosclerosis, fatty liver, and obesity), LPS and other microbial products have significant

influence over hepatic and systemic inflammation[113,369,370]. Apart from models of skeletal injury and liver ischemia-reperfusion, many of the physiological implications of macrophage AMPK *in vivo* were in the contexts of these diseases[171]. Like skeletal injury, AILI evokes a sterile inflammatory response stemming from the release of hepatic DAMPs like HMGB1[35,344]. A recent study compared the inflammatory phenotype of LPS to different redox states of HMGB1 and observed that while a transcriptomic analysis showed an overlapping gene expression profile, HMGB1 stimulation induced a polarization state that was distinct compared to LPS[371]. Given that not all TLR4 agonists are the same, it would be interesting to expand our knowledge on macrophage AMPK signaling and immunometabolism with different hepatic DAMPs in a cell culture system. To date, it has been reported that AMPK activation with AICAR and metformin induces HMGB1 engulfment and inflammation[372]. In addition, *in vitro* stimulation with specific hepatic DAMPS, future work could look at AMPK deletion in cultured BMDMs and KCs treated with conditioned media from APAP-treated hepatocytes. This approach would be the first step prior to the *in vivo* investigation of APAP overdose in KC AMPK KO mice[121]. Finally, in addition to LPS, IL-10 treatment in BMDMs activates AMPK. However, despite the relevance of IL-10 in the resolution of APAP-induced injury, we observed the same degree of residual necrosis 48 hours post-injection in our AMPK MacKO mice.

Basal AMPK activity in the macrophage and hepatocyte compartments does not influence AILI; this may be due to the reported suppression of activity. To address this, we introduced an allosteric activator of AMPK. MK-8722 is a potent and specific pan-AMPK activator that binds to the ADaM site[199]. In a fluorescent reporter of AMPK activation, Ex Rai AMPKAR clearly showed MK-8722 activates all compartmentalized pools of AMPK, including in the nucleus[373]. While mitochondrial

and lysosomal AMPK were still activated in the LKB1 KO MEFs, maximal cytoplasmic activation still relied on the upstream kinase for phosphorylation[204]. To our knowledge, whether LKB1 activity is downregulated during APAP overdose is unknown. Nonetheless, Hwang *et al.* (2015) showed that another allosteric activator, A-769662, attenuated APAP-induced necrosis by buffering ATP depletion through increased glycolysis[353]. While this work provided strong evidence as to the benefit of priming hepatic AMPK, we did not observe protective effects with systemic delivery of MK-8722. Although we were assessing injury after 24 hours of APAP, we may directly compare the effects of MK-8722 to their findings by assessing necrosis 6 hours post-overdose.

To exclude the effects of AMPK activation on intracellular processes of hepatocellular death, we implemented a drug delivery system to target KCs[361]. Unlike systemic delivery of MK-8722 1-hour prior to APAP overdose, we chose to administer NP-MK8722 immediately following APAP injection. Moreover, although this precedes KC activation by a few hours, this timing allowed for KC uptake and subsequent release of MK-8722. Moreover, we selected this time point to avoid any delivery issues associated with APAP-induced dysfunction in the microcirculation[46]. While we did not observe any treatment effects with targeted activation of KC AMPK, it is possible to make several adjustments to the formulation. These include altering the rate of drug release and increasing retention time in circulation (we observed NP-A750 present in the kidneys)[358,359,374]. Importantly, A-769962 encapsulation in the same formulation PLGA-PEG NPs shows that compared to free drug, NP delivery to cultured hepatocytes results in a more potent and prolonged activation of AMPK (**Figure S4.4**). This highlights not only the therapeutic advantages of NPs but also the stability of the drug after endocytosis and release from the lysosome[374].

Macrophage AMPK signaling has proven to be anti-inflammatory and protective in a multitude of inflammatory contexts including acute lung and skeletal muscle injury[256,257]. Recently, the protective effect of hepatic AMPK has been extended to sterile hepatic inflammation concerning hepatic apoptosis during ischemia-reperfusion[259]. In the setting of AILI, we observed that AMPK signaling and activation in both hepatocytes and macrophages is inconsequential to APAP-induced hepatic necrosis and inflammation. This discrepancy between our findings and that of Zhang *et al.* (2023)[259] sheds light on the relevance of hepatic AMPK across different types of liver injury and its role in particular mechanisms of cell death and inflammation.

4.7 Figures

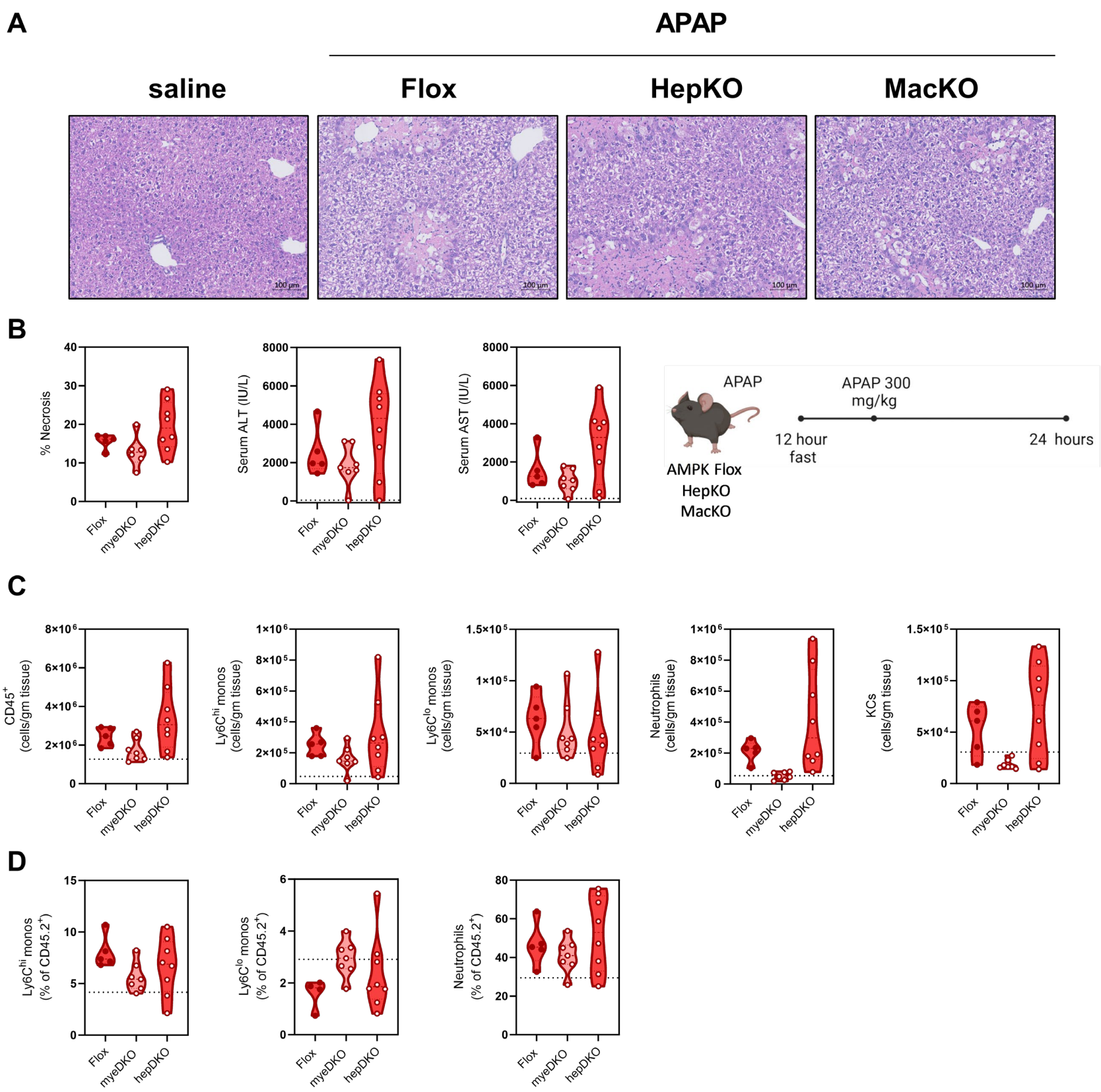

Figure 4.1. Hepatocellular and macrophage AMPK do not affect AILI. A) Experiment schematic and representative H&E-stained liver sections of APAP-overdosed male Flox, MacKO and HepKO mice (20x magnification, 100 µM scale bar), B) Quantification of hepatic necrosis (necrosis expressed as a percentage of whole liver section area), C) Serum levels of liver injury markers ALT and AST. D) Hepatic immune cells (NPCs); total leukocytes ($CD45^+$, live cells), KCs ($TIM4^+$, $F4/80^{hi}$ $CD11b^{lo}$, $CD45.2^+$, live cells), monocytes ($CD115^+$, $Ly6G^-$, $F4/80^{lo}$ $CD11b^{hi}$, $CD45.2^+$, live cells), neutrophils ($Ly6G^+$, $F4/80^{lo}$ $CD11b^{hi}$, $CD45.2^+$, live cells), E) Blood immune cells; monocytes ($CD115^+$, $Ly6G^-$, $F4/80^{lo}$ $CD11b^{hi}$, $CD45.2^+$, live cells), neutrophils ($Ly6G^+$, $F4/80^{lo}$ $CD11b^{hi}$, $CD45.2^+$, live cells). Data was analyzed by One-way ANOVA with Dunnett's test for multiple comparisons of Flox vs. MacKO or HepKO. Saline groups comprised 2 mice, and APAP groups comprised 5-8 mice. The saline average is represented by a hashed line.

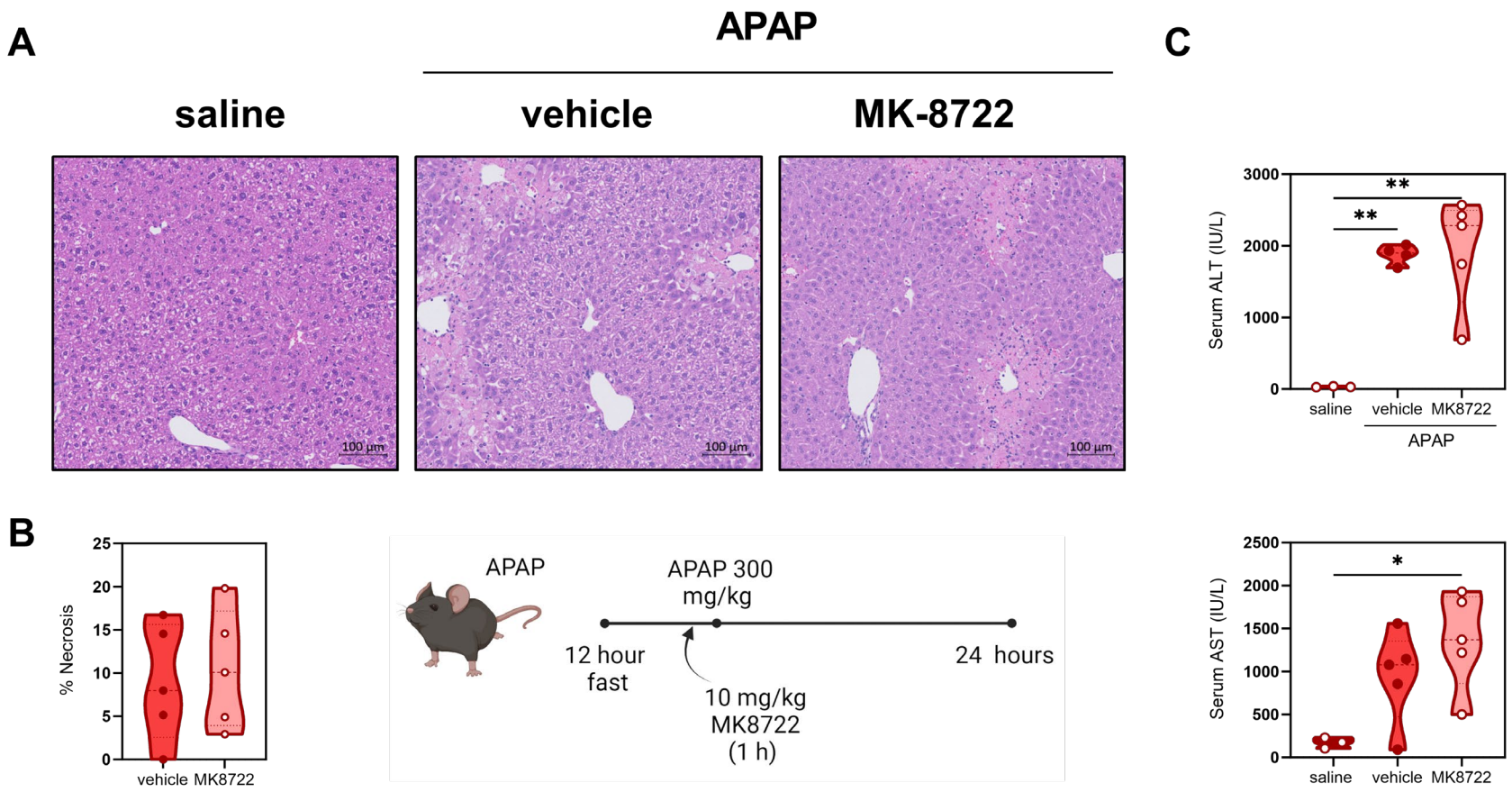

Figure 4.2. Systemic MK-8722 is not protective against APAP-induced hepatic necrosis. A) Representative H&E-stained liver sections of APAP-overdosed male WT mice injected 1 hour prior with systemic 10 mg/kg MK8722 (20x magnification, 100 µM scale bar), B) Quantification of hepatic necrosis (necrosis expressed as a percentage of whole liver section area), C) Serum levels of liver injury markers ALT and AST. Data was analyzed by unpaired two-tailed t-test to compare vehicle vs. MK8722 where * and **represent $p<0.05$ and $p<0.01$, respectively. Saline groups were comprised of 3 mice and APAP groups were comprised of 5 mice.

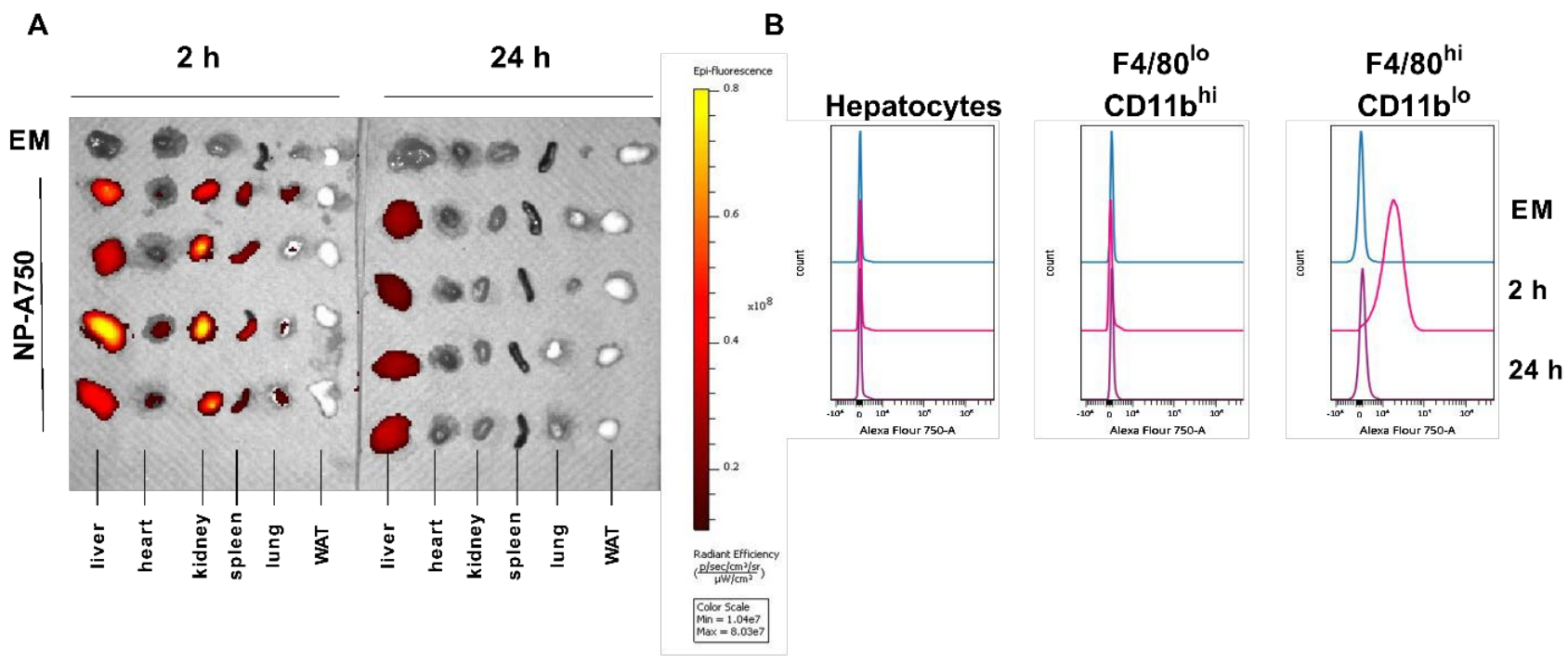

Figure 4.3. NPs accumulate in hepatic macrophages. Optical imaging (IVIS Spectrum) of PBS-perfused mouse tissues 2- and 24-hours post-injection of PLGA-PEG NPs conjugated with Alexa Fluor 750 (NP-A750) or empty NPs (EM), B) Representative flow histograms of NP-A750 fluorescence in hepatic populations - hepatocytes ($CD45.2^-$, live cells), monocytes and neutrophils ($F4/80l^oCD11b^{hi}$, $CD45.2^+$, live cells) and macrophages ($F4/80^{hi}CD11b^{lo}$, $CD45.2^+$, live cells).

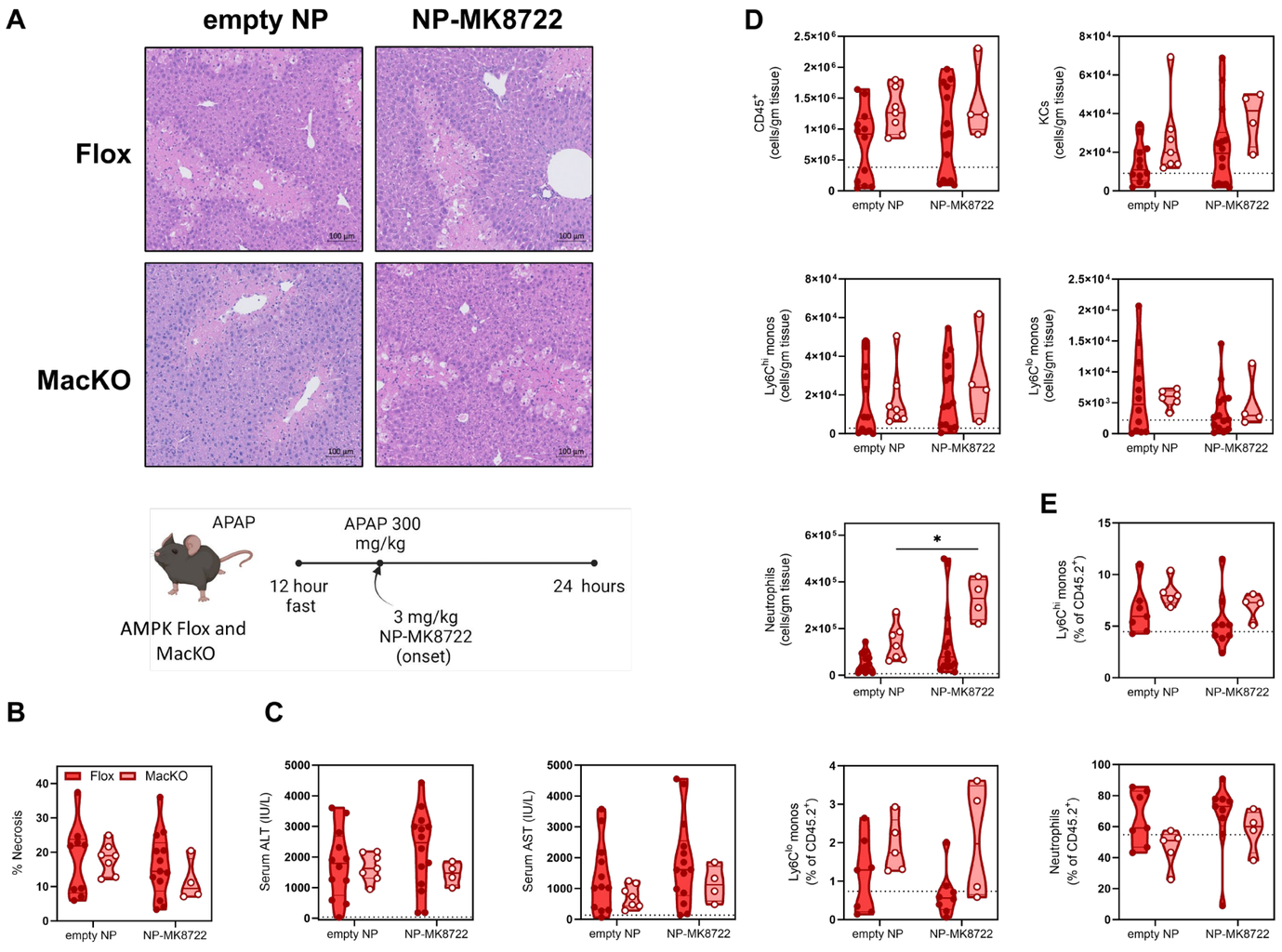

Figure 4.4. NP-MK8722 targeting of KC AMPK does not influence AILI. A) Experiment schematic and representative H&E-stained liver sections of APAP-overdosed male Flox and MacKO mice injected empty PLGA-PEG NPs (empty NP) or MK8722 encapsulated PLGA-PEG NPs (NP-MK8722) (20x magnification, 100 µM scale bar), B) Quantification of hepatic necrosis (necrosis expressed as a percentage of whole liver section area), C) Serum levels of liver injury markers ALT and AST. D) Hepatic immune cells (NPCs); total leukocytes ($CD45^+$, live cells), KCs ($TIM4^+$, $F4/80^{hi}$ $CD11b^{lo}$, $CD45.2^+$, live cells), monocytes ($CD115^+$, $Ly6G^-$, $F4/80^{lo}$ $CD11b^{hi}$, $CD45.2^+$, live cells), neutrophils ($Ly6G^+$, $F4/80^{lo}$ $CD11b^{hi}$, $CD45.2^+$, live cells), E) Blood immune cells; monocytes ($CD115^+$, $Ly6G^-$, $F4/80^{lo}$ $CD11b^{hi}$, $CD45.2^+$, live cells), neutrophils ($Ly6G^+$, $F4/80^{lo}$ $CD11b^{hi}$, $CD45.2^+$, live cells). Data was analyzed by Two-way ANOVA with Tukey's test for multiple comparisons where * represents $p<0.05$. Saline groups comprised 6 mice, and APAP groups comprised 4-11 mice. The saline average is represented by a hashed line.

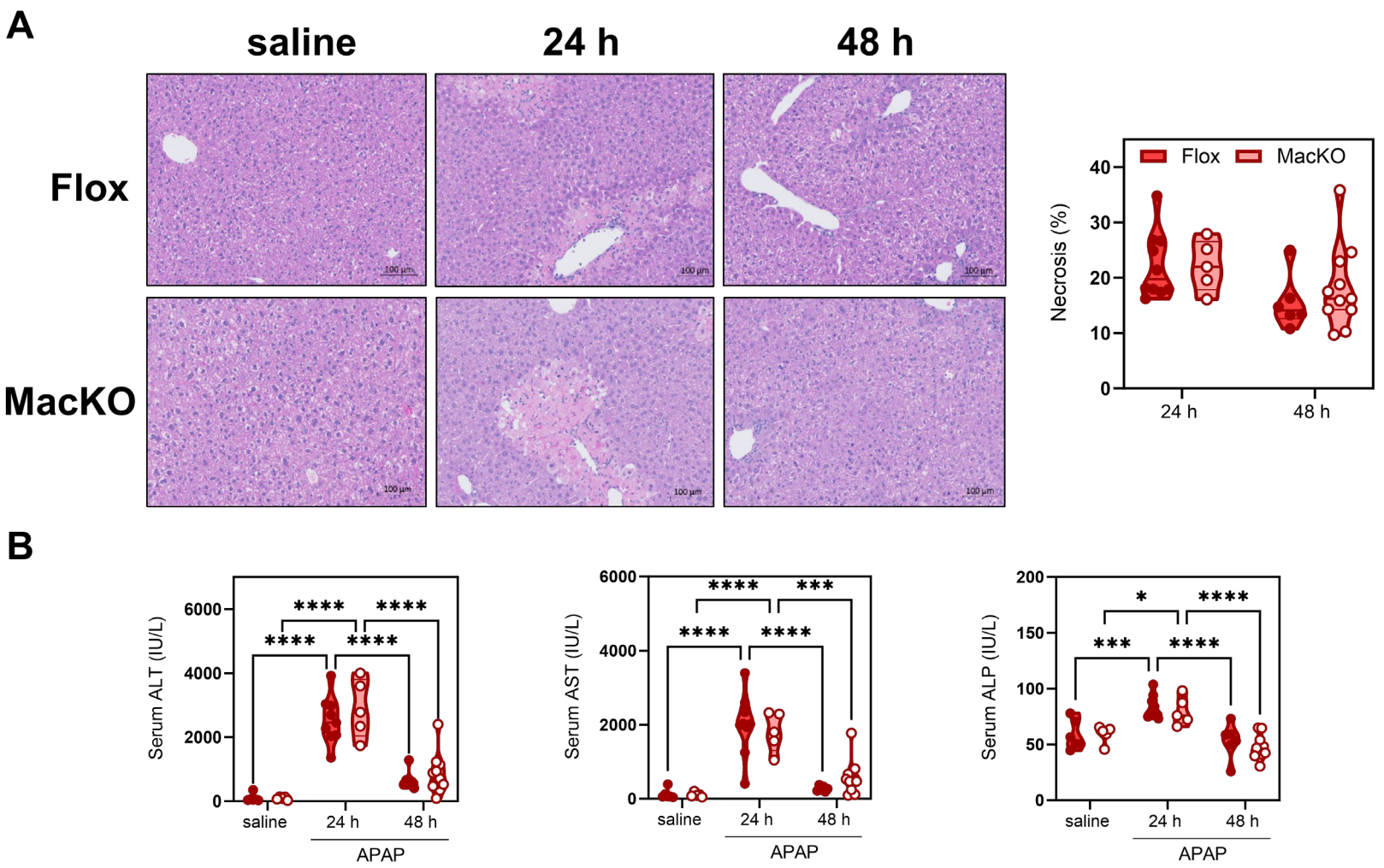

Supplemental Figure 4.1. Macrophage AMPK does not influence APAP-induced hepatic necrosis or recovery. A) Representative H&E-stained liver sections (20x magnification, 100 µM scale bar) from APAP-overdosed male Flox and MacKO mice and quantification of hepatic necrosis (necrosis expressed as a percentage of whole liver section area), B) Serum levels of liver injury markers ALT, AST, ALP. Data was analyzed by Two-way ANOVA with Tukey's test for multiple comparisons where *, *** and **** represent $p<0.05$,$p<0.001$ and $p<0.0001$, respectively. Saline groups comprised 5-6 mice, and APAP groups comprised 8-10 mice.

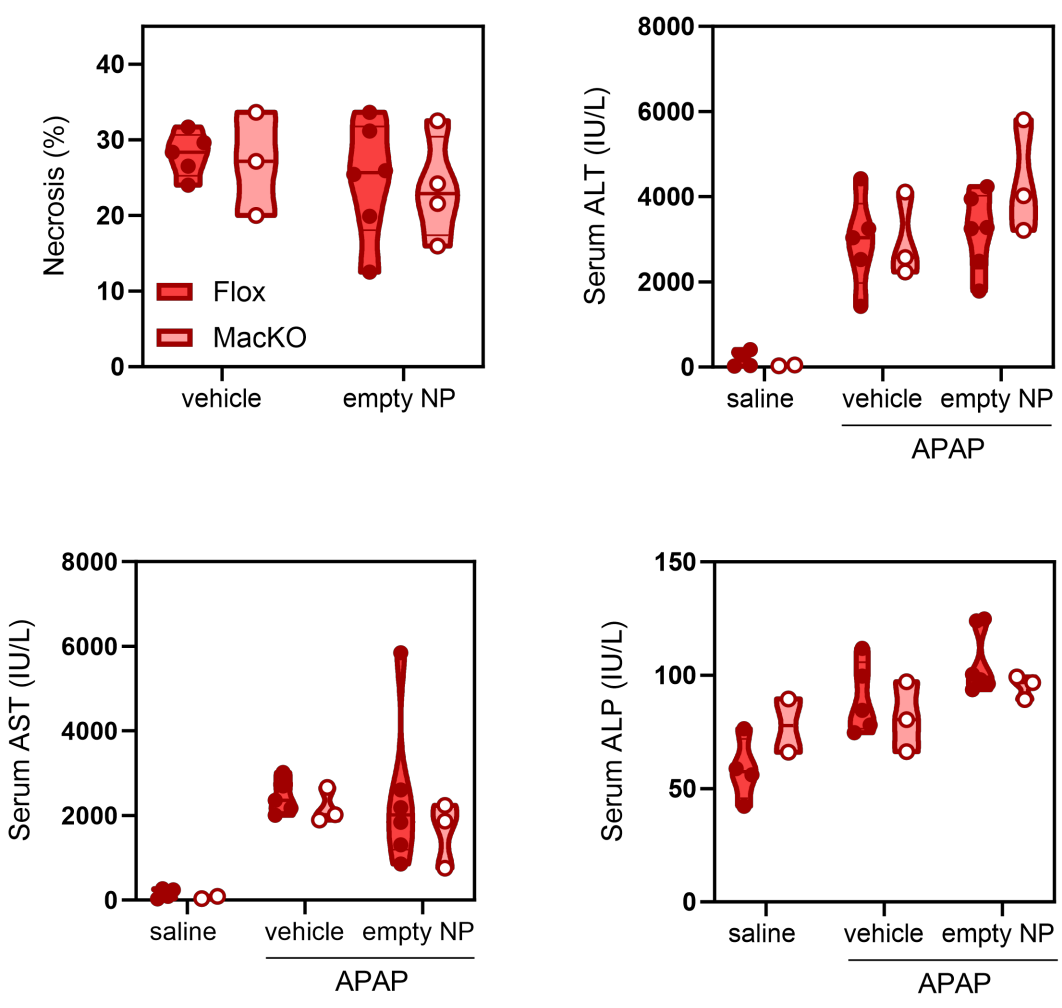

Supplemental Figure 4.2. Empty NPs exhibit no effect in AILI. Quantification of hepatic APAP-overdosed male Flox and MacKO mice injected with saline or empty PLGA-PEG NPs (empty NP) (necrosis expressed as a percentage of whole liver section area) and serum levels of liver injury markers ALT, AST, ALP. Data was analyzed by Two-way ANOVA with Tukey's test for multiple comparisons. Saline groups comprised 2-4 mice, and APAP groups comprised 3-6 mice.

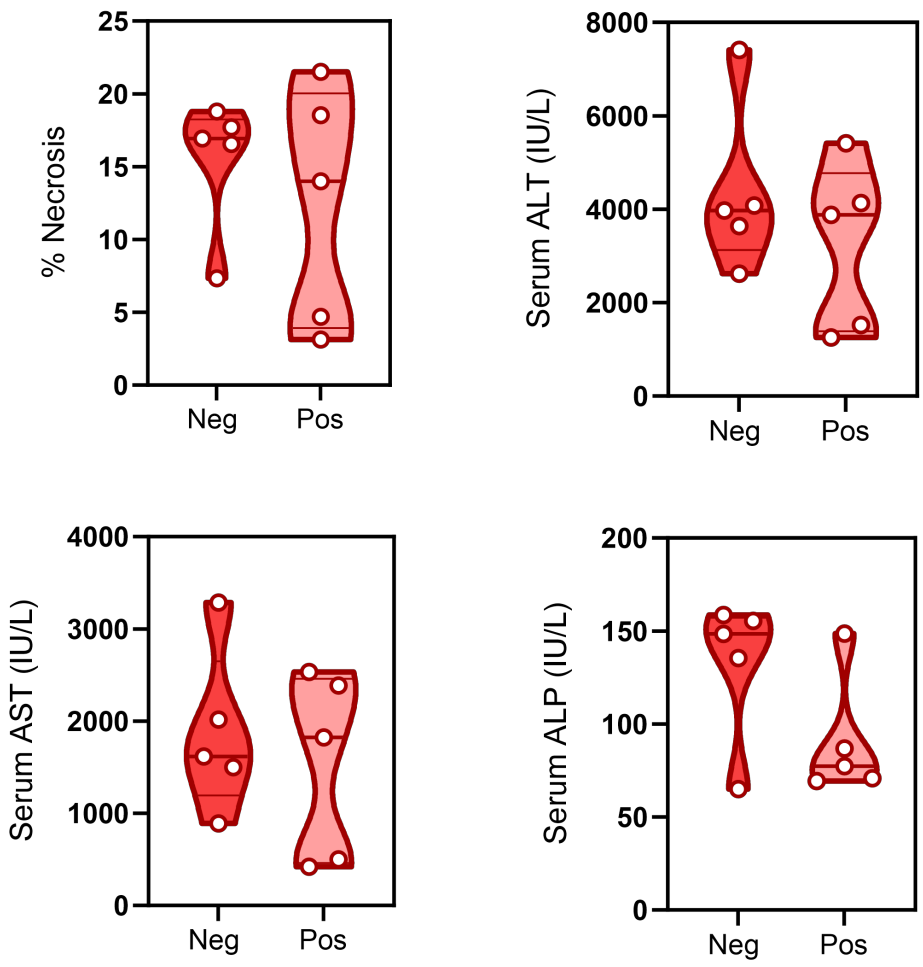

Supplemental Figure 4.3. LysM-Cre has no off-target effects on AILI. Quantification of hepatic APAP-overdosed male LysM-Cre mice (necrosis expressed as a percentage of whole liver section area) and serum levels of liver injury markers ALT, AST, ALP. Data was analyzed by unpaired two-tailed t-test. APAP groups comprised of 5 mice.

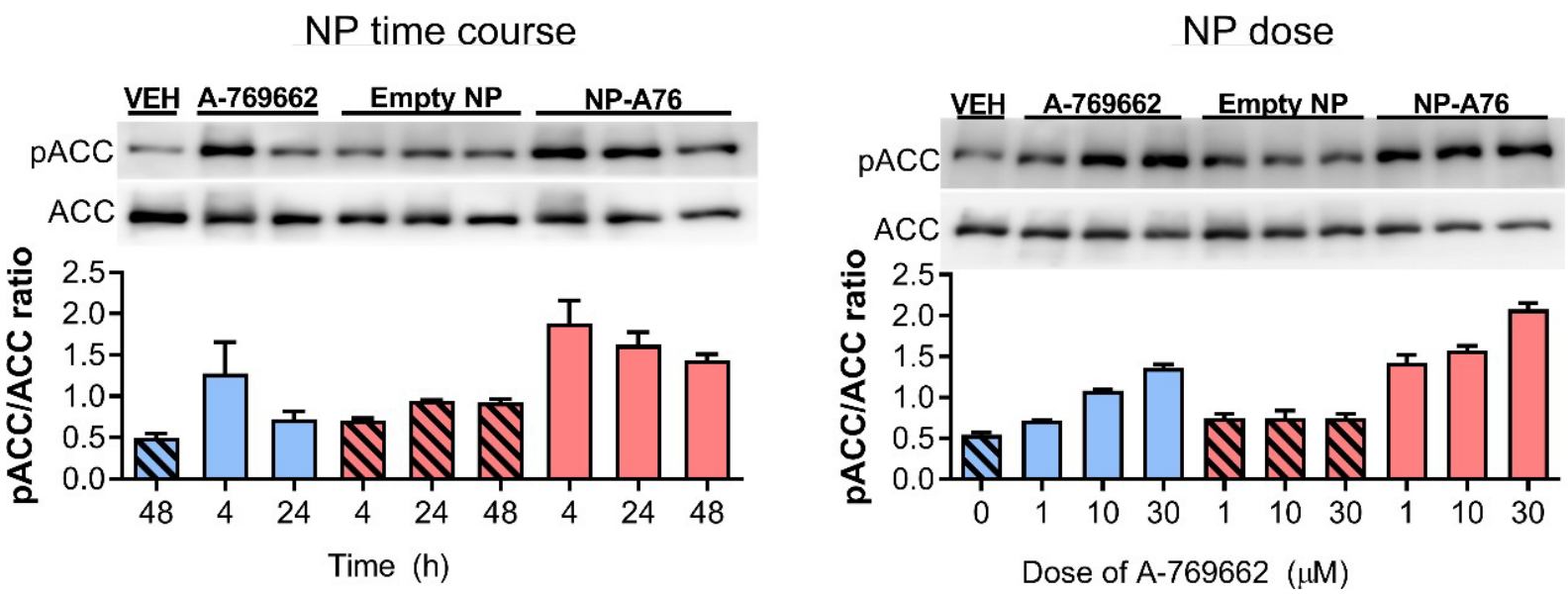

Supplemental Figure 4.4. NP-A76 exhibit a more potent and sustained activation of AMPK than free drug. Primary hepatocytes treated with vehicle (DMSO), A-769662, PLGA-PEG empty NPs (Empty NP) or A-769662 encapsulated PLGA-PEG NPs (NP-A76) A) pACC/ACC Western blots of time course (4, 24, 48 hours) treatment of 100 μM A-769662 and equivalent PLGA-PEG polymer amounts in empty NPs and NP-A76 B) pACC/ACC Western blots of different doses of A-769662 (10, 30, 100 μM) and equivalent PLGA-PEG polymer amounts in empty NPs and NP-A76.

Table S4.1 – Flow stain

Reagent	Catalog number (supplier)	Dilution
CD45.2-PE (clone 104)	45-0454-80 (eBioscience)	1:400
CD45.2-PerCP-Cy5.5(clone 104)	109808 (Biolegend)	1:400
CD11b-biotin (clone M1/70)	109808 133307 (Biolegend)	1:600
Streptavadin-BUV395	564176 (BD Bioscience)	1:200
F4/80-PE (BM8)	12-4801-82 (eBioscience)	1:100
TIMD4-Alexa Flour 647 (clone 21H12)	564177 (BC Bioscience)	1:400
Ly6G-FITC (clone 1A8)	127605 (Biolegend)	1:800
Ly6C-Alexa Flour 700 (clone HK1.4)	128024 (Biolegend)	1:600
CD115-BUV737 (clone AFS98)	750948 (BD Bioscience)	1:200
Live/dead blue	L34961 (Thermo Fisher)	1:500
CD16/CD32 (clone 93)	101302 (Biolegend)	1:250

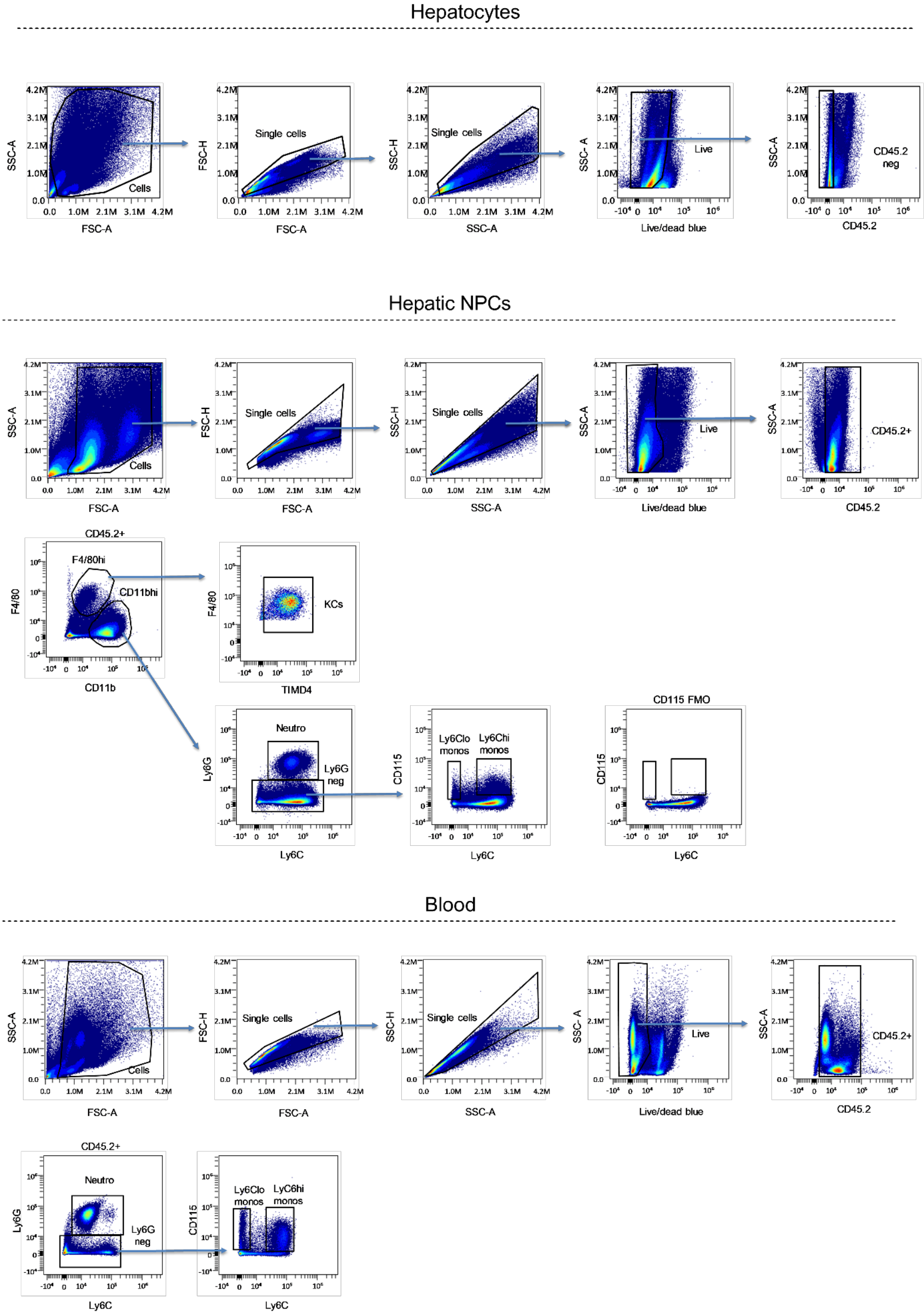

Supplemental Figure 4.5. Flow cytometry gating strategy for hepatic NPCs, blood leukocytes and hepatocytes. Gating strategy for flow analysis of hepatic immune cells (NPCs) (total leukocytes, KCs, monocytes, and neutrophils), blood leukocytes (monocytes and neutrophils) and hepatocytes.

4.8 Acknowledgments

The authors would like to thank the University of Ottawa Louise Pelletier Histology Core Facility for the processing, staining, and scanning of the liver tissues, as well as Dr. Vera Tang and the Faculty of Medicine Flow Cytometry and Virometry Core Facility (RRID: SCR_023306). BioRender was used to create the schematics (publication license MR25AFBM7S).

4.9 Funding

This research was funded by project grants from the Canadian Institutes of Health Research (CIHR) (PJT148634 to M.D.F) and a uOttawa Faculty of Medicine Translational Research Grant (M.D.F). J.R.C.N and C.P. were supported by Ontario Graduate Scholarships or Queen Elizabeth II Graduate Scholarship, and T.K.T.S was supported by a CIHR Vanier Scholarship.

Conflict of Interest statement: The authors have no conflict of interest to declare.

Chapter 5: General Discussion and Future Directions

The liver is susceptible to injury from insults ranging from toxins to overnutrition. While acute liver injury resolves quickly, chronic injury relies on fibrosis to maintain organ integrity. Common to both are hepatocellular death, activation of KCs in response to hepatic DAMPS and immune infiltration[375]. During the resolution phase of acute injury, infiltrating monocytes differentiate into phagocytic pro-resolving macrophages[62]. KC survival is affected in both acute and chronic injury; however, persistent damage leaves an immunological void that is replaced by MoKCs[118]. Like pro-resolving macrophages in acute injury, chronic low-grade inflammation triggers the differentiation of monocytes into temporary macrophages, including subsets such as LAMs[122–126].

This thesis research was particularly focused on whether macrophage AMPK signaling played a role in AILI and NASH, but first I wanted to assess the translational relevance of different mouse models of liver injury. While AILI is initiated and defined by a singular insult, the dynamics of NASH progression and its relationship to metabolic syndrome are difficult to model[129,135]. This is particularly true of NASH-induced hepatic fibrosis, where mouse models that achieve this phenotype are typically divorced from the other aspects of metabolic syndrome[129,135]. In **Chapter 2**, I aimed to overcome this limitation and remove the physiological barriers that chronic cold stress has on WD-induced NASH progression[148–151]. After 16 weeks of feeding, we observed that T_N-housed male mice gained more weight, had elevated liver injury enzymes and had a mild increase in liver TG. Female mice remained mostly protected, apart from increased expression of some profibrotic and macrophage marker genes. Induction of hepatic fibrosis was also limited to transcriptional upregulation in male mice. The most striking of all was the increased glucose

tolerance observed in T_N-housed male mice; however, IR was unaffected, highlighting that these mice may have improved insulin secretion (insulin measurements during the GTT would have been beneficial)[149]. Given these results, we highlighted that the implementation of fructose in the drinking water could exacerbate IR but that an overall investigation of T_N after 24 weeks of WD-feeding is warranted[90,129].

One of the most important considerations for this study is determining what temperature corresponds to the T_N zone. The strain of the mouse, age (as it relates to body)adiposity), and cage density (including bedding) can influence core temperature[295,312]. Like Giles *et al.* (2016), many studies looking at thermoregulation assess its effects on singly housed mice[148,311,376–378]. However, we are not alone in choosing group housing when it comes to looking at disease pathology[151,152,379]. Although the objective of this model was the development of hepatic fibrosis, we were interested in the relative effects of housing. For this reason, we chose to compare housing temperatures using the "conventional" group-housed setting implemented in NASH studies, instead of cold stressing our control group. Regarding the temperature range we selected, we and others have extrapolated from the thermoregulatory studies performed on singly housed mice. Moreover, an important limitation of this work is that for the reasons previously mentioned (age, adiposity), consistently maintaining mice within their T_N zone is not possible[295,312,380]. To add another layer of complexity, Škop *et al.* (2020) challenged the concept of the T_N zone by showing that energy expenditure fluctuates between the light and dark cycles, thereby affecting the temperature required to maintain mice at their T_N point[311]. It was their recommendation (amongst that of others) that C57BL/6J mice be housed at the lower T_N point of 29 °C since mice are better equipped to deal with heat conservation than dissipation.

In **Chapter 3**, we investigated the role of macrophage AMPK during NASH. Given that our TN model did not produce hepatic fibrosis, we selected a nutrient-deficient dietary model of NASH. CDAHFD-feeding accelerates NASH progression to the point of F2 fibrosis after only 8 weeks[142], while the "metabolically faithful" WD takes 24 weeks even with 2% cholesterol[129]. While there is a vast body of literature regarding hepatocellular and macrophage AMPK signaling[171,333], we are the first to assess how macrophage AMPK affects NASH-induced crosstalk in the liver. Specifically, while Galic *et al.* (2011)[258] look at the hematopoietic deletion of AMPK, KC AMPK signaling during liver injury has remained unexplored (apart from Zhang *et al.* (2023)[259] who looked ischemic-reperfusion injury using a *Prkaa1* fl/fl-LysM-Cre model). Moreover, this is an exciting time to study how AMPK may influence the immunometabolism of emerging macrophage subsets like MoKCs and LAMs[122–124,124,125]. Whole liver lysate analysis clearly shows the downregulation of AMPK during overnutrition. To overcome this suppression in the activity, we included metformin at low doses in the drinking water following 4 weeks of CDAHFD. Overall, our findings revealed that macrophage AMPK deficiency and metformin intervention did not affect any parameters of NASH or hepatic fibrosis in either male or female mice.

Despite these results, some important discussion points may reveal the appropriate future directions. First, as previously mentioned, within the NASH immune environment are heterogeneous populations of residential and infiltrating macrophages. Although our MacKO model targets primarily macrophages and monocytes, AMPK deletion in all these macrophage subsets may be an important confounder to consider. Only recently have these populations been identified, and the research on the immunometabolism of each subset has only begun to emerge.

While we did not observe an overall effect on NASH progression, it is possible that spatial transcriptomics could reveal whether AMPK influences the crosstalk of these subsets with other hepatic compartments[381]. Since KCs are spatially polarized to the periportal region (also observed during bacterial infection[382]), it would be especially interesting to see if AMPK could influence the immune zonation during NASH[116]. On the other hand, we could address KC AMPK signaling specifically using NP-based delivery of an AMPK activator. Importantly, we could prime KCs from the beginning to ensure activation prior to their NASH-induced depletion[118]. On the same note, another interesting avenue would be the investigation of KC AMPK signaling and immunometabolism during NASH onset and regression (replacement of CDAHFD with a low-fat control diet)[278].

Finally, we cannot rule out the effects of our dietary model. Regarding hepatocyte AMPK and metformin activation, choline deficiency impairs FAO[383], thereby eliminating one mechanism of AMPK-dependent reduction of hepatic steatosis. Moreover, given that CDAHFD-fed mice only exhibit mild IR and lack a high dietary intake of carbohydrates[142], it's possible that DNL is not a strong contributor to hepatic steatosis. This leaves metformin action on hepatocellular death (AMPK-Caspase-6[281]) and subsequent inflammation and fibrosis. Macrophage AMPK deletion would reveal the degree to which these effects are a consequence of inflammatory signaling. Overall, the lack of phenotype may be model-specific, and it is possible that the anti-inflammatory effects of macrophage AMPK would be more evident in another NASH model. Moreover, while our metformin regime would primarily target infiltrating macrophages, priming of KCs with an earlier intervention warrants investigation[118].

In sharp contrast to NASH-induced chronic injury, in **Chapter 4,** we addressed how AMPK signaling influences the dynamics of APAP-induced hepatic necrosis. We selected this model of acute liver injury for several reasons. First, AILI evokes a sterile inflammatory response, unlike NASH, since APAP overdose does not affect the gut-liver axis[35,344]. This allowed us to address macrophage AMPK signaling after exposure to hepatic DAMPs, while most studies worked either directly with LPS or in a disease setting that involves gut microbial products (NAFLD, atherosclerosis, obesity)[171,333]. Another reason is that, unlike our CDAHFD model, 24 hours of APAP overdose does not involve macrophage subsets other than KCs. Finally, AILI is directly translational to human ALF, which requires alternatives to NAC treatment and liver transplantation[41]. Overall, AILI is an acute translational model of DAMP-mediated activation of KCs that informs on crosstalk between the immune response and hepatocellular death. However, a limitation of this model is the sex dependence of hepatic injury. While we used male and female mice in **Chapters 2** and **3**, female mice are relatively protected against APAP overdose[132] and, therefore, require high doses, which I tested and verified. Since this prevents cross-sex comparison, we chose the more susceptible sex. Overall, for this chapter, we assessed the effects of both hepatocellular and macrophage AMPK signaling and observed no significant effects on hepatic necrosis or immune populations. In addition to AMPK deficiency in these compartments, systemic activation and targeted activation of KC AMPK with NP-MK8722 also proved to be inconsequential. Future work could look to modulate the rate of NP drug release and assessment of the activation during the resolution phase of AILI. We could also compare our systemic MK-8722 delivery to Hwang *et al*. (2015)[353] and determine whether AMPK allosteric activators lose their protective effect observed after 6 hours of overdose.

As previously mentioned, macrophage expression of the AMPK catalytic subunit is largely restricted to AMPKα1. Carling *et al.* (2008) demonstrated a 20-fold higher expression of *Prkaa1* in BMDMs relative to *Prkaa2*, with no detectable protein expression of AMPKα2[246]. Naturally, most studies interested in the immune functions of AMPK have utilized *Prkaa1*fl/fl mice crossed to the Cre of their choice[256,257,259,263,266]. Consistent with *in vitro* studies, the deleterious effects of myeloid AMPKα1 deletion have been observed in models of atherosclerosis, liver injury and skeletal muscle repair. Notably, hematopoietic and myeloid-specific AMPKβ1 deletion has also been implicated in HFD-induced hepatic inflammation[258] and sodium-sulphate-induced colitis, respectively[254,384]. On the contrary, deletion of both AMPKα1 and α2 has mostly been studied in non-immune cells like hepatocytes[215,279,281], requiring either cell type-specificity or an inducible system to evade embryonic lethality[385]. In addition to my thesis work, we previously showed that the MacKO mice were also equally susceptible to atherogenesis induced by AAV expression of a gain-of-function PCSK9 and WD feeding[267]. Setting aside the caveats associated with AMPK activation, I strongly believe that the discrepancies between LysM-Cre deletion of *Prkaa1* and *Prkaa1*/*Prkaa2* should be addressed. Specifically, future work could compare myeloid-specific AMPKα1 KO to our MacKO mice using our models of AILI and NASH. Conversely, I would be interested in using our MacKO to see if we can reproduce the phenotype observed in myeloid-specific AMPKα1 KO mice during liver ischemia-reperfusion[259].

Due to its relationship with the gut through the portal vein, the liver exhibits an immunotolerant nature largely maintained by KCs. Moreover, the immunosuppressive phenotype of KCs is regulated and maintained by other hepatic populations[386,387]. For example, in communication with hepatocytes, LSECs and HSCs, infiltrating monocytes adopt the KC identity through induced

expression of ID3 and LXRα[120,121]. Moreover, transcription factor ZEB2, known for its role in epithelial to mesenchymal transition, was found to be crucial for LXRα-regulated KC identity and survival. Cell surface receptor TIMD4 also mediates KC immunotolerance during homeostasis, and deletion of TIMD4 impaired the resolution of ischemia-reperfusion injury[388]. The majority of these studies are based on experimental KC depletion (clodronate liposomes, for example) and the infiltrating monocytes that adopt KC identity thereafter[119–121]. While their ontogeny differs from that of KCs, this population of macrophages is transcriptionally nearly identical to KCs[119]. On the contrary, MoKCs that arise during NASH are more proinflammatory than their embryonic counterparts[118]. Taking these novel findings together, I am interested in whether AMPK signaling in infiltrating monocytes is relevant for the adoption of KC identity. Moreover, how would this signaling differ depending on the instigator of KC disappearance, that is, to compare NASH-induced proinflammatory MoKCs to monocytes that infiltrate following experimental KC depletion.

Another interesting avenue to explore is the implementation of T_N housing in both models of liver injury. Giles *et al.* (2016) not only showed that T_N housing exacerbated NAFLD progression but also promoted the acute inflammatory response to LPS stimulation in the presence of lower corticosterone levels[148] . For this reason, TN housing likely worsens APAP-induced necrosis and the associated inflammation. On the contrary, AMPK activity is vital for the immunosuppressive effects of glucocorticoids[256], so it stands to reason that macrophage AMPK deletion could impair the effects of cold stressed-induced corticosterone. It is possible, however, that the anti-inflammatory effects of AMPK activation in the absence of cold stress immunosuppression would be more evident.

My thesis work has furthered our understanding of liver pathophysiology in several ways. First, it highlights the importance of relieving mice from cold stress and how this facilitates the translational modeling of NASH. Although CDAHFD has its limitations (such as impaired FAO), it is appropriate for investigation of the downstream effects of hepatic steatosis, like inflammation. We concluded that macrophage deletion of both AMPKα1 and AMPKα2 and low-dose metformin was inconsequential to NASH progression. Similarly, deletion of both catalytic subunits in the hepatocellular or macrophage compartments does not influence APAP-induced hepatic necrosis or immune infiltration. Finally, we observed that even administration of a specific allosteric activator of AMPK (MK-8722), both systemic and NP-targeted delivery, was ineffective. My thesis sheds light on the challenges associated with NASH dietary models, LysM-Cre targeting and hepatic macrophage heterogeneity, and finally, the importance of targeted activation when investigating the complexities of macrophage crosstalk with other cellular compartments. To this end, we are the first address to the role of AMPK expressed in both KCs and infiltrating monocytes/macrophages during acute (apart from Zhang *et al.* (2023)[259]) and chronic liver injury. We are also among the three recent papers that expanded on the work of Giles *et al.* (2016)[148]. While the two other studies focused on the influence of mice strain genetics and implementation of various NASH diets[150,151], we addressed whether T_N housing could accelerate NASH progression during WD-feeding[149]. Finally, in addition to the clinical importance of NASH and AILI, future work should also look at macrophage AMPK signaling during acute-on-chronic liver injury[26,43] and the increased susceptibility to bacterial infection following AILI[389,390]. Overall, this thesis work is likely only the beginning of research on hepatic macrophage AMPK and how cold stress could influence signaling during acute and chronic liver injury.

References

1. Kalra, A., Yetiskul, E., Wehrle, C. J. & Tuma, F. Physiology, Liver. in *StatPearls* (StatPearls Publishing, 2023).
2. Trefts, E., Gannon, M. & Wasserman, D. H. The liver. *Curr. Biol. CB* **27**, R1147–R1151 (2017).
3. Ben-Moshe, S. & Itzkovitz, S. Spatial heterogeneity in the mammalian liver. *Nat. Rev. Gastroenterol. Hepatol.* **16**, 395–410 (2019).
4. Rappaport, A. M., Borowy, Z. J., Lougheed, W. M. & Lotto, W. N. Subdivision of hexagonal liver lobules into a structural and functional unit. Role in hepatic physiology and pathology. *Anat. Rec.* **119**, 11–33 (1954).
5. Jungermann, K. Dynamics of zonal hepatocyte heterogeneity. Perinatal development and adaptive alterations during regeneration after partial hepatectomy, starvation and diabetes. *Acta Histochem. Suppl.* **32**, 89–98 (1986).
6. Deane, H. W. A cytological study of the diurnal cycle of the liver of the mouse in relation to storage and secretion. *Anat. Rec.* **88**, 39–65 (1944).
7. Kater, J. McA. Comparative and experimental studies on the cytology of the liver. *Z. Für Zellforsch. Mikrosk. Anat.* **17**, 217–246 (1933).
8. Chiquoine, A. D. The distribution of glucose-6-phosphatase in the liver and kidney of the mouse. *J. Histochem. Cytochem. Off. J. Histochem. Soc.* **1**, 429–435 (1953).
9. Jungermann, K. & Katz, N. Functional specialization of different hepatocyte populations. *Physiol. Rev.* **69**, 708–764 (1989).
10. Preziosi, M., Okabe, H., Poddar, M., Singh, S. & Monga, S. P. Endothelial Wnts regulate β-catenin signaling in murine liver zonation and regeneration: A sequel to the Wnt-Wnt situation. *Hepatol. Commun.* **2**, 845–860 (2018).
11. Sasse, D., Katz, N. & Jungermann, K. Functional heterogeneity of rat liver parenchyma and of isolated hepatocytes. *FEBS Lett.* **57**, 83–88 (1975).
12. Distribution of organelles and membranes between hepatocytes and nonhepatocytes in the rat liver parenchyma. A stereological study. *J. Cell Biol.* **72**, 441–455 (1977).
13. Tacke, F. & Zimmermann, H. W. Macrophage heterogeneity in liver injury and fibrosis. *J. Hepatol.* **60**, 1090–1096 (2014).
14. Marra, F. Hepatic stellate cells and the regulation of liver inflammation. *J. Hepatol.* **31**, 1120–1130 (1999).
15. Fraser, R., Dobbs, B. R. & Rogers, G. W. Lipoproteins and the liver sieve: the role of the fenestrated sinusoidal endothelium in lipoprotein metabolism, atherosclerosis, and cirrhosis. *Hepatol. Baltim. Md* **21**, 863–874 (1995).
16. Braet, F. *et al.* Comparative atomic force and scanning electron microscopy: an investigation on fenestrated endothelial cells in vitro. *J. Microsc.* **181**, 10–17 (1996).
17. Wisse, E. An electron microscopic study of the fenestrated endothelial lining of rat liver sinusoids. *J. Ultrastruct. Res.* **31**, 125–150 (1970).
18. Bilzer, M., Roggel, F. & Gerbes, A. L. Role of Kupffer cells in host defense and liver disease. *Liver Int. Off. J. Int. Assoc. Study Liver* **26**, 1175–1186 (2006).
19. Sato, K., Yabuki, K., Haba, T. & Maekawa, T. Role of Kupffer cells in the induction of tolerance after liver transplantation. *J. Surg. Res.* **63**, 433–438 (1996).

20. Ju, C., McCoy, J. P., Chung, C. J., Graf, M. L. M. & Pohl, L. R. Tolerogenic role of Kupffer cells in allergic reactions. *Chem. Res. Toxicol.* **16**, 1514–1519 (2003).
21. Ju, C. & Pohl, L. R. Tolerogenic role of Kupffer cells in immune-mediated adverse drug reactions. *Toxicology* **209**, 109–112 (2005).
22. Callery, M. P., Mangino, M. J. & Flye, M. W. Kupffer cell prostaglandin-E2 production is amplified during hepatic regeneration. *Hepatol. Baltim. Md* **14**, 368–372 (1991).
23. Knolle, P. *et al.* Human Kupffer cells secrete IL-10 in response to lipopolysaccharide (LPS) challenge. *J. Hepatol.* **22**, 226–229 (1995).
24. European Association for the Study of the Liver. Electronic address: easloffice@easloffice.eu *et al.* EASL Clinical Practical Guidelines on the management of acute (fulminant) liver failure. *J. Hepatol.* **66**, 1047–1081 (2017).
25. Hadem, J. *et al.* Etiologies and outcomes of acute liver failure in Germany. *Clin. Gastroenterol. Hepatol. Off. Clin. Pract. J. Am. Gastroenterol. Assoc.* **10**, 664-669.e2 (2012).
26. Bernal, W. & Wendon, J. Acute liver failure. *N. Engl. J. Med.* **369**, 2525–2534 (2013).
27. Sharma, A. & Nagalli, S. Chronic Liver Disease. in *StatPearls* (StatPearls Publishing, 2023).
28. Weiskirchen, R. & Tacke, F. Liver Fibrosis: From Pathogenesis to Novel Therapies. *Dig. Dis. Basel Switz.* **34**, 410–422 (2016).
29. Krenkel, O. & Tacke, F. Liver macrophages in tissue homeostasis and disease. *Nat. Rev. Immunol.* **17**, 306–321 (2017).
30. Mantovani, A. *et al.* Complications, morbidity and mortality of nonalcoholic fatty liver disease. *Metabolism* **111**, 154170 (2020).
31. Wree, A. & Marra, F. The inflammasome in liver disease. *J. Hepatol.* **65**, 1055–1056 (2016).
32. Ahmed, O., Robinson, M. W. & O'Farrelly, C. Inflammatory processes in the liver: divergent roles in homeostasis and pathology. *Cell. Mol. Immunol.* **18**, 1375–1386 (2021).
33. Marra, F. & Tacke, F. Roles for Chemokines in Liver Disease. *Gastroenterology* **147**, 577-594.e1 (2014).
34. Heymann, F. & Tacke, F. Immunology in the liver — from homeostasis to disease. *Nat. Rev. Gastroenterol. Hepatol.* **13**, 88–110 (2016).
35. Woolbright, B. L. & Jaeschke, H. The impact of sterile inflammation in acute liver injury. *J. Clin. Transl. Res.* **3**, 170–188 (2017).
36. Cordero-Espinoza, L. & Huch, M. The balancing act of the liver: tissue regeneration versus fibrosis. *J. Clin. Invest.* **128**, 85–96.
37. Charan, H. V., Dwivedi, D. K., Khan, S. & Jena, G. Mechanisms of NLRP3 inflammasome-mediated hepatic stellate cell activation: Therapeutic potential for liver fibrosis. *Genes Dis.* **10**, 480–494 (2023).
38. Hammerich, L. & Tacke, F. Hepatic inflammatory responses in liver fibrosis. *Nat. Rev. Gastroenterol. Hepatol.* **20**, 633–646 (2023).
39. Tsuchida, T. & Friedman, S. L. Mechanisms of hepatic stellate cell activation. *Nat. Rev. Gastroenterol. Hepatol.* **14**, 397–411 (2017).
40. Lee, W. M. Acetaminophen (APAP) hepatotoxicity—Isn't it time for APAP to go away? *J. Hepatol.* **67**, 1324–1331 (2017).
41. Yoon, E., Babar, A., Choudhary, M., Kutner, M. & Pyrsopoulos, N. Acetaminophen-Induced Hepatotoxicity: a Comprehensive Update. *J. Clin. Transl. Hepatol.* **4**, 131–142 (2016).

42. Doycheva, I. & Thuluvath, P. J. Acute-on-chronic liver failure in liver transplant candidates with non-alcoholic steatohepatitis. *Transl. Gastroenterol. Hepatol.* **5**, (2020).
43. Begriche, K., Penhoat, C., Bernabeu-Gentey, P., Massart, J. & Fromenty, B. Acetaminophen-Induced Hepatotoxicity in Obesity and Nonalcoholic Fatty Liver Disease: A Critical Review. *Livers* **3**, 33–53 (2023).
44. McGill, M. R. & Jaeschke, H. METABOLISM AND DISPOSITION OF ACETAMINOPHEN: RECENT ADVANCES IN RELATION TO HEPATOTOXICITY AND DIAGNOSIS. *Pharm. Res.* **30**, 2174–2187 (2013).
45. Jaeschke, H., McGill, M. R. & Ramachandran, A. OXIDANT STRESS, MITOCHONDRIA AND CELL DEATH MECHANISMS IN DRUG-INDUCED LIVER INJURY: LESSONS LEARNED FROM ACETAMINOPHEN HEPATOTOXICITY. *Drug Metab. Rev.* **44**, 88–106 (2012).
46. Luo, G., Huang, L. & Zhang, Z. The molecular mechanisms of acetaminophen-induced hepatotoxicity and its potential therapeutic targets. *Exp. Biol. Med.* **248**, 412–424 (2023).
47. Jaeschke, H., Duan, L., Nguyen, N. & Ramachandran, A. Mitochondrial Damage and Biogenesis in Acetaminophen-induced Liver Injury. *Liver Res.* **3**, 150–156 (2019).
48. Ramachandran, A. & Jaeschke, H. Acetaminophen Toxicity: Novel Insights Into Mechanisms and Future Perspectives. *Gene Expr.* **18**, 19–30 (2018).
49. Kolodziejczyk, A. A. *et al.* Acute liver failure is regulated by MYC- and microbiome-dependent programs. *Nat. Med.* **26**, 1899–1911 (2020).
50. Mossanen, J. C. *et al.* Chemokine (C-C motif) receptor 2–positive monocytes aggravate the early phase of acetaminophen-induced acute liver injury. *Hepatology* **64**, 1667–1682 (2016).
51. Zhao, J. *et al.* Macrophage-Inducible C-Type Lectin Signaling Exacerbates Acetaminophen-Induced Liver Injury by Promoting Kupffer Cell Activation in Mice. *Mol. Pharmacol.* **99**, 92–103 (2021).
52. Ju, C. *et al.* Protective Role of Kupffer Cells in Acetaminophen-Induced Hepatic Injury in Mice. *Chem. Res. Toxicol.* **15**, 1504–1513 (2002).
53. Nguyen, N. T., Umbaugh, D. S., Sanchez-Guerrero, G., Ramachandran, A. & Jaeschke, H. Kupffer cells regulate liver recovery through induction of chemokine receptor CXCR2 on hepatocytes after acetaminophen overdose in mice. *Arch. Toxicol.* **96**, 305–320 (2022).
54. Michael, S. L., Pumford, N. R., Mayeux, P. R., Niesman, M. R. & Hinson, J. A. Pretreatment of mice with macrophage inactivators decreases acetaminophen hepatotoxicity and the formation of reactive oxygen and nitrogen species. *Hepatology* **30**, 186–195 (1999).
55. Fisher, J. E. *et al.* Role of Kupffer cells and toll-like receptor 4 in acetaminophen-induced acute liver failure. *J. Surg. Res.* **180**, 147–155 (2013).
56. Neutrophils in the activation and regulation of innate and adaptive immunity | Nature Reviews Immunology. https://www.nature.com/articles/nri3024.
57. Liu, Z.-X., Han, D., Gunawan, B. & Kaplowitz, N. Neutrophil depletion protects against murine acetaminophen hepatotoxicity. *Hepatology* **43**, 1220–1230 (2006).
58. Dose-dependent pleiotropic role of neutrophils during acetaminophen-induced liver injury in male and female mice | SpringerLink. https://link.springer.com/article/10.1007/s00204-023-03478-4#Fig8.
59. Ishida, Y. *et al.* Opposite roles of neutrophils and macrophages in the pathogenesis of acetaminophen-induced acute liver injury. *Eur. J. Immunol.* **36**, 1028–1038 (2006).

60. Liu, J. *et al.* Modulation of HMGB1 Release in APAP-Induced Liver Injury: A Possible Strategy of Chikusetsusaponin V Targeting NETs Formation. *Front. Pharmacol.* **12**, 723881 (2021).
61. Williams, C. D., Bajt, M. L., Farhood, A. & Jaeschke, H. Acetaminophen-induced hepatic neutrophil accumulation and inflammatory liver injury in CD18-deficient mice. *Liver Int.* **30**, 1280–1292 (2010).
62. Yang, W. *et al.* Neutrophils promote the development of reparative macrophages mediated by ROS to orchestrate liver repair. *Nat. Commun.* **10**, 1076 (2019).
63. You, Q. *et al.* Role of hepatic resident and infiltrating macrophages in liver repair after acute injury. *Biochem. Pharmacol.* **86**, 836–843 (2013).
64. Zigmond, E. *et al.* Infiltrating Monocyte-Derived Macrophages and Resident Kupffer Cells Display Different Ontogeny and Functions in Acute Liver Injury. *J. Immunol.* **193**, 344–353 (2014).
65. Yang, W. *et al.* Proteomic analysis reveals a protective role of specific macrophage subsets in liver repair. *Sci. Rep.* **9**, 2953 (2019).
66. Stutchfield, B. M. *et al.* CSF1 Restores Innate Immunity After Liver Injury in Mice and Serum Levels Indicate Outcomes of Patients With Acute Liver Failure. *Gastroenterology* **149**, 1896-1909.e14 (2015).
67. Zagórska, A., Través, P. G., Lew, E. D., Dransfield, I. & Lemke, G. Diversification of TAM receptor tyrosine kinase function. *Nat. Immunol.* **15**, 920–928 (2014).
68. Triantafyllou, E. *et al.* MerTK expressing hepatic macrophages promote the resolution of inflammation in acute liver failure. *Gut* **67**, 333–347 (2018).
69. Ludwig, J., Viggiano, T. R., McGill, D. B. & Oh, B. J. Nonalcoholic steatohepatitis: Mayo Clinic experiences with a hitherto unnamed disease. *Mayo Clin. Proc.* **55**, 434–438 (1980).
70. Eslam, M. *et al.* A new definition for metabolic dysfunction-associated fatty liver disease: An international expert consensus statement. *J. Hepatol.* **73**, 202–209 (2020).
71. Eslam, M., Sanyal, A. J., George, J., & International Consensus Panel. MAFLD: A Consensus-Driven Proposed Nomenclature for Metabolic Associated Fatty Liver Disease. *Gastroenterology* **158**, 1999-2014.e1 (2020).
72. Estes, C., Razavi, H., Loomba, R., Younossi, Z. & Sanyal, A. J. Modeling the epidemic of nonalcoholic fatty liver disease demonstrates an exponential increase in burden of disease. *Hepatol. Baltim. Md* **67**, 123–133 (2018).
73. European Association for the Study of the Liver (EASL), E. A. for the S. of D. (EASD), European Association for the Study of Obesity (EASO). EASL-EASD-EASO Clinical Practice Guidelines for the Management of Non-Alcoholic Fatty Liver Disease. *Obes. Facts* **9**, 65–90 (2016).
74. Chalasani, N. *et al.* The diagnosis and management of nonalcoholic fatty liver disease: Practice guidance from the American Association for the Study of Liver Diseases. *Hepatol. Baltim. Md* **67**, 328–357 (2018).
75. Nassir, F., Rector, R. S., Hammoud, G. M. & Ibdah, J. A. Pathogenesis and Prevention of Hepatic Steatosis. *Gastroenterol. Hepatol.* **11**, 167–175 (2015).
76. Kleiner, D. E. & Makhlouf, H. R. Histology of NAFLD and NASH in Adults and Children. *Clin. Liver Dis.* **20**, 293–312 (2016).

77. Heyens, L. J. M., Busschots, D., Koek, G. H., Robaeys, G. & Francque, S. Liver Fibrosis in Non-alcoholic Fatty Liver Disease: From Liver Biopsy to Non-invasive Biomarkers in Diagnosis and Treatment. *Front. Med.* **8**, 615978 (2021).
78. Alves-Bezerra, M. & Cohen, D. E. Triglyceride metabolism in the liver. *Compr. Physiol.* **8**, 1–8 (2017).
79. Matsuzaka, T. & Shimano, H. Molecular mechanisms involved in hepatic steatosis and insulin resistance. *J. Diabetes Investig.* **2**, 170–175 (2011).
80. Godoy-Matos, A. F., Silva Júnior, W. S. & Valerio, C. M. NAFLD as a continuum: from obesity to metabolic syndrome and diabetes. *Diabetol. Metab. Syndr.* **12**, 60 (2020).
81. Chen, G., Liang, G., Ou, J., Goldstein, J. L. & Brown, M. S. Central role for liver X receptor in insulin-mediated activation of Srebp-1c transcription and stimulation of fatty acid synthesis in liver. *Proc. Natl. Acad. Sci. U. S. A.* **101**, 11245–11250 (2004).
82. Grefhorst, A. *et al.* Stimulation of lipogenesis by pharmacological activation of the liver X receptor leads to production of large, triglyceride-rich very low density lipoprotein particles. *J. Biol. Chem.* **277**, 34182–34190 (2002).
83. Mitro, N. *et al.* The nuclear receptor LXR is a glucose sensor. *Nature* **445**, 219–223 (2007).
84. Iizuka, K., Bruick, R. K., Liang, G., Horton, J. D. & Uyeda, K. Deficiency of carbohydrate response element-binding protein (ChREBP) reduces lipogenesis as well as glycolysis. *Proc. Natl. Acad. Sci. U. S. A.* **101**, 7281–7286 (2004).
85. Iizuka, K., Miller, B. & Uyeda, K. Deficiency of carbohydrate-activated transcription factor ChREBP prevents obesity and improves plasma glucose control in leptin-deficient (ob/ob) mice. *Am. J. Physiol. Endocrinol. Metab.* **291**, E358-364 (2006).
86. Ide, T. *et al.* SREBPs suppress IRS-2-mediated insulin signalling in the liver. *Nat. Cell Biol.* **6**, 351–357 (2004).
87. Shimano, H. *et al.* Isoform 1c of sterol regulatory element binding protein is less active than isoform 1a in livers of transgenic mice and in cultured cells. *J. Clin. Invest.* **99**, 846–854 (1997).
88. Yahagi, N. *et al.* Absence of sterol regulatory element-binding protein-1 (SREBP-1) ameliorates fatty livers but not obesity or insulin resistance in Lep(ob)/Lep(ob) mice. *J. Biol. Chem.* **277**, 19353–19357 (2002).
89. Samuel, V. T. *et al.* Mechanism of hepatic insulin resistance in non-alcoholic fatty liver disease. *J. Biol. Chem.* **279**, 32345–32353 (2004).
90. Yu, S., Li, C., Ji, G. & Zhang, L. The Contribution of Dietary Fructose to Non-alcoholic Fatty Liver Disease. *Front. Pharmacol.* **12**, (2021).
91. Hodson, L., Rosqvist, F. & Parry, S. A. The influence of dietary fatty acids on liver fat content and metabolism. *Proc. Nutr. Soc.* **79**, 30–41 (2020).
92. Cross, E., Dearlove, D. J. & Hodson, L. Nutritional regulation of hepatic de novo lipogenesis in humans. *Curr. Opin. Clin. Nutr. Metab. Care* **26**, 65–71 (2023).
93. Day, C. P. & James, O. F. W. Steatohepatitis: A tale of two "hits"? *Gastroenterology* **114**, 842–845 (1998).
94. Tilg, H. & Moschen, A. R. Evolution of inflammation in nonalcoholic fatty liver disease: The multiple parallel hits hypothesis. *Hepatology* **52**, 1836–1846 (2010).
95. Buzzetti, E., Pinzani, M. & Tsochatzis, E. A. The multiple-hit pathogenesis of non-alcoholic fatty liver disease (NAFLD). *Metabolism.* **65**, 1038–1048 (2016).

96. Malhi, H. & Gores, G. J. Molecular Mechanisms of Lipotoxicity in Nonalcoholic Fatty Liver Disease. *Semin. Liver Dis.* **28**, 360–369 (2008).
97. Méndez-Sánchez, N., Arrese, M., Zamora-Valdés, D. & Uribe, M. Current concepts in the pathogenesis of nonalcoholic fatty liver disease. *Liver Int.* **27**, 423–433 (2007).
98. Trauner, M., Arrese, M. & Wagner, M. Fatty liver and lipotoxicity. *Biochim. Biophys. Acta BBA - Mol. Cell Biol. Lipids* **1801**, 299–310 (2010).
99. Cortes, V. A. *et al.* Physiological and pathological implications of cholesterol. *Front. Biosci. Landmark Ed.* **19**, 416–428 (2014).
100. Min, H.-K. *et al.* Increased Hepatic Synthesis and Dysregulation of Cholesterol Metabolism Is Associated with the Severity of Nonalcoholic Fatty Liver Disease. *Cell Metab.* **15**, 665–674 (2012).
101. Caballero, F. *et al.* Enhanced free cholesterol, SREBP-2 and StAR expression in human NASH. *J. Hepatol.* **50**, 789–796 (2009).
102. Rada, P., González-Rodríguez, Á., García-Monzón, C. & Valverde, Á. M. Understanding lipotoxicity in NAFLD pathogenesis: is CD36 a key driver? *Cell Death Dis.* **11**, 1–15 (2020).
103. Fu, S., Watkins, S. M. & Hotamisligil, G. S. The Role of Endoplasmic Reticulum in Hepatic Lipid Homeostasis and Stress Signaling. *Cell Metab.* **15**, 623–634 (2012).
104. Feng, B. *et al.* The endoplasmic reticulum is the site of cholesterol-induced cytotoxicity in macrophages. *Nat. Cell Biol.* **5**, 781–792 (2003).
105. Zhang, J., Zhang, K., Li, Z. & Guo, B. ER Stress-induced Inflammasome Activation Contributes to Hepatic Inflammation and Steatosis. *J. Clin. Cell. Immunol.* **7**, 457 (2016).
106. Dixon, L., Berk, M., Thapaliya, S., Papouchado, B. G. & Feldstein, A. E. Caspase 1-mediated regulation of fibrogenesis in diet-induced steatohepatitis. *Lab. Investig. J. Tech. Methods Pathol.* **92**, 713–723 (2012).
107. Lebeaupin, C. *et al.* Endoplasmic reticulum stress signalling and the pathogenesis of non-alcoholic fatty liver disease. *J. Hepatol.* **69**, 927–947 (2018).
108. Montero, J. *et al.* Cholesterol and peroxidized cardiolipin in mitochondrial membrane properties, permeabilization and cell death. *Biochim. Biophys. Acta BBA - Bioenerg.* **1797**, 1217–1224 (2010).
109. Yu, W. *et al.* Altered Cholesterol Metabolism in Niemann-Pick Type C1 Mouse Brains Affects Mitochondrial Function. *J. Biol. Chem.* **280**, 11731–11739 (2005).
110. Campbell, A. M. & Chan, S. H. P. Mitochondrial membrane cholesterol, the voltage dependent anion channel (VDAC), and the Warburg effect. *J. Bioenerg. Biomembr.* **40**, 193–197 (2008).
111. Campbell, A. M. & Chan, S. H. P. The voltage dependent anion channel affects mitochondrial cholesterol distribution and function. *Arch. Biochem. Biophys.* **466**, 203–210 (2007).
112. Fernandez-Checa, J. C. & Kaplowitz, N. Hepatic mitochondrial glutathione: transport and role in disease and toxicity. *Toxicol. Appl. Pharmacol.* **204**, 263–273 (2005).
113. Ferro, D. *et al.* New Insights into the Pathogenesis of Non-Alcoholic Fatty Liver Disease: Gut-Derived Lipopolysaccharides and Oxidative Stress. *Nutrients* **12**, 2762 (2020).
114. Kessoku, T. *et al.* Endotoxins and Non-Alcoholic Fatty Liver Disease. *Front. Endocrinol.* **12**, (2021).

115. Coombes, J. D. *et al.* Osteopontin is a proximal effector of leptin-mediated non-alcoholic steatohepatitis (NASH) fibrosis. *Biochim. Biophys. Acta BBA - Mol. Basis Dis.* **1862**, 135–144 (2016).
116. Huby, T. & Gautier, E. L. Immune cell-mediated features of non-alcoholic steatohepatitis. *Nat. Rev. Immunol.* **22**, 429–443 (2022).
117. Blériot, C. *et al.* A subset of Kupffer cells regulates metabolism through the expression of CD36. *Immunity* **54**, 2101-2116.e6 (2021).
118. Tran, S. *et al.* Impaired Kupffer Cell Self-Renewal Alters the Liver Response to Lipid Overload during Non-alcoholic Steatohepatitis. *Immunity* **53**, 627-640.e5 (2020).
119. Scott, C. L. *et al.* Bone marrow-derived monocytes give rise to self-renewing and fully differentiated Kupffer cells. *Nat. Commun.* **7**, 10321 (2016).
120. Bonnardel, J. *et al.* Stellate Cells, Hepatocytes, and Endothelial Cells Imprint the Kupffer Cell Identity on Monocytes Colonizing the Liver Macrophage Niche. *Immunity* **51**, 638-654.e9 (2019).
121. Sakai, M. *et al.* Liver-Derived Signals Sequentially Reprogram Myeloid Enhancers to Initiate and Maintain Kupffer Cell Identity. *Immunity* **51**, 655-670.e8 (2019).
122. Xiong, X. *et al.* Landscape of Intercellular Crosstalk in Healthy and NASH Liver Revealed by Single-Cell Secretome Gene Analysis. *Mol. Cell* **75**, 644-660.e5 (2019).
123. Seidman, J. S. *et al.* Niche-Specific Reprogramming of Epigenetic Landscapes Drives Myeloid Cell Diversity in Nonalcoholic Steatohepatitis. *Immunity* **52**, 1057-1074.e7 (2020).
124. Remmerie, A. *et al.* Osteopontin Expression Identifies a Subset of Recruited Macrophages Distinct from Kupffer Cells in the Fatty Liver. *Immunity* **53**, 641-657.e14 (2020).
125. Ramachandran, P. *et al.* Resolving the fibrotic niche of human liver cirrhosis at single-cell level. *Nature* **575**, 512–518 (2019).
126. Daemen, S. *et al.* Dynamic Shifts in the Composition of Resident and Recruited Macrophages Influence Tissue Remodeling in NASH. *Cell Rep.* **34**, 108626 (2021).
127. Krenkel, O. *et al.* Myeloid cells in liver and bone marrow acquire a functionally distinct inflammatory phenotype during obesity-related steatohepatitis. *Gut* **69**, 551–563 (2020).
128. Ramos, M. J., Bandiera, L., Menolascina, F. & Fallowfield, J. A. In vitro models for non-alcoholic fatty liver disease: Emerging platforms and their applications. *iScience* **25**, 103549 (2022).
129. Gallage, S. *et al.* A researcher's guide to preclinical mouse NASH models. *Nat. Metab.* **4**, 1632–1649 (2022).
130. Hefler, J. *et al.* Preclinical models of acute liver failure: a comprehensive review. *PeerJ* **9**, e12579 (2021).
131. Soares, R. O. S., Losada, D. M., Jordani, M. C., Évora, P. & Castro-e-Silva, O. Ischemia/Reperfusion Injury Revisited: An Overview of the Latest Pharmacological Strategies. *Int. J. Mol. Sci.* **20**, 5034 (2019).
132. Du, K., Williams, C. D., McGill, M. R. & Jaeschke, H. Lower Susceptibility of Female Mice to Acetaminophen Hepatotoxicity: Role of Mitochondrial Glutathione, Oxidant Stress and c-Jun N-Terminal Kinase. *Toxicol. Appl. Pharmacol.* **281**, 58–66 (2014).
133. Im, Y. R. *et al.* A Systematic Review of Animal Models of NAFLD Finds High-Fat, High-Fructose Diets Most Closely Resemble Human NAFLD. *Hepatology* **74**, 1884–1901 (2021).
134. Eng, J. M. & Estall, J. L. Diet-Induced Models of Non-Alcoholic Fatty Liver Disease: Food for Thought on Sugar, Fat, and Cholesterol. *Cells* **10**, 1805 (2021).

135. Santhekadur, P. K., Kumar, D. P. & Sanyal, A. J. Preclinical models of non-alcoholic fatty liver disease. *J. Hepatol.* **68**, 230–237 (2018).
136. Ioannou, G. N. *et al.* Cholesterol crystallization within hepatocyte lipid droplets and its role in murine NASH. *J. Lipid Res.* **58**, 1067–1079 (2017).
137. Zhang, X. *et al.* Dietary cholesterol drives fatty liver-associated liver cancer by modulating gut microbiota and metabolites. *Gut* **70**, 761–774 (2021).
138. Asgharpour, A. *et al.* A diet-induced animal model of non-alcoholic fatty liver disease and hepatocellular cancer. *J. Hepatol.* **65**, 579–588 (2016).
139. Itagaki, H., Shimizu, K., Morikawa, S., Ogawa, K. & Ezaki, T. Morphological and functional characterization of non-alcoholic fatty liver disease induced by a methionine-choline-deficient diet in C57BL/6 mice. *Int. J. Clin. Exp. Pathol.* **6**, 2683–2696 (2013).
140. Jha, P. *et al.* Role of adipose tissue in methionine–choline-deficient model of non-alcoholic steatohepatitis (NASH). *Biochim. Biophys. Acta BBA - Mol. Basis Dis.* **1842**, 959–970 (2014).
141. Rinella, M. E. & Green, R. M. The methionine-choline deficient dietary model of steatohepatitis does not exhibit insulin resistance. *J. Hepatol.* **40**, 47–51 (2004).
142. Wei, G. *et al.* Comparison of murine steatohepatitis models identifies a dietary intervention with robust fibrosis, ductular reaction, and rapid progression to cirrhosis and cancer. *Am. J. Physiol. - Gastrointest. Liver Physiol.* **318**, G174–G188 (2020).
143. Anstee, Q. M., Reeves, H. L., Kotsiliti, E., Govaere, O. & Heikenwalder, M. From NASH to HCC: current concepts and future challenges. *Nat. Rev. Gastroenterol. Hepatol.* **16**, 411–428 (2019).
144. Kawashita, E., Ishihara, K., Nomoto, M., Taniguchi, M. & Akiba, S. A comparative analysis of hepatic pathological phenotypes in C57BL/6J and C57BL/6N mouse strains in non-alcoholic steatohepatitis models. *Sci. Rep.* **9**, 204 (2019).
145. Fujii, M. *et al.* A murine model for non-alcoholic steatohepatitis showing evidence of association between diabetes and hepatocellular carcinoma. *Med. Mol. Morphol.* **46**, 141–152 (2013).
146. Bastías-Pérez, M. *et al.* Impact of Adaptive Thermogenesis in Mice on the Treatment of Obesity. *Cells* **9**, 316 (2020).
147. Abreu-Vieira, G., Xiao, C., Gavrilova, O. & Reitman, M. L. Integration of body temperature into the analysis of energy expenditure in the mouse. *Mol. Metab.* **4**, 461–470 (2015).
148. Giles, D. A. *et al.* Thermoneutral housing exacerbates nonalcoholic fatty liver disease in mice and allows for sex-independent disease modeling. *Nat. Med.* **23**, 829–838 (2017).
149. Nunes, J. R. C. *et al.* Thermoneutral housing does not accelerate metabolic dysfunction-associated fatty liver disease in male or female C57Bl/6J mice fed a Western diet. *Am. J. Physiol. Endocrinol. Metab.* **325**, E10–E20 (2023).
150. Oates, J. R. *et al.* Thermoneutral housing shapes hepatic inflammation and damage in mouse models of non-alcoholic fatty liver disease. *Front. Immunol.* **14**, 1095132 (2023).
151. Benegiamo, G. *et al.* The genetic background shapes the susceptibility to mitochondrial dysfunction and NASH progression. *J. Exp. Med.* **220**, e20221738 (2023).
152. Morrow, M. R. *et al.* Inhibition of ATP-citrate lyase improves NASH, liver fibrosis, and dyslipidemia. *Cell Metab.* **34**, 919-936.e8 (2022).
153. Carlson, C. A. & Kim, K. H. Regulation of hepatic acetyl coenzyme A carboxylase by phosphorylation and dephosphorylation. *J. Biol. Chem.* **248**, 378–380 (1973).

154. Beg, Z. H., Allmann, D. W. & Gibson, D. M. Modulation of 3-hydroxy-3-methylglutaryl coenzyme A reductase activity with cAMP and with protein fractions of rat liver cytosol. *Biochem. Biophys. Res. Commun.* **54**, 1362–1369 (1973).
155. Atkinson, D. E. The energy charge of the adenylate pool as a regulatory parameter. Interaction with feedback modifiers. *Biochemistry* **7**, 4030–4034 (1968).
156. Atkinson, D. E. Adenine nucleotides as universal stoichiometric metabolic coupling agents. *Adv. Enzyme Regul.* **9**, 207–219 (1970).
157. Yeh, L. A., Lee, K. H. & Kim, K. H. Regulation of rat liver acetyl-CoA carboxylase. Regulation of phosphorylation and inactivation of acetyl-CoA carboxylase by the adenylate energy charge. *J. Biol. Chem.* **255**, 2308–2314 (1980).
158. Ingebritsen, T. S., Lee, H. S., Parker, R. A. & Gibson, D. M. Reversible modulation of the activities of both liver microsomal hydroxymethylglutaryl coenzyme A reductase and its inactivating enzyme. Evidence for regulation by phosphorylation-dephosphorylation. *Biochem. Biophys. Res. Commun.* **81**, 1268–1277 (1978).
159. Munday, M. R., Campbell, D. G., Carling, D. & Hardie, D. G. Identification by amino acid sequencing of three major regulatory phosphorylation sites on rat acetyl-CoA carboxylase. *Eur. J. Biochem.* **175**, 331–338 (1988).
160. Carling, D., Zammit, V. A. & Hardie, D. G. A common bicyclic protein kinase cascade inactivates the regulatory enzymes of fatty acid and cholesterol biosynthesis. *FEBS Lett.* **223**, 217–222 (1987).
161. Carling, D. *et al.* Mammalian AMP-activated protein kinase is homologous to yeast and plant protein kinases involved in the regulation of carbon metabolism. *J. Biol. Chem.* **269**, 11442–11448 (1994).
162. Davies, S. P. *et al.* Purification of the AMP-activated protein kinase on ATP-γ-Sepharose and analysis of its subunit structure. *Eur. J. Biochem.* **223**, 351–357 (1994).
163. Mitchelhill, K. I. *et al.* Mammalian AMP-activated protein kinase shares structural and functional homology with the catalytic domain of yeast Snf1 protein kinase. *J. Biol. Chem.* **269**, 2361–2364 (1994).
164. Stapleton, D. *et al.* Mammalian AMP-activated Protein Kinase Subfamily (∗). *J. Biol. Chem.* **271**, 611–614 (1996).
165. Chen, Z. *et al.* Expression of the AMP-activated protein kinase β1 and β2 subunits in skeletal muscle. *FEBS Lett.* **460**, 343–348 (1999).
166. Thornton, C., Snowden, M. A. & Carling, D. Identification of a Novel AMP-activated Protein Kinase β Subunit Isoform That Is Highly Expressed in Skeletal Muscle *. *J. Biol. Chem.* **273**, 12443–12450 (1998).
167. Cheung, P. C. F., Salt, I. P., Davies, S. P., Hardie, D. G. & Carling, D. Characterization of AMP-activated protein kinase γ-subunit isoforms and their role in AMP binding. (2000).
168. Ross, F. A., MacKintosh, C. & Hardie, D. G. AMP-activated protein kinase: a cellular energy sensor that comes in 12 flavours. *Febs J.* **283**, 2987–3001 (2016).
169. Steinberg, G. R. & Kemp, B. E. AMPK in Health and Disease. *Physiol. Rev.* **89**, 1025–1078 (2009).
170. Chen, L. *et al.* Structural insight into the autoinhibition mechanism of AMP-activated protein kinase. *Nature* **459**, 1146–1149 (2009).
171. Steinberg, G. R. & Hardie, D. G. New insights into activation and function of the AMPK. *Nat. Rev. Mol. Cell Biol.* **24**, 255–272 (2023).

172. Xiao, B. *et al.* Structure of mammalian AMPK and its regulation by ADP. *Nature* **472**, 230–233 (2011).
173. Crute, B. E., Seefeld, K., Gamble, J., Kemp, B. E. & Witters, L. A. Functional Domains of the α1 Catalytic Subunit of the AMP-activated Protein Kinase *. *J. Biol. Chem.* **273**, 35347–35354 (1998).
174. Langendorf, C. G. & Kemp, B. E. Choreography of AMPK activation. *Cell Res.* **25**, 5–6 (2015).
175. Xiao, B. *et al.* Structural basis for AMP binding to mammalian AMP-activated protein kinase. *Nature* **449**, 496–500 (2007).
176. Kemp, B. E., Oakhill, J. S. & Scott, J. W. AMPK Structure and Regulation from Three Angles. *Structure* **15**, 1161–1163 (2007).
177. Gu, X. *et al.* Deconvoluting AMP-activated protein kinase (AMPK) adenine nucleotide binding and sensing. *J. Biol. Chem.* **292**, 12653–12666 (2017).
178. Yan, Y. *et al.* Structure of an AMPK complex in an inactive, ATP-bound state. *Science* **373**, 413–419 (2021).
179. Hawley, S. A. *et al.* Complexes between the LKB1 tumor suppressor, STRADα/β and MO25α/β are upstream kinases in the AMP-activated protein kinase cascade. *J. Biol.* **2**, 28 (2003).
180. Shaw, R. J. *et al.* The tumor suppressor LKB1 kinase directly activates AMP-activated kinase and regulates apoptosis in response to energy stress. *Proc. Natl. Acad. Sci.* **101**, 3329–3335 (2004).
181. Woods, A. *et al.* LKB1 Is the Upstream Kinase in the AMP-Activated Protein Kinase Cascade. *Curr. Biol.* **13**, 2004–2008 (2003).
182. Xin, F.-J., Wang, J., Zhao, R.-Q., Wang, Z.-X. & Wu, J.-W. Coordinated regulation of AMPK activity by multiple elements in the α-subunit. *Cell Res.* **23**, 1237–1240 (2013).
183. Hawley, S. A. *et al.* Phosphorylation by Akt within the ST loop of AMPK-α1 down-regulates its activation in tumour cells. *Biochem. J.* **459**, 275–287 (2014).
184. Li, X. *et al.* Structural basis of AMPK regulation by adenine nucleotides and glycogen. *Cell Res.* **25**, 50–66 (2015).
185. Horman, S. *et al.* Insulin Antagonizes Ischemia-induced Thr172 Phosphorylation of AMP-activated Protein Kinase α-Subunits in Heart via Hierarchical Phosphorylation of Ser485/491*. *J. Biol. Chem.* **281**, 5335–5340 (2006).
186. Hurley, R. L. *et al.* Regulation of AMP-activated Protein Kinase by Multisite Phosphorylation in Response to Agents That Elevate Cellular cAMP *>. *J. Biol. Chem.* **281**, 36662–36672 (2006).
187. Ling, N. X. Y. *et al.* mTORC1 directly inhibits AMPK to promote cell proliferation under nutrient stress. *Nat. Metab.* **2**, 41–49 (2020).
188. Morrison, K. R. *et al.* An AMPKα2-specific phospho-switch controls lysosomal targeting for activation. *Cell Rep.* **38**, (2022).
189. Hawley, S. A. *et al.* 5′-AMP Activates the AMP-activated Protein Kinase Cascade, and Ca2+/Calmodulin Activates the Calmodulin-dependent Protein Kinase I Cascade, via Three Independent Mechanisms (*). *J. Biol. Chem.* **270**, 27186–27191 (1995).
190. Hawley, S. A. *et al.* Calmodulin-dependent protein kinase kinase-β is an alternative upstream kinase for AMP-activated protein kinase. *Cell Metab.* **2**, 9–19 (2005).
191. Woods, A. *et al.* Ca2+/calmodulin-dependent protein kinase kinase-β acts upstream of AMP-activated protein kinase in mammalian cells. *Cell Metab.* **2**, 21–33 (2005).

192. Hurley, R. L. *et al.* The Ca2+/Calmodulin-dependent Protein Kinase Kinases Are AMP-activated Protein Kinase Kinases *. *J. Biol. Chem.* **280**, 29060–29066 (2005).
193. Phosphoproteomics reveals conserved exercise-stimulated signaling and AMPK regulation of store-operated calcium entry. https://www.embopress.org/doi/epdf/10.15252/embj.2019102578 doi:10.15252/embj.2019102578.
194. Jia, J. *et al.* AMPK, a Regulator of Metabolism and Autophagy, Is Activated by Lysosomal Damage via a Novel Galectin-Directed Ubiquitin Signal Transduction System. *Mol. Cell* **77**, 951-969.e9 (2020).
195. Herrero-Martín, G. *et al.* TAK1 activates AMPK-dependent cytoprotective autophagy in TRAIL-treated epithelial cells. *EMBO J.* **28**, 677–685 (2009).
196. Momcilovic, M., Hong, S.-P. & Carlson, M. Mammalian TAK1 Activates Snf1 Protein Kinase in Yeast and Phosphorylates AMP-activated Protein Kinase in Vitro*. *J. Biol. Chem.* **281**, 25336–25343 (2006).
197. Dite, T. A. *et al.* The autophagy initiator ULK1 sensitizes AMPK to allosteric drugs. *Nat. Commun.* **8**, 571 (2017).
198. Xiao, B. *et al.* Structural basis of AMPK regulation by small molecule activators. *Nat. Commun.* **4**, 3017 (2013).
199. Myers, R. W. *et al.* Systemic pan-AMPK activator MK-8722 improves glucose homeostasis but induces cardiac hypertrophy. *Science* **357**, 507–511 (2017).
200. Cool, B. *et al.* Identification and characterization of a small molecule AMPK activator that treats key components of type 2 diabetes and the metabolic syndrome. *Cell Metab.* **3**, 403–416 (2006).
201. Cokorinos, E. C. *et al.* Activation of Skeletal Muscle AMPK Promotes Glucose Disposal and Glucose Lowering in Non-human Primates and Mice. *Cell Metab.* **25**, 1147-1159.e10 (2017).
202. Pinkosky, S. L. *et al.* Long-chain fatty acyl-CoA esters regulate metabolism via allosteric control of AMPK β1 isoforms. *Nat. Metab.* **2**, 873–881 (2020).
203. Afinanisa, Q., Cho, M. K. & Seong, H.-A. AMPK Localization: A Key to Differential Energy Regulation. *Int. J. Mol. Sci.* **22**, 10921 (2021).
204. Zong, Y. *et al.* Hierarchical activation of compartmentalized pools of AMPK depends on severity of nutrient or energy stress. *Cell Res.* **29**, 460–473 (2019).
205. Celenza, J. L. & Carlson, M. A Yeast Gene That Is Essential for Release from Glucose Repression Encodes a Protein Kinase. *Science* **233**, 1175–1180 (1986).
206. SALT, I. P., JOHNSON, G., ASHCROFT, S. J. H. & HARDIE, D. G. AMP-activated protein kinase is activated by low glucose in cell lines derived from pancreatic β cells, and may regulate insulin release. *Biochem. J.* **335**, 533–539 (1998).
207. Zhang, C.-S. *et al.* Fructose-1,6-bisphosphate and aldolase mediate glucose sensing by AMPK. *Nature* **548**, 112–116 (2017).
208. Ma, T. *et al.* Low-dose metformin targets the lysosomal AMPK pathway through PEN2. *Nature* **603**, 159–165 (2022).
209. Scott, J. W., Norman, D. G., Hawley, S. A., Kontogiannis, L. & Hardie, D. G. Protein kinase substrate recognition studied using the recombinant catalytic domain of AMP-activated protein kinase and a model substrate11Edited by J. Karn. *J. Mol. Biol.* **317**, 309–323 (2002).
210. Dale, S., Wilson, W. A., Edelman, A. M. & Hardie, D. G. Similar substrate recognition motifs for mammalian AMP-activated protein kinase, higher plant HMG-CoA reductase kinase-

A, yeast SNF1, and mammalian calmodulin-dependent protein kinase I. *FEBS Lett.* **361**, 191–195 (1995).
211. Weekes, J., Ball, K. L., Caudwell, F. B. & Hardie, D. G. Specificity determinants for the AMP-activated protein kinase and its plant homologue analysed using synthetic peptides. *FEBS Lett.* **334**, 335–339 (1993).
212. Fullerton, M. D. *et al.* Single phosphorylation sites in Acc1 and Acc2 regulate lipid homeostasis and the insulin-sensitizing effects of metformin. *Nat. Med.* **19**, 1649–1654 (2013).
213. Li, Y. *et al.* AMPK Phosphorylates and Inhibits SREBP Activity to Attenuate Hepatic Steatosis and Atherosclerosis in Diet-Induced Insulin-Resistant Mice. *Cell Metab.* **13**, 376–388 (2011).
214. Han, Y. *et al.* Post-translational regulation of lipogenesis via AMPK-dependent phosphorylation of insulin-induced gene. *Nat. Commun.* **10**, 623 (2019).
215. Boudaba, N. *et al.* AMPK Re-Activation Suppresses Hepatic Steatosis but its Downregulation Does Not Promote Fatty Liver Development. *EBioMedicine* **28**, 194–209 (2018).
216. Loh, K. *et al.* Inhibition of Adenosine Monophosphate-Activated Protein Kinase-3-Hydroxy-3-Methylglutaryl Coenzyme A Reductase Signaling Leads to Hypercholesterolemia and Promotes Hepatic Steatosis and Insulin Resistance. *Hepatol. Commun.* **3**, 84–98 (2019).
217. Inoki, K., Zhu, T. & Guan, K.-L. TSC2 Mediates Cellular Energy Response to Control Cell Growth and Survival. *Cell* **115**, 577–590 (2003).
218. Gwinn, D. M. *et al.* AMPK Phosphorylation of Raptor Mediates a Metabolic Checkpoint. *Mol. Cell* **30**, 214–226 (2008).
219. Dai, X. *et al.* AMPK-dependent phosphorylation of the GATOR2 component WDR24 suppresses glucose-mediated mTORC1 activation. *Nat. Metab.* **5**, 265–276 (2023).
220. Lippai, M. *et al.* SNF4Aγ, the Drosophila AMPK γ subunit is required for regulation of developmental and stress-induced autophagy. *Autophagy* **4**, 476–486 (2008).
221. Meley, D. *et al.* AMP-activated Protein Kinase and the Regulation of Autophagic Proteolysis *. *J. Biol. Chem.* **281**, 34870–34879 (2006).
222. Park, J.-M., Lee, D.-H. & Kim, D.-H. Redefining the role of AMPK in autophagy and the energy stress response. *Nat. Commun.* **14**, 2994 (2023).
223. Young, N. P. *et al.* AMPK governs lineage specification through Tfeb-dependent regulation of lysosomes. *Genes Dev.* **30**, 535–552 (2016).
224. Paquette, M. *et al.* AMPK-dependent phosphorylation is required for transcriptional activation of TFEB and TFE3. *Autophagy* **17**, 3957–3975 (2021).
225. Toyama, E. Q. *et al.* AMP-activated protein kinase mediates mitochondrial fission in response to energy stress. *Science* **351**, 275–281 (2016).
226. Ducommun, S. *et al.* Motif affinity and mass spectrometry proteomic approach for the discovery of cellular AMPK targets: Identification of mitochondrial fission factor as a new AMPK substrate. *Cell. Signal.* **27**, 978–988 (2015).
227. Rabinovitch, R. C. *et al.* AMPK Maintains Cellular Metabolic Homeostasis through Regulation of Mitochondrial Reactive Oxygen Species. *Cell Rep.* **21**, 1–9 (2017).
228. Hotamisligil, G. S., Shargill, N. S. & Spiegelman, B. M. Adipose expression of tumor necrosis factor-alpha: direct role in obesity-linked insulin resistance. *Science* **259**, 87–91 (1993).
229. Kelly, B. & O'Neill, L. A. Metabolic reprogramming in macrophages and dendritic cells in innate immunity. *Cell Res.* **25**, 771–784 (2015).
230. Warburg, O. On the origin of cancer cells. *Science* **123**, 309–314 (1956).

231. Makowski, L., Chaib, M. & Rathmell, J. C. Immunometabolism: From basic mechanisms to translation. *Immunol. Rev.* **295**, 5–14 (2020).
232. Mills, E. L. *et al.* Succinate Dehydrogenase Supports Metabolic Repurposing of Mitochondria to Drive Inflammatory Macrophages. *Cell* **167**, 457-470.e13 (2016).
233. Lampropoulou, V. *et al.* Itaconate Links Inhibition of Succinate Dehydrogenase with Macrophage Metabolic Remodeling and Regulation of Inflammation. *Cell Metab.* **24**, 158–166 (2016).
234. McFadden, B. A. & Purohit, S. Itaconate, an isocitrate lyase-directed inhibitor in Pseudomonas indigofera. *J. Bacteriol.* **131**, 136–144 (1977).
235. Michelucci, A. *et al.* Immune-responsive gene 1 protein links metabolism to immunity by catalyzing itaconic acid production. *Proc. Natl. Acad. Sci. U. S. A.* **110**, 7820–7825 (2013).
236. Mills, E. L. *et al.* Itaconate is an anti-inflammatory metabolite that activates Nrf2 via alkylation of KEAP1. *Nature* **556**, 113–117 (2018).
237. Batista-Gonzalez, A., Vidal, R., Criollo, A. & Carreño, L. J. New Insights on the Role of Lipid Metabolism in the Metabolic Reprogramming of Macrophages. *Front. Immunol.* **10**, 2993 (2020).
238. Cardoso, D. & Perucha, E. Cholesterol metabolism: a new molecular switch to control inflammation. *Clin. Sci. Lond. Engl. 1979* **135**, 1389–1408 (2021).
239. York, A. G. *et al.* Limiting Cholesterol Biosynthetic Flux Spontaneously Engages Type I IFN Signaling. *Cell* **163**, 1716–1729 (2015).
240. Varshney, P., Yadav, V. & Saini, N. Lipid rafts in immune signalling: current progress and future perspective. *Immunology* **149**, 13–24 (2016).
241. Jeong, A., Suazo, K. F., Wood, W. G., Distefano, M. D. & Li, L. Isoprenoids and protein prenylation: implications in the pathogenesis and therapeutic intervention of Alzheimer's disease. *Crit. Rev. Biochem. Mol. Biol.* **53**, 279–310 (2018).
242. Bekkering, S. *et al.* Metabolic Induction of Trained Immunity through the Mevalonate Pathway. *Cell* **172**, 135-146.e9 (2018).
243. Fessler, M. B. The Intracellular Cholesterol Landscape: Dynamic Integrator of the Immune Response. *Trends Immunol.* **37**, 819–830 (2016).
244. Guo, C. *et al.* Cholesterol Homeostatic Regulator SCAP-SREBP2 Integrates NLRP3 Inflammasome Activation and Cholesterol Biosynthetic Signaling in Macrophages. *Immunity* **49**, 842-856.e7 (2018).
245. Kusnadi, A. *et al.* The Cytokine TNF Promotes Transcription Factor SREBP Activity and Binding to Inflammatory Genes to Activate Macrophages and Limit Tissue Repair. *Immunity* **51**, 241-257.e9 (2019).
246. Sag, D., Carling, D., Stout, R. D. & Suttles, J. AMP-activated protein kinase promotes macrophage polarization to an anti-inflammatory functional phenotype. *J. Immunol. Baltim. Md 1950* **181**, 8633–8641 (2008).
247. Yang, Z., Kahn, B. B., Shi, H. & Xue, B. Macrophage α1 AMP-activated Protein Kinase (α1AMPK) Antagonizes Fatty Acid-induced Inflammation through SIRT1. *J. Biol. Chem.* **285**, 19051–19059 (2010).
248. Giri, S. *et al.* 5-Aminoimidazole-4-Carboxamide-1-β-4-Ribofuranoside Inhibits Proinflammatory Response in Glial Cells: A Possible Role of AMP-Activated Protein Kinase. *J. Neurosci.* **24**, 479–487 (2004).

249. Carroll, K. C., Viollet, B. & Suttles, J. AMPKα1 deficiency amplifies proinflammatory myeloid APC activity and CD40 signaling. *J. Leukoc. Biol.* **94**, 1113–1121 (2013).
250. Pilon, G., Dallaire, P. & Marette, A. Inhibition of Inducible Nitric-oxide Synthase by Activators of AMP-activated Protein Kinase: A NEW MECHANISM OF ACTION OF INSULIN-SENSITIZING DRUGS *. *J. Biol. Chem.* **279**, 20767–20774 (2004).
251. Vasamsetti, S. B. *et al.* Metformin Inhibits Monocyte-to-Macrophage Differentiation via AMPK-Mediated Inhibition of STAT3 Activation: Potential Role in Atherosclerosis. *Diabetes* **64**, 2028–2041 (2015).
252. Postler, T. S., Peng, V., Bhatt, D. M. & Ghosh, S. Metformin selectively dampens the acute inflammatory response through an AMPK-dependent mechanism. *Sci. Rep.* **11**, 18721 (2021).
253. Phair, I. R. *et al.* AMPK integrates metabolite and kinase-based immunometabolic control in macrophages. *Mol. Metab.* **68**, 101661 (2023).
254. Banskota, S. *et al.* Salicylates Ameliorate Intestinal Inflammation by Activating Macrophage AMPK. *Inflamm. Bowel Dis.* **27**, 914–926 (2020).
255. Guma, M., Wang, Y., Viollet, B. & Liu-Bryan, R. AMPK Activation by A-769662 Controls IL-6 Expression in Inflammatory Arthritis. *PLoS ONE* **10**, e0140452 (2015).
256. Caratti, G. *et al.* Macrophagic AMPKα1 orchestrates regenerative inflammation induced by glucocorticoids. *EMBO Rep.* **24**, e55363 (2023).
257. R, M. *et al.* AMPKα1 regulates macrophage skewing at the time of resolution of inflammation during skeletal muscle regeneration. *Cell Metab.* **18**, (2013).
258. Galic, S. *et al.* Hematopoietic AMPK β1 reduces mouse adipose tissue macrophage inflammation and insulin resistance in obesity. *J. Clin. Invest.* **121**, 4903–4915 (2011).
259. Zhang, T. *et al.* Metabolic orchestration of cell death by AMPK-mediated phosphorylation of RIPK1. *Science* **380**, 1372–1380 (2023).
260. Wang, J., Ma, A., Zhao, M. & Zhu, H. AMPK activation reduces the number of atheromata macrophages in ApoE deficient mice. *Atherosclerosis* **258**, 97–107 (2017).
261. Lee, M. K. S. *et al.* Defective AMPK regulation of cholesterol metabolism accelerates atherosclerosis by promoting HSPC mobilization and myelopoiesis. *Mol. Metab.* **61**, 101514 (2022).
262. Ma, A., Wang, J., Yang, L., An, Y. & Zhu, H. AMPK activation enhances the anti-atherogenic effects of high density lipoproteins in apoE−/− mice. *J. Lipid Res.* **58**, 1536–1547 (2017).
263. Cao, Q. *et al.* Myeloid Deletion of α1AMPK Exacerbates Atherosclerosis in LDL Receptor Knockout (LDLRKO) Mice. *Diabetes* **65**, 1565–1576 (2016).
264. Fisslthaler, B. *et al.* Myeloid-Specific Deletion of the AMPKα2 Subunit Alters Monocyte Protein Expression and Atherogenesis. *Int. J. Mol. Sci.* **20**, 3005 (2019).
265. Seneviratne, A. *et al.* Metformin directly suppresses atherosclerosis in normoglycaemic mice via haematopoietic adenosine monophosphate-activated protein kinase. *Cardiovasc. Res.* **117**, 1295–1308 (2021).
266. Zhang, M. *et al.* AMP-activated protein kinase α1 promotes atherogenesis by increasing monocyte-to-macrophage differentiation. *J. Biol. Chem.* **292**, 7888–7903 (2017).
267. LeBlond, N. D. *et al.* Myeloid deletion and therapeutic activation of AMPK do not alter atherosclerosis in male or female mice. *J. Lipid Res.* **61**, 1697–1706 (2020).
268. Yang, Q. *et al.* Prkaa1 Metabolically Regulates Monocyte/Macrophage Recruitment and Viability in Diet-Induced Murine Metabolic Disorders. *Front. Cell Dev. Biol.* **8**, 611354 (2021).

269. Dzamko, N. *et al.* AMPK β1 Deletion Reduces Appetite, Preventing Obesity and Hepatic Insulin Resistance *. *J. Biol. Chem.* **285**, 115–122 (2010).
270. Nakamuta, M. *et al.* The significance of differences in fatty acid metabolism between obese and non-obese patients with non-alcoholic fatty liver disease. *Int. J. Mol. Med.* **22**, 663–667 (2008).
271. Ruderman, N. B., Carling, D., Prentki, M. & Cacicedo, J. M. AMPK, insulin resistance, and the metabolic syndrome. *J. Clin. Invest.* **123**, 2764–2772 (2013).
272. Cusi, K. *et al.* Efficacy and safety of PXL770, a direct AMP kinase activator, for the treatment of non-alcoholic fatty liver disease (STAMP-NAFLD): a randomised, double-blind, placebo-controlled, phase 2a study. *Lancet Gastroenterol. Hepatol.* **6**, 889–902 (2021).
273. Esquejo, R. M. *et al.* Activation of Liver AMPK with PF-06409577 Corrects NAFLD and Lowers Cholesterol in Rodent and Primate Preclinical Models. *EBioMedicine* **31**, 122–132 (2018).
274. Gluais-Dagorn, P. *et al.* Direct AMPK Activation Corrects NASH in Rodents Through Metabolic Effects and Direct Action on Inflammation and Fibrogenesis. *Hepatol. Commun.* **6**, 101–119 (2022).
275. Foretz, M. *et al.* Metformin inhibits hepatic gluconeogenesis in mice independently of the LKB1/AMPK pathway via a decrease in hepatic energy state. *J. Clin. Invest.* **120**, 2355–2369 (2010).
276. Foretz, M., Guigas, B. & Viollet, B. Metformin: update on mechanisms of action and repurposing potential. *Nat. Rev. Endocrinol.* **19**, 460–476 (2023).
277. Woods, A. *et al.* Liver-Specific Activation of AMPK Prevents Steatosis on a High-Fructose Diet. *Cell Rep.* **18**, 3043–3051 (2017).
278. Garcia, D. *et al.* Genetic Liver-Specific AMPK Activation Protects against Diet-Induced Obesity and NAFLD. *Cell Rep.* **26**, 192-208.e6 (2019).
279. Foretz, M., Even, P. C. & Viollet, B. AMPK Activation Reduces Hepatic Lipid Content by Increasing Fat Oxidation In Vivo. *Int. J. Mol. Sci.* **19**, 2826 (2018).
280. Zhang, J. *et al.* Molecular Profiling Reveals a Common Metabolic Signature of Tissue Fibrosis. *Cell Rep. Med.* **1**, 100056 (2020).
281. Zhao, P. *et al.* An AMPK-caspase-6 axis controls liver damage in nonalcoholic steatohepatitis. *Science* **367**, 652–660 (2020).
282. Da Silva Morais, A. *et al.* Development of hepatic fibrosis occurs normally in AMPK-deficient mice. *Clin. Sci.* **118**, 411–420 (2010).
283. Ford, R. J. *et al.* Metformin and salicylate synergistically activate liver AMPK, inhibit lipogenesis and improve insulin sensitivity. *Biochem. J.* **468**, 125–132 (2015).
284. Stephenson, K. *et al.* Updates on Dietary Models of Nonalcoholic Fatty Liver Disease: Current Studies and Insights. *Gene Expr.* **18**, 5–17 (2018).
285. Hebbard, L. & George, J. Animal models of nonalcoholic fatty liver disease. *Nat. Rev. Gastroenterol. Hepatol.* **8**, 35–44 (2011).
286. Loomba, R., Sirlin, C. B., Schwimmer, J. B. & Lavine, J. E. Advances in pediatric nonalcoholic fatty liver disease. *Hepatology* **50**, 1282–1293 (2009).
287. Thieme E-Journals - Seminars in Liver Disease / Abstract. https://www.thieme-connect.de/products/ejournals/abstract/10.1055/s-0028-1091980.
288. Pacifico, L. *et al.* Nonalcoholic fatty liver disease and the heart in children and adolescents. *World J. Gastroenterol. WJG* **20**, 9055–9071 (2014).
289. Targher, G. *et al.* Prevalence of Nonalcoholic Fatty Liver Disease and Its Association With Cardiovascular Disease Among Type 2 Diabetic Patients. *Diabetes Care* **30**, 1212–1218 (2007).

290. Duan, X.-Y., Zhang, L., Fan, J.-G. & Qiao, L. NAFLD leads to liver cancer: Do we have sufficient evidence? *Cancer Lett.* **345**, 230–234 (2014).
291. Anstee, Q. M. & Day, C. P. The genetics of NAFLD. *Nat. Rev. Gastroenterol. Hepatol.* **10**, 645–655 (2013).
292. Dufour, J.-F. *et al.* Current therapies and new developments in NASH. *Gut* **71**, 2123–2134 (2022).
293. Best, C. H. & Huntsman, M. E. The effect of choline on the liver fat of rats in various states of nutrition. *J. Physiol.* **83**, 255–274 (1935).
294. Febbraio, M. A. *et al.* Preclinical Models for Studying NASH-Driven HCC: How Useful Are They? *Cell Metab.* **29**, 18–26 (2019).
295. Keijer, J., Li, M. & Speakman, J. R. What is the best housing temperature to translate mouse experiments to humans? *Mol. Metab.* **25**, 168–176 (2019).
296. Ahmed, B. A. *et al.* Lower brown adipose tissue activity is associated with non-alcoholic fatty liver disease but not changes in the gut microbiota. *Cell Rep. Med.* **2**, (2021).
297. Giles, D. A. *et al.* Modulation of ambient temperature promotes inflammation and initiates atherosclerosis in wild type C57BL/6 mice. *Mol. Metab.* **5**, 1121–1130 (2016).
298. Liang, J. Q. *et al.* Dietary cholesterol promotes steatohepatitis related hepatocellular carcinoma through dysregulated metabolism and calcium signaling. *Nat. Commun.* **9**, 4490 (2018).
299. Colesevelam ameliorates non-alcoholic steatohepatitis and obesity in mice | Hepatology International. https://link.springer.com/article/10.1007/s12072-022-10296-w.
300. Lytle, K. A. & Jump, D. B. Is Western Diet-Induced Nonalcoholic Steatohepatitis in Ldlr-/- Mice Reversible? *PLOS ONE* **11**, e0146942 (2016).
301. Differences in metabolic and liver pathobiology induced by two dietary mouse models of nonalcoholic fatty liver disease | American Journal of Physiology-Endocrinology and Metabolism. https://journals.physiology.org/doi/full/10.1152/ajpendo.00321.2020.
302. Dudele, A. *et al.* Effects of ambient temperature on glucose tolerance and insulin sensitivity test outcomes in normal and obese C57 male mice. *Physiol. Rep.* **3**, e12396 (2015).
303. Bligh, E. G. & Dyer, W. J. A RAPID METHOD OF TOTAL LIPID EXTRACTION AND PURIFICATION. *Can. J. Biochem. Physiol.* **37**, 911–917 (1959).
304. Livak, K. J. & Schmittgen, T. D. Analysis of Relative Gene Expression Data Using Real-Time Quantitative PCR and the 2−ΔΔCT Method. *Methods* **25**, 402–408 (2001).
305. Small, L., Gong, H., Yassmin, C., Cooney, G. J. & Brandon, A. E. Thermoneutral housing does not influence fat mass or glucose homeostasis in C57BL/6 mice. *J. Endocrinol.* **239**, 313–324 (2018).
306. Bissig-Choisat, B. *et al.* A human liver chimeric mouse model for non-alcoholic fatty liver disease. *JHEP Rep.* **3**, (2021).
307. Ghallab, A. *et al.* Spatio-Temporal Multiscale Analysis of Western Diet-Fed Mice Reveals a Translationally Relevant Sequence of Events during NAFLD Progression. *Cells* **10**, 2516 (2021).
308. Casimiro, I., Stull, N. D., Tersey, S. A. & Mirmira, R. G. Phenotypic sexual dimorphism in response to dietary fat manipulation in C57BL/6J mice. *J. Diabetes Complications* **35**, 107795 (2021).
309. Reynolds, T. H. *et al.* The impact of age and sex on body composition and glucose sensitivity in C57BL/6J mice. *Physiol. Rep.* **7**, e13995 (2019).

310. Yang, Y., Smith, D. L., Keating, K. D., Allison, D. B. & Nagy, T. R. Variations in body weight, food intake and body composition after long-term high-fat diet feeding in C57BL/6J Mice. *Obes. Silver Spring Md* **22**, 2147–2155 (2014).
311. Škop, V. *et al.* Mouse Thermoregulation: Introducing the Concept of the Thermoneutral Point. *Cell Rep.* **31**, 107501 (2020).
312. Fischer, A. W., Cannon, B. & Nedergaard, J. Optimal housing temperatures for mice to mimic the thermal environment of humans: An experimental study. *Mol. Metab.* **7**, 161–170 (2018).
313. Bogatyrev, S. R., Rolando, J. C. & Ismagilov, R. F. Self-reinoculation with fecal flora changes microbiota density and composition leading to an altered bile-acid profile in the mouse small intestine. *Microbiome* **8**, 19 (2020).
314. Zhou, D. *et al.* Total fecal microbiota transplantation alleviates high-fat diet-induced steatohepatitis in mice via beneficial regulation of gut microbiota. *Sci. Rep.* **7**, 1529 (2017).
315. Sadler, D. G., Treas, L., Sikes, J. D. & Porter, C. A modest change in housing temperature alters whole body energy expenditure and adipocyte thermogenic capacity in mice. *Am. J. Physiol.-Endocrinol. Metab.* **323**, E517–E528 (2022).
316. Choi, B. S.-Y. *et al.* Feeding diversified protein sources exacerbates hepatic insulin resistance via increased gut microbial branched-chain fatty acids and mTORC1 signaling in obese mice. *Nat. Commun.* **12**, 3377 (2021).
317. Farrell, G. *et al.* Mouse Models of Nonalcoholic Steatohepatitis: Toward Optimization of Their Relevance to Human Nonalcoholic Steatohepatitis. *Hepatology* **69**, 2241 (2019).
318. Marcher, A.-B. *et al.* Transcriptional regulation of Hepatic Stellate Cell activation in NASH. *Sci. Rep.* **9**, 2324 (2019).
319. Guilliams, M. & Scott, C. L. Liver macrophages in health and disease. *Immunity* **55**, 1515–1529 (2022).
320. Steneberg, P. *et al.* PAN-AMPK activator O304 improves glucose homeostasis and microvascular perfusion in mice and type 2 diabetes patients. *JCI Insight* **3**, e99114, 99114 (2018).
321. Hawley, S. A. *et al.* The ancient drug salicylate directly activates AMP-activated protein kinase. *Science* **336**, 918–922 (2012).
322. Feng, W. *et al.* Randomized trial comparing the effects of gliclazide, liraglutide, and metformin on diabetes with non-alcoholic fatty liver disease. *J. Diabetes* **9**, 800–809 (2017).
323. Tian, F., Zheng, Z., Zhang, D., He, S. & Shen, J. Efficacy of liraglutide in treating type 2 diabetes mellitus complicated with non-alcoholic fatty liver disease. *Biosci. Rep.* **38**, BSR20181304 (2018).
324. Zhang, R. *et al.* Metformin and Diammonium Glycyrrhizinate Enteric-Coated Capsule versus Metformin Alone versus Diammonium Glycyrrhizinate Enteric-Coated Capsule Alone in Patients with Nonalcoholic Fatty Liver Disease and Type 2 Diabetes Mellitus. *Gastroenterol. Res. Pract.* **2017**, 8491742 (2017).
325. Loomba, R. *et al.* Clinical trial: pilot study of metformin for the treatment of non-alcoholic steatohepatitis. *Aliment. Pharmacol. Ther.* **29**, 172–182 (2009).
326. Martini, T., Naef, F. & Tchorz, J. S. Spatiotemporal Metabolic Liver Zonation and Consequences on Pathophysiology. *Annu. Rev. Pathol.* **18**, 439–466 (2023).
327. Okishio, S. *et al.* PPARα agonist and metformin co-treatment ameliorates NASH in mice induced by a choline-deficient, amino acid-defined diet with 45% fat. *Sci. Rep.* **10**, 19578 (2020).

328. Matsumoto, M. *et al.* An improved mouse model that rapidly develops fibrosis in non-alcoholic steatohepatitis. *Int. J. Exp. Pathol.* **94**, 93–103 (2013).
329. Viollet, B. *et al.* The AMP-activated protein kinase α2 catalytic subunit controls whole-body insulin sensitivity. *J. Clin. Invest.* **111**, 91–98 (2003).
330. Clausen, B. E., Burkhardt, C., Reith, W., Renkawitz, R. & Förster, I. Conditional gene targeting in macrophages and granulocytes using LysMcre mice. *Transgenic Res.* **8**, 265–277 (1999).
331. Bankhead, P. *et al.* QuPath: Open source software for digital pathology image analysis. *Sci. Rep.* **7**, 16878 (2017).
332. Daemen, S., Chan, M. M. & Schilling, J. D. Comprehensive analysis of liver macrophage composition by flow cytometry and immunofluorescence in murine NASH. *STAR Protoc.* **2**, 100511 (2021).
333. Steinberg, G. R. & Carling, D. AMP-activated protein kinase: the current landscape for drug development. *Nat. Rev. Drug Discov.* **18**, 527–551 (2019).
334. Dong, C. *et al.* RNA sequencing and transcriptomal analysis of human monocyte to macrophage differentiation. *Gene* **519**, 279–287 (2013).
335. Abram, C. L., Roberge, G. L., Hu, Y. & Lowell, C. A. Comparative analysis of the efficiency and specificity of myeloid-Cre deleting strains using ROSA-EYFP reporter mice. *J. Immunol. Methods* **408**, 89–100 (2014).
336. Greenhalgh, S. N., Conroy, K. P. & Henderson, N. C. Cre-ativity in the liver: Transgenic approaches to targeting hepatic nonparenchymal cells. *Hepatol. Baltim. Md* **61**, 2091–2099 (2015).
337. Zhou, G. *et al.* Role of AMP-activated protein kinase in mechanism of metformin action. *J. Clin. Invest.* **108**, 1167–1174 (2001).
338. Clarke, J. D. *et al.* Mechanism of Altered Metformin Distribution in Nonalcoholic Steatohepatitis. *Diabetes* **64**, 3305–3313 (2015).
339. Katsura, A. *et al.* MicroRNA profiles following metformin treatment in a mouse model of non-alcoholic steatohepatitis. *Int. J. Mol. Med.* **35**, 877–884 (2015).
340. Li, Y.-L., Li, X.-Q., Wang, Y.-D., Shen, C. & Zhao, C.-Y. Metformin alleviates inflammatory response in non-alcoholic steatohepatitis by restraining signal transducer and activator of transcription 3-mediated autophagy inhibition in vitro and in vivo. *Biochem. Biophys. Res. Commun.* **513**, 64–72 (2019).
341. Y, K. *et al.* Metformin prevents and reverses inflammation in a non-diabetic mouse model of nonalcoholic steatohepatitis. *PloS One* **7**, (2012).
342. Vara Ciruelos, D. *et al.* Phenformin, but not metformin, delays development of T-cell acute lymphoblastic leukemia/lymphoma via cell-autonomous AMPK activation. *Cell Rep.* **27**, 690-698.e4 (2019).
343. Krenkel, O., Mossanen, J. C. & Tacke, F. Immune mechanisms in acetaminophen-induced acute liver failure. *Hepatobiliary Surg. Nutr.* **3**, 331–343 (2014).
344. Jaeschke, H. & Ramachandran, A. Mechanisms and pathophysiological significance of sterile inflammation during acetaminophen hepatotoxicity. *Food Chem. Toxicol.* **138**, 111240 (2020).
345. Saberi, B. *et al.* Protein kinase C (PKC) participates in acetaminophen hepatotoxicity through JNK dependent and independent signaling pathways. *Hepatol. Baltim. Md* **59**, 1543–1554 (2014).

346. Zhang, J. *et al.* Apigenin Attenuates Acetaminophen-Induced Hepatotoxicity by Activating AMP-Activated Protein Kinase/Carnitine Palmitoyltransferase I Pathway. *Front. Pharmacol.* **11**, (2020).
347. Yan, M. *et al.* Cajaninstilbene Acid Ameliorates Acetaminophen-Induced Liver Injury Through Enhancing Sestrin2/AMPK-Mediated Mitochondrial Quality Control. *Front. Pharmacol.* **13**, (2022).
348. Lv, H. *et al.* Corilagin alleviates acetaminophen-induced hepatotoxicity via enhancing the AMPK/GSK3β-Nrf2 signaling pathway. *Cell Commun. Signal.* **17**, 2 (2019).
349. Leng, J. *et al.* NF-κB and AMPK/PI3K/Akt signaling pathways are involved in the protective effects of Platycodon grandiflorum saponins against acetaminophen-induced acute hepatotoxicity in mice. *Phytother. Res. PTR* **32**, 2235–2246 (2018).
350. Cui, B.-W. *et al.* Thymoquinone Attenuates Acetaminophen Overdose-Induced Acute Liver Injury and Inflammation Via Regulation of JNK and AMPK Signaling Pathway. *Am. J. Chin. Med.* **47**, 577–594 (2019).
351. Wu, J. *et al.* Ferulic acid ameliorates acetaminophen-induced acute liver injury by promoting AMPK-mediated protective autophagy. *IUBMB Life* **74**, 880–895 (2022).
352. Ramachandran, R. & Saraswathy, M. Up-regulation of nuclear related factor 2 (NRF2) and antioxidant responsive elements by metformin protects hepatocytes against the acetaminophen toxicity. *Toxicol. Res.* **3**, 350–358 (2014).
353. Hwang, J. H. *et al.* Enhanced Production of Adenosine Triphosphate by Pharmacological Activation of Adenosine Monophosphate-Activated Protein Kinase Ameliorates Acetaminophen-Induced Liver Injury. *Moleucles Cells* **38**, 843–850 (2015).
354. Mossanen, J. & Tacke, F. Acetaminophen-induced acute liver injury in mice. *Lab. Anim.* **49**, 30–36 (2015).
355. Martínez Rivas, C. J. *et al.* Nanoprecipitation process: From encapsulation to drug delivery. *Int. J. Pharm.* **532**, 66–81 (2017).
356. Bachurski, D. *et al.* Extracellular vesicle measurements with nanoparticle tracking analysis – An accuracy and repeatability comparison between NanoSight NS300 and ZetaView. *J. Extracell. Vesicles* **8**, 1596016 (2019).
357. Troutman, T. D. *et al.* Purification of mouse hepatic non-parenchymal cells or nuclei for use in ChIP-seq and other next-generation sequencing approaches. *STAR Protoc.* **2**, 100363 (2021).
358. Suk, J. S., Xu, Q., Kim, N., Hanes, J. & Ensign, L. M. PEGylation as a strategy for improving nanoparticle-based drug and gene delivery. *Adv. Drug Deliv. Rev.* **99**, 28–51 (2016).
359. Danhier, F. *et al.* PLGA-based nanoparticles: An overview of biomedical applications. *J. Controlled Release* **161**, 505–522 (2012).
360. Sylvestre, M., Pun, S. H. & Crane, C. A. Progress on Modulating Tumor-Associated Macrophages with Biomaterials. *Adv. Mater. Deerfield Beach Fla* **32**, e1902007 (2020).
361. Ngo, W. *et al.* Why nanoparticles prefer liver macrophage cell uptake in vivo. *Adv. Drug Deliv. Rev.* **185**, 114238 (2022).
362. Colino, C. I., Lanao, J. M. & Gutierrez-Millan, C. Targeting of Hepatic Macrophages by Therapeutic Nanoparticles. *Front. Immunol.* **11**, (2020).
363. Jaeschke, H. & Ramachandran, A. Acetaminophen-induced apoptosis: Facts versus fiction. *J. Clin. Transl. Res.* **6**, 36–47 (2020).

364. Jaeschke, H., Duan, L., Akakpo, J. Y., Farhood, A. & Ramachandran, A. The role of apoptosis in acetaminophen hepatotoxicity. *Food Chem. Toxicol. Int. J. Publ. Br. Ind. Biol. Res. Assoc.* **118**, 709–718 (2018).
365. Dara, L. *et al.* Receptor Interacting Protein Kinase-1 mediates murine acetaminophen toxicity independent of the necrosome and not through necroptosis. *Hepatol. Baltim. Md* **62**, 1847–1857 (2015).
366. Jaeschke, H., Ramachandran, A., Chao, X. & Ding, W.-X. EMERGING AND ESTABLISHED MODES OF CELL DEATH DURING ACETAMINOPHEN-INDUCED LIVER INJURY. *Arch. Toxicol.* **93**, 3491–3502 (2019).
367. Iorga, A. *et al.* Interaction of RIPK1 and A20 modulates MAPK signaling in murine acetaminophen toxicity. *J. Biol. Chem.* **296**, (2021).
368. Shi, J., Hua, L., Harmer, D., Li, P. & Ren, G. Cre Driver Mice Targeting Macrophages. *Methods Mol. Biol. Clifton NJ* **1784**, 263–275 (2018).
369. Gorabi, A. M. *et al.* Implications for the role of lipopolysaccharide in the development of atherosclerosis. *Trends Cardiovasc. Med.* **32**, 525–533 (2022).
370. Hersoug, L.-G., Møller, P. & Loft, S. Role of microbiota-derived lipopolysaccharide in adipose tissue inflammation, adipocyte size and pyroptosis during obesity. *Nutr. Res. Rev.* **31**, 153–163 (2018).
371. Biomolecules | Free Full-Text | Transcriptomic Profiling Reveals That HMGB1 Induces Macrophage Polarization Different from Classical M1. https://www.mdpi.com/2218-273X/12/6/779.
372. Yang, X. *et al.* Promoting AMPK/SR-A1-mediated clearance of HMGB1 attenuates chemotherapy-induced peripheral neuropathy. *Cell Commun. Signal.* **21**, 99 (2023).
373. Schmitt, D. L. *et al.* Spatial regulation of AMPK signaling revealed by a sensitive kinase activity reporter. *Nat. Commun.* **13**, 3856 (2022).
374. Sahle, F. F. Polymeric Nanoparticles-Based Drug and Gene Delivery to Macrophages. in *Macrophage Targeted Delivery Systems: Basic Concepts and Therapeutic Applications* (eds. Gupta, S. & Pathak, Y. V.) 145–167 (Springer International Publishing, 2022). doi:10.1007/978-3-030-84164-5_7.
375. Hoque, R., Farooq, A. & Mehal, W. Z. Sterile inflammation in the liver and pancreas. *J. Gastroenterol. Hepatol.* **28**, 61–67 (2013).
376. Clayton, Z. S. & McCurdy, C. E. Short-term thermoneutral housing alters glucose metabolism and markers of adipose tissue browning in response to a high-fat diet in lean mice. *Am. J. Physiol.-Regul. Integr. Comp. Physiol.* **315**, R627–R637 (2018).
377. Fischer, A. W. *et al.* Thermoneutrality-Induced Macrophage Accumulation in Brown Adipose Tissue Does Not Impair the Tissue's Competence for Cold-Induced Thermogenic Recruitment. *Front. Endocrinol.* **11**, (2020).
378. Raun, S. H. *et al.* Housing temperature influences exercise training adaptations in mice. *Nat. Commun.* **11**, 1560 (2020).
379. Povinelli, B. J. *et al.* Standard Sub-Thermoneutral Caging Temperature Influences Radiosensitivity of Hematopoietic Stem and Progenitor Cells. *PLOS ONE* **10**, e0120078 (2015).
380. Speakman, J. R. & Keijer, J. Not so hot: Optimal housing temperatures for mice to mimic the thermal environment of humans. *Mol. Metab.* **2**, 5–9 (2013).
381. Halpern, K. B. *et al.* Single-cell spatial reconstruction reveals global division of labour in the mammalian liver. *Nature* **542**, 352–356 (2017).

382. Gola, A. *et al.* Commensal-driven immune zonation of the liver promotes host defence. *Nature* **589**, 131–136 (2021).
383. Corbin, K. D. & Zeisel, S. H. Choline Metabolism Provides Novel Insights into Non-alcoholic Fatty Liver Disease and its Progression. *Curr. Opin. Gastroenterol.* **28**, 159–165 (2012).
384. Banskota, S. *et al.* Inhibition of NADPH Oxidase (NOX) 2 Mitigates Colitis in Mice with Impaired Macrophage AMPK Function. *Biomedicines* **11**, 1443 (2023).
385. Viollet, B. *et al.* AMPK: Lessons from transgenic and knockout animals. *Front. Biosci. Landmark Ed.* **14**, 19–44 (2009).
386. Guilliams, M. *et al.* Spatial proteogenomics reveals distinct and evolutionarily conserved hepatic macrophage niches. *Cell* **185**, 379-396.e38 (2022).
387. Zhao, D. *et al.* ALK1 signaling is required for the homeostasis of Kupffer cells and prevention of bacterial infection. *J. Clin. Invest.* **132**, (2022).
388. Ni, M. *et al.* T-Cell Immunoglobulin and Mucin Domain-Containing Protein-4 Is Critical for Kupffer Cell Homeostatic Function in the Activation and Resolution of Liver Ischemia Reperfusion Injury. *Hepatol. Baltim. Md* **74**, 2118–2132 (2021).
389. Lopes, M. E. *et al.* Susceptibility to Infections During Acute Liver Injury Depends on Transient Disruption of Liver Macrophage Niche. *Front. Immunol.* **13**, (2022).
390. Triantafyllou, E. *et al.* PD-1 blockade improves Kupffer cell bacterial clearance in acute liver injury. *J. Clin. Invest.* **131**, e140196.

Appendix

Rights and Permissions

Chapter 1: General Introduction

Chapter 1 - Figures	Licenses	Provider
Figure 1.1.	5632791270020	Springer Nature and Copyright Clearance Centre Inc.
Figure 1.2.	1398453-1	Copyright Clearance Centre Inc. on behalf of American Society for Clinical Investigation.
Figure 1.3.	CC BY-NC 4.0	Creative Commons.
Figure 1.4.	5632800235222	Springer Nature and Copyright Clearance Centre Inc.
Figure 1.5.	5632800512605	Springer Nature and Copyright Clearance Centre Inc.
Figure 1.6.	5632800837723	Springer Nature and Copyright Clearance Centre Inc.

Chapter 2: Thermoneutral housing does not accelerate metabolic dysfunction-associated fatty liver disease in male or female C57Bl/6J mice fed a Western diet.

American Journal of Physiology publication process

REUSE OF APS CONTENT BY APS AUTHORS

Authors of APS articles may reuse their content in the following situations:

Type of Use	Allowed?	Terms*
Reuse in New Works	**Yes**	Full citation is required.
Meeting Presentations and Conferences	**Yes**	A copyright fee will apply if there is a charge to the user or if the meeting is commercially supported. Full citation is required.
Theses and Dissertations	**Yes**	Whole articles may be reproduced in dissertations and posted to thesis repositories. Full citation is required.
Open Courseware	**Yes**	A copyright fee will apply to a book chapter or during the first 12 months of a journal article's publication. Full citation is required.
Posting to Websites	No	Articles may not be posted to any website including social and research networking platforms. Instead, authors should post a link to the journal article using the digital object identifier (DOI).
Posting to Institutional Repositories (Non-Theses)	**Yes**	Articles may be posted if • embargoed for 12-months from the date of final publication; • accompanied by a link to the article on the APS journal website; • not used for commercial purposes; Self-archived articles are without warranty of any kind.

*__Exception:__ Articles published with **APS Open Access** under a Creative Commons license (CC-BY 4.0) may be shared and reused immediately with full citation.

(Information for Authors: Publication Process (physiology.org))

Chapter 3: Myeloid AMPK signaling is dispensable for, and low-dose metformin does not improve diet-induced NASH in male and female mice.

Journal of Lipid Research publication process

Submission declaration and verification

Submission of an article implies that the work described has not been published previously (except in the form of an abstract, a published lecture, academic thesis, or preprint, see 'Multiple, redundant or concurrent publication' for more information), that it is not under consideration for publication elsewhere, that its publication is approved by all authors and tacitly or explicitly by the responsible authorities where the work was carried out, and that, if accepted, it will not be published elsewhere in the same form, in English or in any other language, including electronically without the written consent of the copyright-holder. To verify originality, your article may be checked by the originality detection service Crossref Similarity Check.

(Guide for authors - Journal of Lipid Research - ISSN 0022-2275 | ScienceDirect.com by Elsevier)

Appendix: Metformin again? Atheroprotection mediated by macrophage AMPK and ATF1

OXFORD UNIVERSITY PRESS LICENSE
TERMS AND CONDITIONS

Sep 21, 2023

This Agreement between University of Ottawa -- Julia Nunes ("You") and Oxford University Press ("Oxford University Press") consists of your license details and the terms and conditions provided by Oxford University Press and Copyright Clearance Center.

The publisher has provided special terms related to this request that can be found at the end of the Publisher's Terms and Conditions.

License Number	5633910540002
License date	Sep 21, 2023
Licensed content publisher	Oxford University Press
Licensed content publication	Cardiovascular Research
Licensed content title	Metformin again? Atheroprotection mediated by macrophage AMPK and ATF1
Licensed content author	Salt, Ian P; Nunes, Julia R C
Licensed content date	Mar 3, 2021
Type of Use	Thesis/Dissertation

ESC European Society of Cardiology
Cardiovascular Research (2021) 117, 1233–1234
doi:10.1093/cvr/cvab065

EDITORIAL

Metformin again? Atheroprotection mediated by macrophage AMPK and ATF1

Ian P. Salt [1]*, Julia R.C. Nunes [2,3], and Morgan D. Fullerton [2,3]

[1]Institute of Cardiovascular and Medical Sciences, College of Medical, Veterinary and Life Sciences, University of Glasgow, Glasgow G12 8QQ, UK; [2]Department of Biochemistry, Microbiology and Immunology, Faculty of Medicine, University of Ottawa, Ottawa, ON K1H 8M5, Canada and [3]Centre for Infection, Immunity and Inflammation, Centre for Catalysis Research and Innovation, University of Ottawa, Ottawa, ON K1H 8M5, Canada

Online publish-ahead-of-print 3 March 2021

This editorial refers to 'Metformin directly suppresses atherosclerosis in normoglycemic mice via haematopoietic Adenosine Monophosphate-Activated Protein Kinase (AMPK)' by A. Seneviratne *et al.*, pp. 1295–1308.

Metformin is a biguanide that has been used as a frontline treatment for type 2 diabetes (T2DM) over the past 60 years, though its medicinal roots date back to medieval times. While new medications have emerged in recent years, metformin remains the most widely prescribed anti-diabetic drug. Despite this, the molecular mechanisms by which metformin acts remain incompletely understood.[1] Twenty years ago, metformin was demonstrated to activate hepatic AMP-activated protein kinase (AMPK),[2] a master regulator of energy homeostasis that exerts control over lipid and carbohydrate metabolism. Although metformin-mediated suppression of hepatic glucose production was subsequently shown to be AMPK-independent,[3] others reported that AMPK activation underlies metformin-mediated improvements in insulin action by maintaining hepatic lipid homeostasis.[4] Given its low cost, well-known tolerance and broad metabolic benefits, there are efforts currently underway to 'repurpose' metformin towards conditions, such as cancers, ageing, and cardiovascular disease. Atherosclerosis is characterized by chronic-low-grade inflammation that is driven by hyperlipidaemia and immune-infiltration that results in the formation of lipid-rich plaque in the arterial intima. Atherosclerotic macrovascular disease is a leading cause of mortality in people with T2DM and growing evidence suggests that metformin has a direct anti-atherogenic action that may be independent of its effect on glycaemia.[5] AMPK activation in vascular tissues has also been demonstrated to exhibit anti-inflammatory and anti-atherogenic actions.[6] Therefore, while potentially not independent, or mutually exclusive of any effect on glycaemia, stimulation of AMPK by metformin may still hold therapeutic promise against atherosclerosis given its role in lipid metabolism and inflammation.

In this study, Seneviratne *et al.*[7] sought to add to the limited pre-clinical understanding we have and examine whether metformin treatment had anti-atherogenic actions in normoglycemic but atherogenic mice and whether this potential benefit was AMPK-mediated. Their studies support a novel mechanism by which metformin suppresses atherogenesis by promoting a protective, pro-resolving macrophage M2-like phenotype that overlaps with a [Mhem] phenotype in an AMPK- and activating transcription factor 1 (ATF1)-dependent manner.

Their study made use of low-density lipoprotein receptor (*Ldlr*) knockout (KO) mice fed a regular chow diet to avoid the hyperglycaemia that accompanies Western diet feeding of *Ldlr* KO mice. A preventative and clinically relevant metformin regime saw a significant reduction in early, macrophage-rich atherosclerotic lesions in these mice without altering glucose or lipid profiles. Given this, the authors focused on the haematopoietic compartment. Transplantation of bone marrow from AMPKb1-deficient (*Prkab1*$^{-/-}$) mice into *Ldlr* KO recipients abrogated the atheroprotective action of metformin, whereas metformin was still effective in mice transplanted with bone marrow from wild type littermate controls. The same group has previously demonstrated that haeme and metformin increase ATF1 phosphorylation in an AMPK-dependent manner in human blood-derived macrophages, leading to the atheroprotective, [Mhem] phenotype.[8] In this study, transcriptional analysis of primary macrophages showed that metformin promoted the expression of atheroprotective genes in an AMPK- and ATF1-dependent manner. These experiments were also extended in human blood macrophages where Mhem-associated atheroprotective genes required the transcriptional activity of ATF1 with metformin treatment. The importance of this pathway was further validated *in vivo*, where metformin stimulated phosphorylation of AMPK, ATF1 and suppressed markers of inflammation in lesional cells. Finally, in contrast to plaque reduction seen in preventative treatment of early atherosclerosis, metformin treatment of the same mice/model with more established atherosclerosis increased the extent of the layer of vascular smooth muscle cells (VSMCs) between the endothelium and the macrophages. A scheme of the proposed mechanism is shown in *Figure 1*.

This work adds to previous studies that have shown a protective effect of metformin in mice and points to a mechanistic role for haematopoietic AMPK. While there was a clear rationale for the use of chow fed *Ldlr* KO mice, thereby removing potential influence of hyperglycaemia from the model system, this also removed an important variable and driver of atherogenesis, hyperlipidaemia. There are, however, no mouse models that perfectly model the progression of human atherosclerosis.

The opinions expressed in this article are not necessarily those of the Editors of *Cardiovascular Research* or of the European Society of Cardiology.

* Corresponding Author. Tel: þ44 (0)141 330 2049, E-mail: ian.salt@glasgow.ac.uk

Published on behalf of the European Society of Cardiology. All rights reserved. © The Author(s) 2021. For permissions, please email: journals.permissions@oup.com.

Downloaded from https://academic.oup.com/cardiovascres/article/117/5/1233/6157826 by guest on 28 September 2023

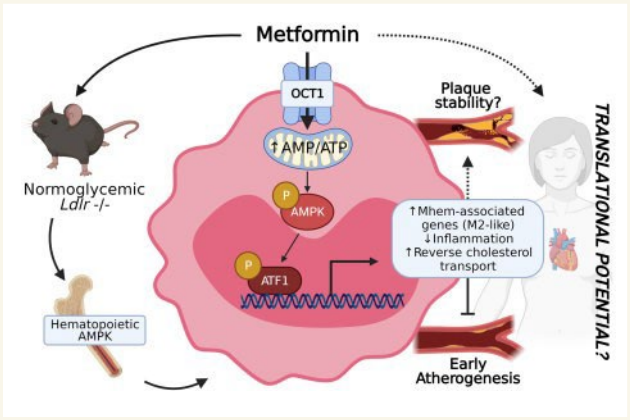

Figure 1 Model of attenuated atherogenesis in response to metformin in macrophages. Metformin is transported into macrophages, likely via the organic cation transporter-1, where it is activates AMPK through inhibition of mitochondrial ATP synthesis, leading to activation of AMPK. AMPK phosphorylates and activates ATF1-mediated transcription of genes concerned with reverse cholesterol transport and resolution of inflammation, leading to a phenotype resembling Mhem. In normoglycemic *Lldr*$^{-/-}$ mice, via haematopoietic AMPK, this subsequently suppresses atherogenesis and may increase stability of established plaques. Created with BioRender.com.

The beneficial effects of metformin described here should be considered in the context of the earliest stages of atherosclerosis. It is, however, also intriguing that metformin shows evidence of increasing plaque stability in more established atherosclerosis, albeit in a model without the potential for advanced plaque. Although the AMPK- or ATF1-dependence of this was not tested in the study of Seneviratne *et al.*,[9] metformin has been reported to increase indices of plaque stability via mechanisms that require AMPK in VSMCs and several atherosclerosis-prone AMPK KO mouse models have been reported to exhibit more advanced, less stable plaques.[6] It will indeed be interesting to test the preventative and therapeutic potential of metformin (and potentially other AMPK activators) in pre-clinical models of more advanced and aggressive atherogenesis.

Overall, Seneviratne *et al.*[5] provide evidence for an atheroprotective effect of metformin involving activation of haematopoietic AMPK and ATF1. The significance of this work lies in the translational appeal for people without diabetes. The epidemiological evidence suggesting that metformin use protects against adverse cardiovascular outcomes in people is not overwhelming, yet there is a therapeutic benefit. However, from a translational perspective, the potential that metformin treatment has to initiate anti-inflammatory and atheroprotective gene programmes in monocytes and macrophages of people both with and without diabetes is a testable hypothesis. Do human immune cells experience the same immune programming upon oral metformin administration? How well does this metformin-induced polarization influence plaque macrophage dynamics? While both are important questions, a final consideration may relate to the appropriate therapeutic window. Could metformin be used to prevent atherogenesis in those at risk regardless of whether they have diabetes? Furthermore, given the finding that a clinically relevant dose of metformin shows evidence of increasing plaque stability, does metformin have the potential to stabilize vulnerable plaque in advanced human lesions, while at the same time favourably altering immunometabolism? Metformin is cost effective and has a long-standing reputation for being safe. It is also worth noting that selective AMPK activators are also currently in clinical trials for the treatment of fatty liver disease and T2DM.[10,11] There may, therefore, also be the potential for targeting macrophage AMPK directly to prevent atherogenesis or stabilize plaques. Addressing these questions could unravel the full potential of metformin for the treatment and management of cardiovascular disease as well as other disorders with an inflammation component, independent of diabetes.

Conflict of interest: none declared.

References

1. Foretz M, Guigas B, Viollet B. Understanding the glucoregulatory mechanisms of metformin in type 2 diabetes mellitus. *Nat Rev Endocrinol* 2019;15:569–589.
2. Zhou G, Myers R, Li Y, Chen Y, Shen X, Fenyk-Melody J, Wu M, Ventre J, Doebber T, Fujii N, Musi N, Hirshman MF, Goodyear LJ, Moller DE. Role of AMP-activated protein kinase in mechanism of metformin action. *J Clin Invest* 2001;108:1167–1174.
3. Foretz M, He´brard S, Leclerc J, Zarrinpashneh E, Soty M, Mithieux G, Sakamoto K, Andreelli F, Viollet B. Metformin inhibits hepatic gluconeogenesis in mice independently of the LKB1/AMPK pathway via a decrease in hepatic energy state. *J Clin Invest* 2010;120:2355–2369.
4. Fullerton MD, Galic S, Marcinko K, Sikkema S, Pulinilkunnil T, Chen ZP, O'Neill HM, Ford RJ, Palanivel R, O'Brien M, Hardie DG, Macaulay SL, Schertzer JD, Dyck JR, van Denderen BJ, Kemp BE, Steinberg GR. Single phosphorylation sites in Acc1 and Acc2 regulate lipid homeostasis and the insulin-sensitizing effects of metformin. *Nat Med* 2013;19:1649–1654.
5. Luo F, Das A, Chen J, Wu P, Li X, Fang Z. Metformin in patients with and without diabetes: a paradigm shift in cardiovascular disease management. *Cardiovasc Diabetol* 2019;18:54.
6. Salt IP, Hardie DG. AMP-activated protein kinase: an ubiquitous signaling pathway with Key roles in the cardiovascular system. *Circ Res* 2017;120:1825–1841.
7. Seneviratne A, Cave L, Hyde G, Moestrup SK, Carling D, Mason JC, Haskard DO, Boyle JJ. Metformin directly suppresses atherosclerosis in normoglycemic mice via haematopoietic Adenosine Monophosphate-Activated Protein Kinase (AMPK). *Cardiovasc Res* 2021;117:1295–1308.
8. Wan X, Huo Y, Johns M, Piper E, Mason JC, Carling D, Haskard DO, Boyle JJ. 5'-AMP-activated protein kinase-activating transcription factor 1 cascade modulates human monocyte-derived macrophages to atheroprotective functions in response to heme or metformin. *Arterioscler Thromb Vasc Biol* 2013;33:2470–2480.
9. Cai Z, Ding Y, Zhang M, Lu Q, Wu S, Zhu H, Song P, Zou MH. Ablation of adenosine monophosphate-activated protein kinase alpha1 in vascular smooth muscle cells promotes diet-induced atherosclerotic calcification in vivo. *Circ Res* 2016;119:422–433.
10. Steneberg P, Lindahl E, Dahl U, Lidh E, Straseviciene J, Backlund F, Kjellkvist E, Berggren E, Lundberg I, Bergqvist I, Ericsson M, Eriksson B, Linde K, Westman J, Edlund T, Edlund H. PAN-AMPK activator O304 improves glucose homeostasis and microvascular perfusion in mice and type 2 diabetes patients. *JCI Insight* 2018;3:e99114.
11. Tomah S, Alkhouri N, Hamdy O. Nonalcoholic fatty liver disease and type 2 diabetes: where do diabetologists stand? *Clin Diabetes Endocrinol* 2020;6:9.

Downloaded from https://academic.oup.com/cardiovascres/article/117/5/1233/6157826 by guest on 28 September 2023

Julia Rolim Cavalcanti Nunes

Objective

I offer six years of experience in immunometabolism and biochemistry with an emphasis in leadership, interdisciplinary collaborations, and excellent communication skills.

Experience

University of Ottawa, Lab of Dr. Morgan Fullerton Ottawa, Ontario

Doctoral candidate 2017-present

To determine the contribution of macrophage and hepatocyte AMPK in metabolic disease, designed and led long-term collaborative studies of immunometabolism with mouse models of atherosclerosis, NASH and APAP-induced liver injury with the goal of 2-3 first-author publications and the rationale for future therapeutics.

To develop a translational mouse model of NASH, designed and executed a study implementing thermoneutral housing for exacerbation of dietary model of NAFLD, with the goal of publication achieved in 2023.

To characterize AMPK-mediated regulation of cholesterol synthesis, designed and executed experiments like overexpression of the potential molecular target, pharmacological activation of AMPK and phosphorylation analysis of the target by mass spectrometry with the goal of expansion of our knowledge of metabolism and a first-author publication.

Canadian Liver Foundation Ottawa, Ontario

Volunteer 2019-2021

To raise funds and awareness to combat liver disease, joined the organizational committee for the virtual Stroll for Liver 2020 to which I was involved in social media, resulting in increased visibility of the event and a fundraising total of $104,000.

To fund a peer support group led by a registered dietitian, wrote grant applications to make healthy living/cooking more accessible to over 65 expectant attendees per session.

Canadian Lipids Journal Club

Graduate student coordinator 2020-2021

To connect trainees in my field during the pandemic, organized a virtual journal club for the Canadian Vascular and Lipid Summit Conference community, where we promote events, resources, and opportunities on a Slack group for research trainees as well chair monthly journal clubs, resulting a close-knit online community of 52 strong.

Biochemistry, Microbiology and Immunology Graduate Student Association Ottawa, Ontario

Vice President of Internal affairs, elected 2018-2019

To improve student community life, served as a departmental graduate student representative that worked across departments, resulting in my involvement with reaccreditation and revitalization of the biochemistry program as well as implementation of student merchandise that I helped organized with the program director.

Vice President of Finance, elected 2020

To manage student council finances, served as the council member with access to bank accounts and budget plans, resulting in sufficient funds for student events and resources.

Pertinent skills

Primary cell isolation and culturing, long-term in vivo studies with mouse models of disease and inducible genetic deletions, immune cell profiling by multi-parameter flow cytometry, preparation and imaging/analysis of histological samples, serum assays, ELISA, Western blots, qPCR, site-directed mutagenesis, immunoprecipitation, transient and stable cell lines (lentiviral packaging), isolation and immortalization of mouse embryonic fibroblasts, phosphorylation site identification by mass spectrometry and SILAC, preparation and pharmacokinetic/dynamic analysis of nanomedicine-based drug delivery systems, extensive experience with excel, word and many other software programs (Prism Graphpad, QuPath, OMIQ etc.).

Publications

Journal articles

Peyman Ghorbani , Sang Yong Kim , Tyler K T Smith , Lucía Minarrieta , Victoria Robert-Gostlin , Marisa K Kilgour , Maja Ilijevska , Irina Alecu , Shayne A Snider , Kaitlyn D Margison , **Julia R C Nunes** , Daniel Woo , Ciara Pember , Conor O'Dwyer , Julie Ouellette , Pavel Kotchetkov , Julie St-Pierre , Steffany A L Bennett , Baptiste Lacoste , Alexandre Blais , Meera G Nair ,Morgan D Fullerton (2023) Choline metabolism underpins macrophage IL-4 polarization and RELMα up-regulation in helminth infection. PLOS Pathog.

Julia R.C. Nunes, Tyler K.T. Smith, Peyman Ghorbani, Conor O'Dwyer, Natasha A. Trzaskalski, Habiba Dergham, Ciara Pember, Marisa K. Kilgour, Erin E. Mulvihill, Morgan D. Fullerton (2023) Thermoneutral housing does not accelerate metabolic dysfunction-associated fatty liver 1 disease in male or female C57Bl/6J mice fed a Western diet. AJP Endo and metab.

Trzaskalski NA, Vulesevic B, Nguyen M, Jeraj N, Fadzeyeva E, Morrow N, Locatelli CAA, Travis N, Hanson A, **Nunes JRC**, O'Dwyer C, Van der Veen JN, Lorenzen-Schmidt I, Seymour R, Pulente SM, Clément AC, Crawley AM, Jacobs R, Doyle M, Cooper C, Kim K, Fullerton MD, Mulvihill EE (2022) Dipeptidyl-peptidase 4 in hepatocytes regulates portal GLP-1 bioactivity, gluconeogenesis and its complete absence alters liver disease progression. JCI Insight

LeBlond ND, Ghorbani P, O'Dwyer C, Ambursley N, **Nunes JRC**, Smith TKT, Trzaskalski NA, Mulvihill EE, Viollet B, Foretz M, Fullerton MD. (2020) Myeloid deletion and therapeutic activation of AMPK do not alter atherosclerosis in male or female mice. J Lipid Res.

LeBlond ND, **Nunes JRC**, Smith TKT, Robichaud S, Gadde S, Cote M, Kemp B, Ouimet M, Fullerton MD. (2020). Foam cell induction activates AMPK but uncouples its regulation of autophagy and lysosomal homeostasis. *Int. J. Mol. Sci.*

Conor O'Dwyer, Rebecca Yaworski, Nicholas D. LeBlond, Peyman Ghorbani1, **Julia R.C. Nunes**, Kaitlyn D. Margison, Tyler T.K. Smith, Kaelan Gobeil Odai1, Shauna Han, Morgan D. Fullerton. (2019). Fatty acid-induced Lipotoxicity in primary hepatocytes and diet-induced obesity in male mice inhibits hepatic choline transport. Hepatology Communications.

Kim Loh, Shanna Tam, Lisa Murray-Segal, Kevin Huynh, Peter J. Meikle, John W. Scott, Bryce van Denderen, Zhiping Chen, Rohan Steel, Nicholas D. LeBlond, Leah A. Burkovsky, Conor O'Dwyer, **Julia R.C. Nunes**, Gregory R. Steinberg, Morgan D. Fullerton, Sandra Galic, and Bruce E. Kemp. (2018). Inhibition of Adenosine Monophosphate-Activated ProteinKinase-3-Hydroxy-3-Methylglutaryl Coenzyme A Reductase

Signaling Leads to Hypercholesterolemia and Promotes Hepatic Steatosis and Insulin Resistance. Hepatology Communications.

Shayne A. Snider, Kaitlyn D. Margison, Peyman Ghorbani, Nicholas D. LeBlond, Conor O'Dwyer, **Julia R.C. Nunes**, Thao Nguyen, Hongbin Xu, Steffany A. Bennett, Morgan D. Fullerton. (2018). Choline transport links macrophage phospholipid metabolism and inflammation. Journal of Biological Chemistry.

Editorial

Salt IP, **Nunes JRC**, Fullerton MD (2021) Metformin again? Atheroprotection mediated by AMPK and ATF1. *Cardiovasc Res.*

Conferences, research day, seminars, awards

Conferences (*oral presentations)

*Julia R.C. Nunes, Tyler K.T. Smith, Conor O'Dwyer, Peyman Ghorbani, Victoria Robert-Gostlin, Ciara Pember, Alexia Cabrera Brutus, Rama El Hakim, Suresh Gadde, Benoit Viollet, Marc Foretz, Morgan D. Fullerton, "The role of macrophage and hepatocyte AMPK in response to acetaminophen-induced liver injury" 12th International Meeting on AMPK, Lorne, Victoria, Australia, October 1-5th, 2023.

*Julia RC Nunes, Conor O'Dwyer, Peyman Ghorbani, Tyler KT Smith, Ciara Pember, Habiba Dergham, Natasha Trzaskalski, Erin Mulvihill, Morgan D Fullerton, "Implementing thermoneutral housing for the development of NASH in mice" Biochemistry Microbiology and Immunology Symposium, Montebello, QB., May 31st, 2022.

Julia R.C. Nunes, Tyler Smith, Conor O'Dwyer, Peyman Ghorbani, Ciara Pember, Suresh Gadde, Morgan D. Fullerton, "AMP-activated protein kinase in macrophage metabolism during liver injury" 2022 Ottawa Institute for Systems Biology Symposium, Cornwall, ON., May 24-25th, 2022.

Julia R.C. Nunes, Conor O'Dwyer, Peyman Ghorbani, Morgan D. Fullerton, "Multifaceted regulation of cholesterol homeostasis by AMP-activated protein kinase" 11th international conference AMPK, virtual mode, September 26-30th, 2021.

Julia Nunes, Peyman Ghorbani, Conor O'Dwyer, Morgan Fullerton, "AMPK: The coupling of cellular energy and cholesterol homeostasis" Final Scientific Program, Canadian Vascular and Lipid Summit, Banff, AB., October 3-6th, 2019.

Julia Nunes, Peyman Ghorbani, Morgan Fullerton, "Validation of the AMPK-SREBP2 pathway and the implications on hepatic cholesterol homeostasis," Final Scientific Program, 43rd Canadian Lipoprotein Conference, Toronto, ON., June 7-10th, 2018.

*Julia Nunes, Peyman Ghorbani, Morgan Fullerton, "Validation of the AMPK-SREBP2 pathway and implications on hepatic cholesterol homeostasis" Biochemistry Microbiology and Immunology Symposium, Montebello, QB., May 17-18th, 2018.

Julia Nunes, Peyman Ghorbani, Morgan Fullerton, "Validation of the AMPK-SREBP2 pathway and implications on hepatic cholesterol homeostasis" Biochemistry Microbiology and Immunology Poster Day, Ottawa, ON., May 3rd, 2018.

Julia Nunes, Morgan D. Fullerton, "Potential for an AMPK, SREBP2 and miR-33 pathway in regulating immunometabolism" Final Scientific Program, 42nd Canadian Lipoprotein Conference, Ottawa, ON., Oct. 19-22nd, 2017.

Research days and seminars (*oral presentations)

Julia R.C. Nunes, Tyler K.T. Smith, Conor O'Dwyer, Peyman Ghorbani, Victoria Robert-Gostlin, Samarth Chauchan, Ciara Pember, Suresh Gadde, Morgan D. Fullerton, "Regulating macrophage metabolism in acute and chronic liver injury", 66th Annual Canadian Society for Molecular Biosciences Conference, May 30th- June 2nd, 2023.

*Julia R.C. Nunes, Tyler Smith, Conor O'Dwyer, Peyman Ghorbani, Ciara Pember, Suresh Gadde, Morgan D. Fullerton, "Targeting macrophage metabolism in acute liver injury" Centre for Catalysis Research and Innovation, virtual mode, March 9th, 2023.

*Julia R.C. Nunes, Tyler Smith, Conor O'Dwyer, Peyman Ghorbani, Ciara Pember, Suresh Gadde, Morgan D. Fullerton, "Regulating macrophage metabolism during acute and chronic liver injury" Immunometabolism Forum Global meeting series, virtual mode, March 3rd, 2023.

Julia R.C. Nunes, Tyler Smith, Conor O'Dwyer, Peyman Ghorbani, Ciara Pember, Samarth Chauhan, Morgan D. Fullerton, "AMPK's modulation of macrophage metabolism during NASH" Biochemistry Microbiology and Immunology Seminar Day, Ottawa, ON., February 23rd, 2023.

Julia R.C. Nunes, Tyler Smith, Conor O'Dwyer, Peyman Ghorbani, Ciara Pember, Suresh Gadde, Morgan D. Fullerton, "AMP-activated protein kinase in macrophage metabolism during liver injury" 2022 Ottawa Cardiovascular Research Day, virtual mode, May 26-27th, 2022.

*Julia RC Nunes, Conor O'Dwyer, Peyman Ghorbani, Tyler KT Smith, Ciara Pember, Habiba Dergham, Natasha Trzaskalski, Erin Mulvihill, Morgan D Fullerton, "Implementing thermoneutral housing for the development of NASH in mice" Biochemistry Microbiology and Immunology Seminar Day, virtual mode, April 21st, 2022.

Julia R.C. Nunes, Conor O'Dwyer, Peyman Ghorbani, Morgan D. Fullerton, "Hepatic AMPK: coupling cellular energy and cholesterol homeostasis" Biochemistry Microbiology and Immunology Seminar Day, virtual mode, April 15th, 2021.

*Julia Nunes, Peyman Ghorbani, Conor O'Dwyer, Morgan Fullerton, "AMPK: The coupling of cellular energy and cholesterol homeostasis" Faculty of Medicine Research Day, virtual mode, September 25th, 2020.

*Julia Nunes, Peyman Ghorbani, Morgan Fullerton, "Validation of the AMPK-SREBP2 pathway and implications on hepatic cholesterol homeostasis" Biochemistry Microbiology and Immunology Seminar Day, Ottawa, ON., February 2019.

Awards

University of Ottawa, Faculty of Medicine

Admission scholarship ($9,000/year for 4 years)	2019-2023
Excellence scholarship (up to $10,000/year)	2019-2020
Excellence scholarship (up to $10,000/year)	2020-2021
Excellence scholarship (up to $10,000/year)	2021-2022
Excellence scholarship (up to $10,000/year)	Summer 2023
Government of Ontario	
Ontario Graduate Scholarship ($15,000 for 1 year)	2019-2020
Ontario Graduate Scholarship ($15,000 for 1 year)	2020-2021
Ontario Graduate Scholarship ($15,000 for 1 year)	2022
Queen Elizabeth II Graduate Scholarship ($15,000 for 1 year)	2023
University of Ottawa, Faculty of Medicine, BMI Department	
3rd place poster award	2018
2nd place poster award	2021